

UNIVERSITY OF CALIFORNIA

Los Angeles

Application of Knowledge-Based Classification Techniques and
Geographic Information Systems (GIS) on Satellite Imagery for Stormwater Management

A dissertation submitted in partial satisfaction of the
requirements for the degree Doctor of Philosophy
in Civil Engineering

by

Lourdes Villanueva Abellera

2005

The dissertation of Lourdes Villanueva Abellera is approved.

Keith Clarke

Steven Margulis

Keith Stolzenbach

Michael K. Stenstrom, Committee Chair

University of California, Los Angeles

2005

Table of Contents

Signature Page ii

Table of Contents iii

List of Figures viii

List of Tables xii

Acknowledgments xv

Vita xvi

Abstract of the Dissertation xviii

1 Introduction 1

1.1 Background 1

1.2 Objectives and Methodology 2

1.3 Overview of the Chapters 3

2 Remote Sensing 6

2.1 Definition 6

2.2 Energy Interactions with Earth Surface Features 6

2.2.1 Vegetation 7

2.2.2 Soil 9

2.2.3 Water 11

2.3 Sensor and Platform Characteristics 12

2.4 The Landsat Program 15

2.4.1 Overview 15

2.4.2	Landsat -4, - 5, -7 Technical Characteristics	17
2.4.3	The Thematic Mapper	18
2.5	Image Data	20
2.6	References	25
3	Digital Image Processing	28
3.1	Image Rectification and Restoration	28
3.2	Image Enhancement	29
3.2.1	Contrast Manipulation	30
3.2.2	Spatial Feature Manipulation	31
3.2.3	Multi-image Manipulation	33
3.3	Image Classification	33
3.3.1	Supervised Classification	35
3.3.1.1	Training Stage	35
3.3.1.2	Parallelepiped Classification	37
3.3.1.3	Minimum Distance to Means Classification	38
3.3.1.4	Maximum Likelihood Classification	39
3.3.1.5	The Jeffries-Matusita (J-M) Distance	41
3.3.2	Unsupervised Classification	42
3.3.3	Accuracy Assessment	44
3.4	References	47
4	Geographic Information Systems	48
4.1	Definitions	48

4.2	Data Structures	49
4.3	Data Conversion	51
4.4	Spatial Manipulation and Analysis	53
4.4.1	Reclassification	53
4.4.2	Interpolation	54
4.4.3	Connectivity Operations	54
4.4.4	Neighborhood Operations	55
4.4.5	Measurement	55
4.4.6	Statistical Analysis	57
4.5	References	58
5	Knowledge-Based Classification	59
5.1	Definitions	59
5.2	Components of a Knowledge-Based System	60
5.3	Knowledge Acquisition	64
5.4	Knowledge Representation	64
5.5	Approaches to Knowledge-Based Classification	67
5.6	References	69
6	Application of Satellite Data for Stormwater Modeling	72
6.1	Introduction	72
6.2	Land Use/Land Cover	74
6.3	Impervious Surface	79
6.4	Other Hydrologic Parameters	81

6.5	Discussion	84
6.6	Summary and Conclusions	87
6.7	References	89
7	Land Use Classification Using Satellite Data: New Approaches	92
7.1	Introduction	92
7.2	Incorporation of Ancillary Data	93
7.3	Contextual Classifiers	94
7.4	Neural Networks	95
7.5	Fuzzy Classifiers	96
7.6	Knowledge-Based Systems	97
7.7	Discussion	98
7.8	References	100
8	Impervious Surface Detection from Satellite Data	103
8.1	Introduction	103
8.2	Data, Materials, and Software	104
8.3	Methodology	108
8.3.1	Calculation of the Jeffries-Matusita Distances	108
8.3.2	Knowledge-Based Classification	113
8.3.3	Maximum Likelihood Classification	119
8.3.4	Calculation of Overall Imperviousness	120
8.3.5	Accuracy Assessment	124
8.4	Results and Discussion	127

8.5	Conclusions	130
8.6	References	136
9	Estimation of Pollutant Loadings from Satellite Data	137
9.1	Introduction	137
9.2	Data, Materials, and Software	138
9.3	Methodology	138
9.3.1	Calculation of Pollutant Loadings	138
9.3.2	Knowledge-Based Classification	141
9.3.3	Accuracy Assessment	151
9.4	Results and Discussion	158
9.5	Conclusions	174
9.6	References	175
10	Assessing the Accuracy of Classifications for Pollutant Loadings Estimation	176
10.1	Introduction	176
10.2	Methodology	176
10.3	Results and Discussion	184
10.4	Conclusions	186
10.5	References	187
11	Conclusions and Future Work	188
	Appendix: Abbreviations and Acronyms	194

List of Figures

- 2.1 A subset of a satellite image 21
- 3.1 Principle of contrast stretch enhancement 31
- 3.2 Concept of convolution 32
- 3.3 Kernel that detects vertical line features 33
- 3.4 Pixel observations from training areas 36
- 3.5 Parallelepiped classification scheme 38
- 3.6 Minimum distance to means classification scheme 39
- 3.7 Clustering by the ISODATA method 43
- 3.8 Confusion matrix 46
- 4.1 Examples of data layers in a GIS 49
- 4.2 Vector data structure 50
- 4.3 Vector to raster conversion of line entity 51
- 4.4 Digitizer 52
- 4.5 Scanner 52
- 4.6 Creating a majority image 56
- 4.7 Original image (a), and image (b) resulting from the application of a 3 x 3 majority filter 56
- 5.1 An example of a semantic net 62
- 5.2 An example of a decision tree 63
- 7.1 An example of a neural network 95

7.2	An example of a decision tree	98
8.1	Vicinity map of the study area	105
8.2	Black and white reproduction of infrared color image of the study area	106
8.3	Normalized Difference Vegetation Index (NDVI) image	110
8.4	Training areas on NDVI image	111
8.5	Knowledge base with spectral data	115
8.6	Knowledge base with spectral data and buffer zone	116
8.7	Neighborhood analysis	117
8.8	Knowledge base with spectral data, buffer zone, and neighborhood information	118
8.9	SCAG land use map (48 classes aggregated to 7 classes)	123
8.10	Knowledge-based classification with spectral data	131
8.11	Knowledge-based classification with spectral data and buffer zone	132
8.12	Knowledge-based classification with spectral data, buffer zone, and neighborhood information	133
8.13	Maximum likelihood classification on raw image	134
8.14	Maximum likelihood classification on NDVI image	135
9.1	“Greenness” component of the tasseled cap transformation	144
9.2	“Wetness” component of the tasseled cap transformation	145
9.3	“Haze” component of the tasseled cap transformation	146
9.4	TSS loadings classification using spectral data (similar flowcharts for BOD5, Total P, and TKN)	147

- 9.5 TSS loadings classification using spectral data and buffer zone (similar flowcharts for BOD5, Total P, and TKN) 148
- 9.6 Neighborhood analysis 149
- 9.7 TSS loadings classification using spectral data, buffer zone, and neighborhood information (similar flowcharts for BOD5, Total P, and TKN) 150
- 9.8 Copper loadings classification using spectral data 152
- 9.9 Copper loadings classification using spectral data and buffer zone 153
- 9.10 Copper loadings classification using spectral data, buffer zone, and neighborhood information 154
- 9.11 O & G loadings classification using spectral data 155
- 9.12 O & G loadings classification using spectral data and buffer zone 156
- 9.13 O & G loadings classification using spectral data, buffer zone, and neighborhood information 157
- 9.14 TSS, BOD5, Total P, and TKN loadings using spectral data 160
- 9.15 TSS, BOD5, Total P, and TKN loadings using spectral data and buffer zone 161
- 9.16 TSS, BOD5, Total P, and TKN loadings using spectral data, buffer zone, and neighborhood information 162
- 9.17 Copper loadings using spectral data 163
- 9.18 Copper loadings using spectral data and buffer zone 164
- 9.19 Copper loadings using spectral data, buffer zone, and neighborhood information 165
- 9.20 O & G loadings using spectral data 166

- 9.21 O & G loadings using spectral data and buffer zone 167
- 9.22 O & G loadings using spectral data, buffer zone, and neighborhood information 168

List of Tables

- 2.1 Characteristics of the Landsat satellites 16
- 2.2 Landsat 7 characteristics 18
- 2.3 Thematic Mapper spectral bands and applications 19
- 2.4 ETM + characteristics 20
- 2.5 Pixel colors on normal color image 22
- 2.6 Pixel colors on infrared color image 22
- 2.7 Terrain signatures on infrared color image 22
- 2.8 Terrain signatures on normal color and infrared color images 23
- 2.9 TM band/color combinations 24
- 3.1 Tasseled cap transformation 34
- 5.1 An example of a frame 63
- 8.1 Raw image characteristics 107
- 8.2 Jeffries-Matusita distances for the NDVI image 112
- 8.3 Jeffries-Matusita distances for the raw image (6 bands) 112
- 8.4 Aggregation of original SCAG classes to categories relevant to stormwater modeling 121
- 8.5 Overall imperviousness determined from SCAG and LACDPW 122
- 8.6 Distribution of test pixels 124
- 8.7 Error matrix (using raw & NDVI images) 125
- 8.8 Error matrix (using raw & NDVI images, & buffer zone) 125

- 8.9 Error matrix (using raw & NDVI images, buffer zone, & neighborhood info.) 126
- 8.10 Error matrix (using MXL on raw image) 126
- 8.11 Error matrix (using MXL on NDVI image) 127
- 8.12 Comparison of classifications 129
- 9.1 Land use characteristics 139
- 9.2 Pollutant concentrations and annual loadings 141
- 9.3 Range and average loadings for the different pollution levels 142
- 9.4 Error matrix for TSS, BOD5, Total P, and TKN, using spectral data 169
- 9.5 Error matrix for TSS, BOD5, Total P, and TKN, using spectral data and buffer zone 169
- 9.6 Error matrix for TSS, BOD5, Total P, and TKN, using spectral data, buffer zone, and neighborhood information 170
- 9.7 Error matrix for copper, using spectral data 170
- 9.8 Error matrix for copper, using spectral data and buffer zone 171
- 9.9 Error matrix for copper, using spectral data, buffer zone, and neighborhood information 171
- 9.10 Error matrix for O & G, using spectral data 172
- 9.11 Error matrix for O & G, using spectral data and buffer zone 172
- 9.12 Error matrix for O & G, using spectral data, buffer zone, and neighborhood information 173
- 9.13 Comparison of classifications 173

10.1	Annual pollutant loadings	177
10.2	Range and average loadings for the different pollution levels	178
10.3	Proportion of pixels distributed into k classes	179
10.4	Agreement weight matrix for copper with variable weights to be computed	182
10.5	Relationship of copper loadings to weights	183
10.6	Agreement weight matrix for copper	183
10.7	Agreement weight matrix for TSS	183
10.8	Agreement weight matrix for BOD5	183
10.9	Agreement weight matrix for Total P	183
10.10	Agreement weight matrix for TKN	184
10.11	Agreement weight matrix for O & G	184
10.12	Accuracy measures for classification with spectral data (in per cent)	185
10.13	Accuracy measures for classification with spectral data and buffer zone (in per cent)	185
10.14	Accuracy measures for classification with spectral data, buffer zone, and neighborhood information (in per cent)	186

ACKNOWLEDGMENTS

I would like to express my gratitude to my advisor, Prof. Michael K. Stenstrom, for his guidance and encouragement throughout my graduate studies. I especially appreciate his availability and prompt action during paper submissions. I also thank the other members of my committee: Prof. Keith Clarke, Prof. Steven Margulis, and Prof. Stolzenbach. The Philippine government, through the Department of Science and Technology, provided support for my Ph.D. studies.

Yafang Su and other staff members of the UCLA Visualization and Modeling Laboratory assisted me with software and hardware difficulties. I also thank the UCLA ATS Statistical Consulting Group for helping me learn STATA 8.2 in a short period of time. My father, Robustiano L. Abellera, illustrated the scanner and digitizer in the GIS Chapter. The Landsat ETM+ and the SCAG data were downloaded from the UCLA GIS Database.

I thank my research group mates for patiently listening to my presentations and providing valuable insights. I am grateful to my dear family, my parents (Robustiano and Lourdes), sister (Evangeline), and brother (Robustiano Jr.), and to Anand Panangadan for their constant love and support. Anand also helped me with technical problems and drove during my fieldwork. I also acknowledge Gabriel whose mere presence brings me respite on stressful days.

VITA

November 13, 1963	Born, Manila, Philippines
1981-1986	Undergraduate Scholarship from the University of the Philippines
1986	B.S., Geodetic Engineering University of the Philippines, Diliman Quezon City, Philippines
1991-1997	Instructor Department of Geodetic Engineering University of the Philippines, Diliman Quezon City, Philippines
1995-1996	Master's Thesis Grant from the Philippine Council for Advanced Science and Technology Research and Development
1997	M.S., Remote Sensing University of the Philippines, Diliman Quezon City, Philippines
1998-2001	Doctoral Fellowship from the Department of Science and Technology
2001	M.S., Civil Engineering University of California, Los Angeles Los Angeles, California, U.S.A.

PUBLICATIONS AND PRESENTATIONS

Abellera, L.V. and Stenstrom, M.K. (2005) Impervious surface detection from satellite imagery with knowledge-based systems and GIS. In *Proceedings of the International Conference on Computing in Civil Engineering*, 12-15 July, Cancun, Mexico, in press.

Abellera, L.V. and Stenstrom, M.K. (2005) Application of remotely sensed environmental data for control and automation. *Journal of Environmental Instrumentation, Control and Automation*, 9 (4): 1-7.

Abellera, L.V. and Stenstrom, M.K. (2005) Assessing the accuracy of satellite image classifications for pollutant loadings estimation. In *Proceedings of the 3rd International Symposium on Remote Sensing and Data Fusion Over Urban Areas (URBAN 2005)*, 14-16 March, Tempe, Arizona, U.S.A., in CD-ROM.

Abellera, L.V. and Stenstrom, M.K. (2005) Evaluation of raw and transformed Landsat ETM+ data for knowledge-based land use and impervious surface identification. In *Abstracts of the Hawaii Water Environment Association 27th Annual Conference*, 16-18 February, Honolulu, Hawaii, U.S.A., Presentation 30.

Abellera, L.V. and Stenstrom, M.K. (2005) Application of satellite data for stormwater modeling. In *Proceedings of the 8th Map India Annual International Conference*, 7-9 February, New Delhi, India, Paper AD 143.

Abellera, L.V. and Stenstrom, M.K. (2005) Estimation of pollutant loadings from remotely-sensed data with knowledge-based systems and GIS. In *Proceedings of the 8th Map India Annual International Conference*, 7-9 February, New Delhi, India, Paper AD 283.

Abellera, L.V. and Dolino, C.N. (2004) Conservation status of the Philippine tarsier. In *Abstracts of the Biology in Asia International Conference*, 7-10 December, Singapore, p. 45.

Abellera, L.V. and Dolino, C.N. (2004) Habitat mapping from satellite imagery. In *Abstracts of the Biology in Asia International Conference*, 7-10 December, Singapore, p. 46.

Abellera, L.V. and Stenstrom, M.K. (2004) Land use classification using satellite data for stormwater management. In *Proceedings of the 25th Asian Conference on Remote Sensing, Volume 2*, 22-26 November, Chiang Mai, Thailand, pp. 1251-1256.

Abellera, L.V. and Veracion, J.G. (2004) Mapping Philippine tarsier habitat using remote sensing and geographic information systems (GIS). In *Proceedings of the 25th Asian Conference on Remote Sensing, Volume 1*, 22-26 November, Chiang Mai, Thailand, pp. 432-437.

Abellera, L.V. (1996) Solid waste disposal site selection using image processing and geographic information systems (GIS) techniques. In *Proceedings of the 17th Asian Conference on Remote Sensing*, 4-8 November, Colombo, Sri Lanka (abstract), online.

Abellera, L.V. (1996) Solid waste disposal site selection using image processing and geographic information systems (GIS) techniques. In *Abstracts of the 18th National Academy of Science and Technology Annual Scientific Meeting*, 10-11 July, Davao City, Philippines.

ABSTRACT OF THE DISSERTATION

Application of Knowledge-Based Classification Techniques and
Geographic Information Systems (GIS) on Satellite Imagery for Stormwater Management

by

Lourdes Villanueva Abellera

Doctor of Philosophy in Civil Engineering

University of California, Los Angeles, 2005

Professor Michael K. Stenstrom, Chair

Stormwater management is concerned with runoff control and water quality optimization. A stormwater model is a tool applied to reach this goal. Hydrologic variables required to run this model are usually obtained from field surveys and aerial photo-interpretation. However, these procedures are slow and difficult. An alternative is the automated processing of satellite imagery. We examined various studies that utilized satellite data to provide inputs to stormwater models. The overall results of the modeling effort are acceptable even if the outputs of satellite data processing are used instead of

those obtained from standard techniques. One important model input parameter is land use because it is associated with the amounts of runoff and pollutants generated in a parcel of land. Hence, we also explored new ways that land use can be identified from satellite imagery.

Next, we demonstrated how the combined technologies of satellite remote sensing, knowledge-based systems, and geographic information systems (GIS) are used to delineate impervious surfaces from a Landsat ETM+ data. Imperviousness is a critical model input parameter because it is proportional to runoff rates and volumes. We found that raw satellite image, normalized difference vegetation image, and ancillary data can provide rules to distinguish impervious surfaces satisfactorily. We also identified different levels of pollutant loadings (high, medium, low) from the same satellite imagery using similar techniques. It is useful to identify areas with high stormwater pollutant emissions so that they can be prioritized for the implementation of best management practices. The contaminants studied were total suspended solids, biochemical oxygen demand, total phosphorus, total Kjeldahl nitrogen, copper, and oil and grease. We observed that raw data, tasseled cap transformed images, and ancillary data can be utilized to make rules for mapping pollution levels. Finally, we devised a method to compute weights associated with the severity of misclassification errors. We proposed the use of the weighted equivalents of the overall accuracy and kappa coefficient to evaluate the quality of classifications for pollutant loadings estimation. Overall, we conclude that the automated classification of satellite imagery can provide valuable information that can be used in stormwater management.

Chapter 1

Introduction

1.1 Background

The goal of stormwater management is to control runoff quantity and maintain water quality. Elevated volumes and flow rates of runoff can have a number of harmful effects including flooding, stream erosion, and habitat destruction. Surface runoff can also carry and distribute sediment, nutrients, oxygen-demanding organics, toxic substances, and pathogens to drainage systems and watercourses. These pollutants may also threaten aquifers.

To solve problems associated with runoff, a stormwater model is used to simulate the movement of stormwater and transported materials through a watershed. Many parameters are required to run a stormwater model. Parameter acquisition is a tedious process because stormwater runoff is a poorly understood environmental system. Innumerable factors affect runoff including topography, precipitation characteristics, and human activities. Also, the large area that needs to be quantified makes data collection using conventional methods too time-consuming and expensive. Hydrologic variables for stormwater modeling are commonly acquired by means of conventional techniques such as field surveys and aerial photo-interpretation. With the introduction of space technologies, satellite data have turned out to be a more expedient option to these

traditional methods. Satellite imagery can be acquired easily, can cover extensive areas, and is compatible with many stormwater modeling software packages.

1.2 Objectives and Methodology

In this investigation, we explore the use of satellite imagery for stormwater management. After discussing how satellite data are applied in stormwater management, we demonstrate the use of knowledge-based systems to classify areas on a satellite image that are of interest to stormwater managers. A knowledge-based system applies rules to a symbolic representation of knowledge to complete a task. Knowledge is in the form of spectral data but ancillary data, like elevation, housing density, or zoning information, are commonly incorporated. As such, knowledge-based classification normally utilizes a geographic information system (GIS), a potent set of techniques that can obtain, store, retrieve, analyze, and display spatial data.

The following are the objectives of this study:

1. To explain the concepts of satellite remote sensing and the procedures to process image data;
2. To present the fundamentals of GIS and its capabilities;
3. To discuss the rudiments of knowledge-based systems and examine the various means by which these systems are applied in image classifications;
4. To explore the ways in which satellite data are used in stormwater modeling;
5. To survey novel approaches for land use classification utilizing satellite imagery;

6. To detect impervious surface in the Marina del Rey area and vicinity using remote sensing, knowledge-based systems, and GIS technologies;
7. To estimate levels of pollution for selected contaminants in the same study area using similar techniques, and
8. To propose a method to assess the accuracy of classifications for pollutant loadings estimation.

1.3 Overview of the Chapters

In Chapter 2, the concepts of remote sensing are discussed. Here, we see how materials with their unique properties interact with electromagnetic radiation. This chapter also tells us how sensors and platforms work to gather remotely sensed data and how the resulting images are formatted and interpreted. Particular emphasis is placed on the Landsat satellites. Processing of satellite imagery to provide useful information is the subject of Chapter 3. The details of image classification are stressed in this chapter. To evaluate the quality of the image classifications, the subject of accuracy assessment is also explained. In Chapter 4, the fundamentals of GIS are outlined. Data structures, data conversion, and standard GIS techniques, such as reclassification and neighborhood operations, are presented.

Chapter 5 explores the basics of knowledge-based systems such as its components, knowledge acquisition, and knowledge representation. The chapter ends with the discussion of the variety of methods in applying knowledge-based systems to image classification. Chapter 6 illustrates how the concepts and techniques of remote

sensing, GIS, and other emerging technologies are utilized in the acquisition of parameters required for stormwater modeling. Examples of these hydrologic variables are land use, impervious surface, and elevation. Chapter 7 discusses how land use can be obtained from satellite data with new approaches like neural networks and fuzzy classifiers. The issues affecting land use classification for stormwater modeling are also treated. Land use is a necessary input parameter to stormwater models because it is related to the amount of runoff and pollutants generated in a parcel of land.

In Chapters 8, 9, and 10, we demonstrate the actual use of the techniques of remote sensing, knowledge-based systems, and GIS for stormwater management applications. In Chapter 8, impervious surface is identified on a Landsat ETM+ data in a highly urbanized portion of the Santa Monica Bay watershed in Los Angeles, the Marina del Rey area. Delineation of impervious surface is important because it is used to determine runoff rates and volumes. Calculating for the size of a storage facility to prevent flooding, for example, requires the knowledge of the amount of impervious surface in the watershed. In this chapter, we will see how well we can distinguish impervious surface from water, vegetation, soil, and beach. We also compared our results to those obtained from the maximum likelihood method, a standard statistical classifier. Next, we used similar strategies to directly estimate levels of pollution using the same imagery. The procedures and analysis are discussed in Chapter 9. The six water quality parameters studied were total suspended solids, biochemical oxygen demand, total phosphorus, total Kjeldahl nitrogen, copper, and oil and grease. It is necessary to know the areas in the watershed that generate high levels of pollution to be able to prioritize

these areas for the implementation of best management practices. In Chapter 10, a method is presented to evaluate the accuracy of the classifications made in Chapter 9. Essentially, we propose the use of the weighted equivalents of the overall accuracy and kappa coefficient to report the quality of the classifications. We also recommend a way to calculate the weights associated with misclassification errors. The specific accuracy measures will provide more information for pollution control. Chapter 11 presents the overall conclusions of this investigation and discusses ways where the techniques learned can be applied to other areas.

Chapter 2

Remote Sensing

2.1 Definition

Remote sensing is the art and science of acquiring information about an object or phenomenon by means of a device not directly in contact with the object or phenomenon under observation. In a technological setting, remote sensing is usually associated with data obtained by sensors and instruments that measure emitted or reflected electromagnetic radiation. The data can be arranged in a digital format that can be analyzed using a computer to yield useful information (Sanchez and Canton, 1999).

2.2 Energy Interactions with Earth Surface Features

When incident electromagnetic radiation or energy from the sun strikes an object on the earth's surface, some of the radiation is absorbed, some is transmitted, and the rest is reflected. This incident radiation is of various types, depending on its location in the electromagnetic spectrum. Not all radiation types are utilized in remote sensing because some of them are scattered and/or absorbed by atmospheric particles. Therefore, only those in the atmospheric windows are utilized for remote sensing. They are the blue (0.4-0.5 μm), green (0.5-0.6 μm), red (0.6-0.7 μm), near infrared (NIR) (0.7-1.3 μm), middle infrared (MIR) (1.3-3 μm), thermal infrared (TIR) (beyond 3 μm), and the microwave

energy (1 mm to 1 m). For a specific object, various kinds of incident energy will result in different amounts of absorbed, transmitted, and reflected energy. Water, for instance, reflects little blue and red energy, and completely absorbs NIR (Lillesand and Kiefer, 1994).

If the reflected energy is plotted against the wavelength, a spectral signature results. The characteristic patterns of spectral signatures of earth surface features are the basis for the recognition of their properties (Lillesand and Kiefer, 1994). There are typical signatures of earth materials, but they can vary according to several factors that are associated with the material itself or the environment (Curran, 1985). Vegetation, soil, and water are dominant surface features and their signatures are examined next.

2.2.1 Vegetation

The basic component of vegetation is the leaf. A leaf is made of layers of structural fibrous organic matter. Inside the leaf are pigmented, water-filled cells, and air spaces. These three characteristics, pigmentation, physiological structure, and water content, affect the way the leaf absorbs, transmits, and reflects the energy incident on it. All healthy green vegetation exhibits low reflectance of red and blue energy, medium reflectance of green energy and high reflectance of near infrared energy. This is due to the combined effects of leaf pigments and physiological structure. However, due to old age and disease, plant pigments can break down. Consequently, stressed vegetation will show a decrease in the amount of reflected near infrared energy and a rise in the reflection of blue and red wavelengths (Curran, 1985). The leaf pigment chlorophyll has

been particularly studied because of its influence on vegetation stress. Chlorosis, a plant disease characterized by yellowing or decoloring, and necrosis, death of narrow areas of living plant tissue, can result from pollution, pests, and agents of disease like bacteria or virus. In those areas affected, the concentration of chlorophyll pigments can diminish. Barton (2001) reported that these small diseased areas exhibit a disproportionately large effect on total leaf reflectance.

Moisture in the plants will cause a decrease in the overall reflected energy. This happens because water generally absorbs energy, regardless of wavelength (Curran, 1985). In analyzing satellite data, however, we do not usually deal with individual leaves or plants. What we see in an image is mostly a plant canopy. A canopy is the topmost expanding branchy stratum of a forest. In this case, factors in the environment can influence the amount of reflected energy. For example, when the sun is high in the sky, electromagnetic radiation will penetrate deeply into the canopy, and reflectance will be low. When the sun is low, radiation will only strike the canopy at shallow depths, and reflectance will be high (Ahmad and Lockwood, 1979). In open canopies, we can detect plant species in the understory (ground level plants). Williams and Hunt (2002) identified a perennial weed called leafy spurge among other green vegetation in northeastern Wyoming because of the unique yellow-green color of its bracts.

Phenology, that branch of science that deals with the relationship between climate and recurrent biological phenomena, has an effect on the reflectance of plants (Steiner, 1970). Wheat, for example, has a relatively high red reflectance, but low NIR reflectance during the winter. In the summer, the opposite is true. Red reflectance is low, while NIR

reflectance is high (Kauth and Thomas, 1976). Lanjeri *et al.* (2001) were able to distinguish different vineyard classes such as abandoned vineyards and young vineyards from multi-temporal remotely sensed data because of their phenology.

2.2.2 Soil

Most types of soils have the same reflectance properties. There is a positive relationship between the reflectance and the wavelength. Reflectance generally increases with the wavelength. There are five factors, which are interrelated, that describe the reflectance of soils. These are moisture content, organic content, texture, structure, and iron oxide content (Hoffer, 1978; Stoner and Baumgardner, 1981).

We refer to two contrasting soil types to be able to see the relationship between texture, structure, and soil moisture. Clay soil particles hold fast to each other, and as a result, clay soil tends to have a strong structure. This leads to rough surface on plowing. Clay soils usually have high moisture content. The combination of these factors causes clay soils to exhibit a fairly low reflectance. Clay is in contrast with a sandy soil which tends to have a weak structure. The particles stick less to each other. This causes a fairly smooth surface on plowing. In addition, sandy soils tend to drain water well, and hence, have low moisture content. Because of all of these, sandy soils exhibit high reflectance (Bowers and Hanks, 1965).

Again, as water generally absorbs energy, its presence in any material will decrease that material's reflectance. The same holds true for soil. In visible wavelengths, the reflectance of soil is greatly decreased by the presence of soil moisture (Jensen and

Hodgson, 1983). However, when the soil becomes saturated, the addition of more moisture will have no effect on reflectance. In the near infrared and middle infrared, the same observation holds, but the decrease in reflectance is more rapid (Curran, 1985).

The presence of dark organic matter will decrease the reflectance of soil. However, when the organic matter content of the soil is more than 5 per cent, the soil is already black. Additional increases in organic matter will have only a slight effect on reflectance (Page, 1974). Many soils have a rusty red color because of the presence of iron oxide, which selectively reflects red light and absorbs green light (Obukhov and Orlov, 1964). With this remarkable property, iron ore deposits can be delineated from satellite images (Vincent, 1973).

The discussion above tells us that the spectral signature of a particular soil can be used to predict its properties. Bendor and Banin (1995) consulted the spectral reflectance curves in the near infrared portion of the electromagnetic spectrum to calculate the following soil properties: organic matter content, carbonate content, clay content, hygroscopic moisture, specific surface area, and cation-exchange capacity. The soils investigated were from arid and semi-arid regions. McCarty *et al.* (2002) referred to the near-infrared and mid-infrared regions to quantify the amount of organic and inorganic carbon in soil. They studied 14 soil series with contrasting temperature and soil moisture characteristics.

2.2.3 Water

The majority of the incident radiation on water is not reflected but is either absorbed or transmitted. In the visible wavelengths, little radiation is absorbed, a small amount, not more than 5 per cent, is reflected. The rest of the majority is transmitted. The near infrared and the middle infrared radiation are strongly absorbed by water, so very little is reflected or transmitted (Wolfe and Zissis, 1978). Because of this, the boundary between water and land shows a sharp contrast.

Factors in the environment affect the reflectance of a water body. The depth of the water, the materials within the water, and the surface roughness of the water are some of the most significant factors (Curran, 1985). In shallow water, the majority of the reflectance comes from the bottom of the water body, not by the water itself. Hence, in these areas, the underlying material, not the water itself, determines the water body's reflectance characteristics and color. Non-organic sediments, tannin, and chlorophyll are the most common suspended materials in water (Curran, 1985). Non-organic silts and clays tend to increase the scatter and reflectance in visible wavelengths (Weisblatt *et al.*, 1973). Using this property, amounts of suspended particulate matter can be calculated in prominently turbid waters (Doxaran *et al.*, 2002).

If the chlorophyll content of water is very high, the water body will partly exhibit the reflectance properties of vegetation where green reflectance is high, and blue and red reflectance are low (Piech *et al.*, 1978). Zeichen and Robinson (2004) concluded that the large segments of water in the north-east Atlantic Ocean showing increased reflectance of visible radiation contained phytoplankton blooms.

The roughness of the water surface can also change the reflectance properties of water. A smooth water surface can show very high or very low reflectance depending upon the location of the sensor. If the surface is very rough, reflectance will increase as there is an increased scattering on the surface (Curran, 1985).

2.3 Sensor and Platform Characteristics

We have seen how surface materials respond to incident energy. These properties are used in remote sensing to gather beneficial information. The remotely-sensed data are acquired by a device or sensor on board a platform. The sensor and the platform together constitute a remote sensing system. A passive remote sensing system utilizes the sun's electromagnetic radiation, while an active remote sensing system supplies its own source of energy to illuminate earth surface features (Lillesand and Kiefer, 1994). Aboard a satellite, remote sensing devices electronically code radiation in numeric format to produce a digital image. The most common sensing devices are the multi-spectral scanners and microwave sensors (Harrison and Jupp, 1989).

The multi-spectral scanners utilize the visible, near infrared, middle infrared, and thermal infrared parts of the electromagnetic spectrum to obtain data. One wavelength range (e.g., 0.4-0.5 μm) corresponds to one band or channel (e.g., blue band) (Lillesand and Kiefer, 1994). Multi-spectral scanners, which depend on natural illumination from the sun (passive system), operate in various ways. There are three types that are categorized according to the mechanism used by the sensor to view each pixel. Electromechanical scanners have a sensor which oscillates from side to side to form the

image. In a linear array scanner, there is an array of detectors that sense the pixel values along a line simultaneously. While in a central perspective scanner, the sensing device does not move during data acquisition. Hence, the sensor views all pixels from the same central position. In this aspect, this sensor is similar to a photographic camera (Harrison and Jupp, 1989).

The microwave sensors function between the wavelengths of about 1-1,000 mm. These devices are employed in both active and passive systems. In active systems, like radar, the device not only supplies the energy but also detects the response from the features of interest. In the passive system, the earth sends out natural radio emission that the microwave devices can sense (Lillesand and Kiefer, 1994). Data from the microwave sensors, however, are not usually utilized for land use classification because of the configuration of the data acquisition process that makes shadows more pronounced (Harrison and Jupp, 1989).

Platforms carry the sensors that gather data. The most common platforms are aircraft and spacecraft (Lillesand and Kiefer, 1994). Some of the multi-spectral and hyperspectral instruments aboard an aircraft are the AMS which operates in 10 wavelength bands in 8-bit and 12-bit resolutions, AVIRIS which utilizes the 400 to 2,500 nm region in 224 channels, CASI which uses the 400 to 1000 nm region in up to 288 channels, and HYDICE with the capability of imaging in 210 spectral bands in the 400 – 2,500 nm range of the electromagnetic spectrum (CARSTAD, 2004).

Spacecraft can be manned or unmanned (Harrison and Jupp, 1989). Mercury, Gemini, Apollo (launched in the 1960s), Skylab (1970s), and the Space Shuttle (1980s)

are some of the manned spacecraft operated by the United States which have taken numerous images of the earth (Sanchez and Canton, 1999). Unmanned spacecraft may be categorized into two general groups: polar orbiting earth observation satellites and geostationary meteorological satellites. Geostationary satellites orbit at an altitude of about 36,000 km above the equator. They always view the same point on the earth's surface. This is caused by the satellite's circling around the earth with the same angular velocity as the earth's rotation. Hence, the satellite views images of the same part of the earth at regular intervals (CEOS, 2003). Some of the satellites that monitor the atmosphere covering the entire globe include Meteosat 7, Insat 3E, Himwari/GMS5, GOES-10 and GOES-12 (Satellite Signals, 2004).

Polar-orbiting satellites invariably pass a specific latitude at the same solar time. They cover regions between the latitudes 82° north and 82° south of the equator. Hence, they are called polar, sun-synchronous satellites. Their orbits in space can vary from 700 km to 1,500 km from the surface of the earth. Because of the orbital characteristics of these satellites, the near global imaging of the earth's surface can be done on a routine and predictable basis (Harrison and Jupp, 1989). The Landsat series of satellites have been the best-known satellites of this nature. Imageries that they acquire are also the most commonly utilized. But there are many other polar orbiters in space. One of these is the SPOT satellite which carries the multi-spectral (MSS) and panchromatic sensors. The MSS operates in three channels; the panchromatic, in one channel. Another example is the NOAA satellite which contains the AVHRR instrument operating in five wavelength bands (Kerr and Ostrovsky, 2003).

Landsat data have been used in many applications in numerous disciplines. This is because Landsat data have a relatively high resolution (30 meters in most bands) which is sufficient for most areas of study. It also has seven bands that can be combined to suit a scientist's particular application. Perhaps the greatest advantage of Landsat data is its availability to the public. Landsat data will be used in this study, and is the topic of the next section.

2.4 The Landsat Program

2.4.1 Overview

In more than thirty-five years of space exploration, many space imaging missions have been flown by countries such as the United States, Britain, Canada, China, Germany, India, Japan, and Russia. Particularly, the United States has been playing a major role in earth remote sensing. Its Landsat program is the longest running mission and has produced the largest collection of earth images available (more than three million) (Sanchez and Canton, 1999).

On June 23, 1972, the first Landsat satellite was launched. From then on, more Landsat satellites were brought in space. Each new satellite carried with it sensors more powerful than their predecessors (Sanchez and Canton, 1999). Table 2.1 shows the essential attributes of the Landsat satellites.

The Landsat satellites can be grouped into three classes. The first group consists of Landsats 1, 2, and 3 which held the Multi-spectral Scanner (MSS) and the Return Beam Vidicon (RBV) camera. Next is the Landsats 4 and 5 group which carried the

Thematic Mapper (TM) in addition to the MSS. The last group combines Landsats 6 and 7 with the Enhanced Thematic Mapper (ETM) and the Enhanced Thematic Mapper Plus (ETM+) sensors on board respectively (Sanchez and Canton, 1999). The more recent satellites have enhanced sensor and communication capabilities and are the only ones to be discussed further. Specifically, we focus our discussion on Landsats 4, 5, and 7. Although Landsat 4 was recently decommissioned, and Landsat 5 will be shut down soon (U.S. Geological Survey, 2003), the images they collected are still available to the public. After reviewing the characteristics of the satellite platform, the sensor Thematic Mapper and its enhanced counterpart will be discussed.

Table 2.1: Characteristics of the Landsat satellites

Satellite	Launch Date	Decommission Date	Sensors
Landsat 1	July 23, 1972	Jan. 16, 1978	MSS, RBV
Landsat 2	Jan. 23, 1975	Feb. 25, 1982	MSS, RBV
Landsat 3	March 5, 1978	March 31, 1983	MSS, RBV
Landsat 4	July 16, 1982	June 15, 2001	MSS, TM
Landsat 5	March 1, 1984	Operational	MSS, TM
Landsat 6	Oct. 5, 1993	Crashed at launch	ETM
Landsat 7	April 15, 1999	Operational	ETM +

(from Sanchez and Canton, 1999; Australian Centre for Remote Sensing, 2003; and Goddard News, 2001)

MSS = Multi-spectral Scanner
 RBV = Return Beam Vidicon
 TM = Thematic Mapper
 ETM = Enhanced Thematic Mapper

2.4.2 Landsat -4, - 5, -7 Technical Characteristics

Landsats 4 and 5 were both positioned on circular, sun-synchronous, near-polar orbits (within 9° of the North Pole). Each spacecraft weighing approximately 4,400 lbs was placed at an altitude of about 705 km above the earth. The solar panels are 1.5 m long and 2.3 m wide. The antennas directly transmit data to receiving stations on earth. The period, the time a satellite takes to complete an entire orbit, is 98.9 minutes. This results in a 16-day repeat cycle. This simply means that a specific point on the earth's surface is viewed by the satellite every 16 days. This also means that the entire globe is covered by the satellite after 16 days. The ground track is the path of the satellite when traced on the surface of the earth. At the equator, the distance between ground tracks is 2,752 km. The equatorial crossing, where the path crosses the equator, takes place at 9:45 AM local time. Because of the earth's rotation, each satellite orbit is placed westward of the preceding one. Hence, everyday, the satellite orbit progresses slowly westward (Sanchez and Canton, 1999). Data are gathered on the illuminated side of the earth on the descending path (northeast to southwest). Because it is a passive system, in the night during the ascending path, the sensors are turned off. The image swath width is 185 km. This means that the sensor sweeps through 185 km of ground in one imaging instance. Coverage of adjacent swaths happens every seven days, and the coverage cycle is 16 days (Sanchez and Canton, 1999). Landsat 7, as can be seen in Table 2.2, is similar to Landsats 4 and 5, except that it contains an enhanced version of the Thematic Mapper.

Table 2.2: Landsat 7 characteristics

Launch date:	April 15, 1999
Sensor data acquired:	ETM (Enhanced Thematic Mapper) +
Data reception commenced:	ETM data from July 6, 1999
Altitude:	705 km
Swath Width:	185 km
Orbit type:	near polar, sun synchronous
Orbit period:	99 minutes
Repeat cycle:	16 days

(from the Australian Centre for Remote Sensing, 2003)

2.4.3 The Thematic Mapper

The Thematic Mapper (TM) is carried on board Landsats 4 and 5. The TM has a flat, oscillating mirror that scans both west-to-east and east-to-west directions. This produces a ground swath of 185 km. The ground track is perpendicular to the orbital track. The satellite movement results in the along-track dimension of the image. The scanning mirror directs the reflected and emitted radiation to the inside of the instrument. Here, various stationary mirrors focus the gathered energy onto a fiber optic collector. From the collector, the energy is transmitted to detectors which are sensitive to seven spectral regions (called bands or channels) (Sanchez and Canton, 1999).

We call the surface area imaged by the sensor at a given instant in time as the instantaneous field of view (IFOV). For the Thematic Mapper, the IFOV is 30 m by 30 m (except for band 6). Remote sensing practitioners often regard the word pixel to mean IFOV. Consequently, we can also say that each TM pixel covers an area 30 m by 30 m. The size of the pixel determines how well we can resolve specific objects on the earth's surface covered by that pixel. Hence, another word for pixel size is resolution or spatial

resolution (Sanchez and Canton, 1999; Harrison and Jupp, 1989). Table 2.3 details the characteristics and applications of TM data.

Table 2.3: Thematic Mapper spectral bands and applications

Band	Resolution	Wavelength (μm)	Spectral Location	Applications
1	30 m	0.45- 0.52	Blue	Water body penetration in coastal water mapping Soil/vegetation discrimination Forest type determination Cultural features identification
2	30 m	0.52- 0.60	Green	Vegetation's green reflectance peak Vegetation type discrimination Vegetation vigor assessment Cultural feature identification
3	30 m	0.63-0.69	Red	Chlorophyll absorption determination Plant species determination Cultural feature identification
4	30 m	0.76-0.90	Near Infrared	Vegetation type determination Vegetation vigor determination Biomass contents determination Delineating water bodies Soil moisture discrimination
5	30 m	1.55-1.75	Mid- Infrared	Vegetation moisture determination Soil moisture determination Snow/clouds differentiation
7	30 m	2.08-2.35	Mid- Infrared	Mineral types determination Rock types determination Vegetation moisture determination
6	120 m	10.4-12.5	Thermal Infrared	Vegetation stress analysis Soil moisture discrimination Thermal mapping

(from Sanchez and Canton, 1999)

Landsat 7 carries the Enhanced Thematic Mapper + which is an improved version of the Thematic Mapper. The resolution of the thermal band was increased to 60 m (120 m for the TM). Also, there is a panchromatic band which has a higher resolution of 15 m. Table 2.4 summarizes the characteristics of the ETM+.

Table 2.4: ETM + characteristics

Band	Resolution	Wavelength (μm)	Spectral Location
1	30 m	0.450- 0.515	Blue
2	30 m	0.525- 0.605	Green
3	30 m	0.63-0.69	Red
4	30 m	0.75-0.90	Near Infrared
5	30 m	1.55-1.75	Mid-Infrared
7	30 m	2.09-2.35	Mid-Infrared
6	60 m	10.4-12.5	Thermal Infrared
Panchromatic	15 m	0.52-0.90	Visible Range

(from Sanchez and Canton, 1999)

2.5 Image Data

The resulting remotely sensed data is an image which has a square or rectangular array format. This raster image (Figure 2.1) which shows different levels of gray is made of square elements called pixels. Each image is associated with one band or channel. Every pixel has a digital number (DN) which represents the reflected energy or reflectance of that parcel of land covered by the pixel. The Thematic Mapper gathers data in 8 bits. Hence, the DN ranges from 0 (black pixel, very low reflectance) to 255 (white pixel, very high reflectance). Any DN in between will show different levels of gray.

Resolution or spatial resolution is the relationship between the pixel size and the size of the ground the pixel captured. An 80-meter resolution, for instance, means that one side of the pixel correlates to 80 m on the earth's surface.

104	102	106	104	105	105	106	119	112	114
99	109	112	105	108	104	103	116	111	109
111	118	105	105	99	102	111	106	101	101
118	118	112	121	106	112	109	96	101	103
117	116	112	116	108	116	106	102	113	105
111	108	114	105	108	107	104	116	109	120
105	106	103	104	118	109	105	116	106	108

Figure 2.1: A subset of a satellite image

Color images actually consist of three images, for example, blue, green, and red bands. These bands can be assigned to the blue, green, and red color guns of the display device (e.g., computer monitor) respectively. These images are superimposed on each other to produce a color image or a composite. Table 2.5 gives examples of pixel colors that will appear in the computer monitor if the above scheme is applied. The resulting image is called a normal color image. If we use the green, red, and near infrared bands instead, and assign them respectively to the blue, green, and red guns of the color monitor, the result is Table 2.6. This image is referred to as an infrared color image. All other color assignments are simply called false color images or composites. Tables 2.7

and 2.8 list the appearances of selected earth surface features in satellite images using the two different color assignments. The infrared color image, however, is more helpful for visual interpretation.

Table 2.5: Pixel colors on normal color image

	DN	DN	DN	DN	DN	DN
Blue Band	255	0	0	0	255	128
Green Band	0	255	0	0	255	128
Red Band	0	0	255	0	255	0
Resulting Color	Blue	Green	Red	Black	White	Light Cyan

(Blue band assigned to blue gun, Green band to green gun, Red band to red gun)

Table 2.6: Pixel colors on infrared color image

	DN	DN	DN	DN	DN	DN
Green Band	255	0	0	0	255	128
Red Band	0	255	0	0	255	128
Near Infrared Band	0	0	255	0	255	0
Resulting Color	Blue	Green	Red	Black	White	Light Cyan

(Green band to blue gun, Red band to green gun, Near infrared band to red gun)

Table 2.7: Terrain signatures on infrared color image

Surface Feature	Infrared Color Image
Green vegetation	Red
Deep, clear water	Dark blue
Turbid water	Bright blue
Red soil	Green
Bright urban areas	Pale blue

(from Harrison and Jupp, 1989)

Table 2.8: Terrain signatures on normal color and infrared color images

Surface Feature	Normal Color Image	Infrared Color Image
Healthy vegetation: Broadleaf type Needle-leaf type	Green Green	Red to magenta Reddish brown to purple
Stressed vegetation: Previsual stage Visual stage	Green Yellowish green	Pink to blue Cyan
Autumn leaves	Red to yellow	Yellow to white
Clear water	Blue-green	Dark blue to black
Silty water	Light green	Light blue
Damp ground	Slightly darker	Distinct dark tones
Shadows	Blue with details visible	Black with few details visible
Water penetration	Good	Green and red bands: same Infrared band: poor
Contacts between land and water	Poor to fair discrimination	Excellent discrimination
Red bed outcrops	Red	Yellow

(from “Introduction to Remote Sensing” Seminar, 1995)

Table 2.9 lists possible band combinations for some applications. Since water strongly absorbs radiation beyond the visible bands, the blue (1), green (2) and red (3) bands should be superimposed to detect patterns in water sediments. For recognizing urban features and vegetation types, the NIR band (4) should be included. It is strongly suggested to incorporate either of the two middle infrared bands (5 or 7) to discriminate between vegetation classes. Choosing any of the visible bands (1 or 2 or 3) plus the NIR band (4) plus either of the two middle infrared bands (5 or 7) will also be advantageous. However, selecting band combinations actually depends on the interpreter and his particular application (NOAA, 1984).

Table 2.9: TM band/color combinations

Blue	Green	Red	Composite	Possible Application
1	2	3	Normal Color	Water sediment patterns
2	3	4	Infrared Color	Urban features/Vegetation types
3	4	5	False Color	Urban features/Vegetation types
3	4	7	False Color	Urban features/Vegetation types
3	5	7	False Color	Vegetation enhancement
4	5	7	False Color	
1	4	7	False Color	

(from NOAA, 1984)

2.6 References

- Ahmad, S.B. and Lockwood, J.G. (1979) Albedo. *Progress in Physical Geography*, 3: 500-543.
- Australian Centre for Remote Sensing (2003) ACRES Facts. <<http://www.auslig.gov.au/acres/facts.htm>>, accessed on 1 Feb. 2003.
- Barton, C.V.M. (2001) A theoretical analysis of the influence of heterogeneity in chlorophyll distribution on leaf reflectance. *Tree Physiology*, 21 (12-13): 789-795.
- Bendor, E. and Banin, A. (1995) Near-infrared analysis as a rapid method to simultaneously evaluate several soil properties. *Soil Science Society of America Journal*, 59 (2): 364-372.
- Bowers, S.A. and Hanks, R.J. (1965) Reflection of radiant energy from soils. *Soil Science*, 100 (2): 130-138.
- CARSTAD (2004) Listing of Instruments Available for Airborne Remote Sensing. <<http://carstad.gsfc.nasa.gov/Topics/instrumentlist.htm>>, accessed on 21 Feb. 2005.
- CEOS (2003) Introduction to Remotely Sensed Data- Platforms and Sensor Systems. <<http://ceos.cnes.fr:8100/cdrom-00b2/ceos1/irsd/page/pss3.htm>>, accessed on 21 Feb. 2005.
- Curran, P.J. (1985) *Principles of Remote Sensing*, Longman Group Limited, New York.
- Doxaran, D., Froidefond, J.M., Lavender, S., and Castaing, P. (2002) Spectral signature of highly turbid waters- Application with SPOT data to quantify suspended particulate matter concentrations. *Remote Sensing of Environment*, 81 (1): 149-161.
- Goddard News (2001) Landsat-4 Decommissioned. <<http://www.gsfc.nasa.gov/gsfcc/news/071301/071301.htm#landsat>>, accessed on 1 Feb. 2003.
- Harrison, B.A. and Jupp, D.L.B. (1989) *Introduction to Remotely Sensed Data*, CSIRO Publications, Australia.
- Hoffer, R.M. (1978) Biological and physical considerations in applying computer-aided analysis techniques to remote sensor data. In *Remote Sensing, the Quantitative Approach* (P.H. Swain and S.M. Davis, Eds.), McGraw Hill, New York, pp. 227-289.
- Introduction to Remote Sensing* (1995) Paper for a seminar presented at the Department of Geodetic Engineering, University of the Philippines, Diliman, 20-31 March.

- Jensen, J.R. and Hodgson, M.E. (1983) Remote sensing brightness maps. *Photogrammetric Engineering and Remote Sensing*, 49: 93-102.
- Kauth, R.J. and Thomas, G.S. (1976) The tasseled cap- A graphic description of the spectral-temporal development of agricultural crops as seen by Landsat. In *Proceedings of the Symposium on Machine Processing of Remotely Sensed Data*, Purdue University, Indiana, pp. 4B.41-4B.51.
- Kerr, J.T. and Ostrovsky, M. (2003) From space to species: Ecological applications for remote sensing. *Trends in Ecology & Evolution*, 18 (6): 299-305.
- Lanjeri, S., Melia, J., and Segarra, D. (2001) A multi-temporal masking classification method for vineyard monitoring in central Spain. *International Journal of Remote Sensing*, 22 (16): 3167-3186.
- Lillesand, T.M. and Kiefer, R.W. (1994) *Remote Sensing and Image Interpretation, 3rd Edition*, John Wiley & Sons, Inc., U.S.A.
- McCarty, G.W., Reeves, J.B., Reeves, V.B., Follett, R.F., and Kimble, J.M. (2002) Mid-infrared and near-infrared diffuse reflectance spectroscopy for soil carbon measurement. *Soil Science Society of America Journal*, 66 (2): 640-646.
- NOAA (1984) Visual interpretation of TM band combinations being studied. *Landsat Data Users Notes*, no. 30.
- Obukhov, A.I. and Orlov, D.S. (1964) Spectral reflectivity of the major soil groups and possibility of using diffuse reflection in soil investigations. *Soviet Soil Science*, 1 (2): 174-184.
- Page, N.R. (1974) Estimation of organic matter in Atlantic coastal plain soils with a colour-difference meter. *Agronomy Journal*, 66: 652-653.
- Piech, K.R., Schott, J.R., and Stewart, K.M. (1978) The blue-to-green reflectance ratio and lake water quality. *Photogrammetric Engineering and Remote Sensing*, 44 (10): 1303-1310.
- Sanchez, J. and Canton, M.P. (1999) *Space Image Processing*, CRC Press LLC, Boca Raton, Florida.
- Satellite Signals (2004) List of Satellites in Geostationary Orbit. < <http://www.satsig.net/sslist.htm>>, accessed on 21 Feb. 2005.
- Steiner, D. (1970) Time dimension for crop surveys from space. *Photogrammetric Engineering*, 36 (2): 187-194.

Stoner, E.R. and Baumgardner, M.E. (1981) Characteristic variations in the reflectance of surface soils. *Soil Science Society of America Journal*, 45: 1161-1165.

U.S. Geological Survey (2003) USGS News. <http://www.usgs.gov/public/press/public_affairs/press_releases/pr1475m.html>, accessed on 1 Feb. 2003.

Vincent, R.K. (1973) An ERTS multispectral scanner experiment for mapping iron compounds. In *Proceedings of the 8th International Symposium on Remote Sensing of Environment*, University of Michigan, Ann Arbor, pp. 1239-1247.

Williams, A.P. and Hunt, E.R. (2002) Estimation of leafy spurge cover from hyperspectral imagery using mixture tuned matched filtering. *Remote Sensing of Environment*, 82 (2-3): 446-456.

Weisblatt, E.A., Zaitzeff, J.B., and Reeves, C.A. (1973) Classification of turbidity levels in the Texas marine coastal zone. In *Proceedings of the Symposium on Machine Processing of Remotely Sensed Data*, Purdue University, Indiana, pp. 3A.42-3A.59.

Wolfe, W.L. and Zissis, G.J. (1978) *The Infrared Handbook*, Office of Naval Research, Department of the Navy, Washington, DC.

Zeichen, M.M. and Robinson, I.S. (2004) Detection and monitoring of algal blooms using SeaWiFS imagery. *International Journal of Remote Sensing*, 25 (7-8): 1389-1395.

Chapter 3

Digital Image Processing

3.1 Image Rectification and Restoration

A raw satellite image cannot be processed immediately for classification. This is because it lacks the geometric integrity of a map. There are many sources of geometric distortions. Examples are the earth's rotation during image acquisition; the curvature of the earth; and differences in the altitude, attitude and velocity of the platform. To correct these errors, one technique is to determine the relationship between the geometrically distorted image and the reference, normally a map (Richards, 1986).

To fix this mathematical relationship, ground control points (GCPs) are chosen. GCPs are points that can be recognized easily both on the image and on the map. In addition, the actual geographic coordinates (Northing and Easting, or latitude and longitude) of these GCPs should be obtainable. Examples are road intersections, bends in rivers, and towers. The pixel address of the GCPs (by row and column coordinates, v and u respectively) and their actual geographic coordinates (x and y) are determined, and these groups of coordinates are related by least squares, a statistical technique (Lillesand and Kiefer, 1994). First, second, or third degree mapping polynomials are possible. The following, for instance, are two equations associated with a second degree polynomial.

$$u = a_0 + a_1x + a_2y + a_3xy + a_4x^2 + a_5y^2 \quad (3.1)$$

$$v = b_0 + b_1x + b_2y + b_3xy + b_4x^2 + b_5y^2 \quad (3.2)$$

When the coefficients a_i and b_i are computed using the GCPs, the location of any other point on the rectified image can be calculated (Richards, 1986).

After the locations of points are corrected, the problem of determining the DNs in the resulting raster or output matrix must be solved. There are three resampling techniques available. Nearest neighbor resampling assigns the DN of the pixel whose center is nearest to the raster cell in the rectified image. Bilinear interpolation method calculates a distance-weighted average of the DNs of the four nearest pixels. Cubic convolution utilizes 16 surrounding pixels using a more complex mathematical scheme (Lillesand and Kiefer, 1994).

3.2 Image Enhancement

Although the human mind is superior at interpreting the spatial characteristics of an image, it is poor at discriminating subtle spectral differences (i.e., color differences). An analyst, for example, knows that the very dark blue irregularly-shaped area in an infrared image is part of the ocean. But it is not immediately clear to him where shallow water is, where reflectance is a little bit higher. The purpose of image enhancement is to emphasize certain attributes of the image for improved visual interpretability.

There are three general enhancement techniques: contrast manipulation, spatial feature manipulation, and multi-image manipulation (Lillesand and Kiefer, 1994). There are innumerable methods under these categories that are available to the analyst. Only

one example for each category is presented here. The choice of method generally depends upon the purpose and oftentimes a matter of personal preference.

3.2.1 Contrast Manipulation

In contrast manipulation, the contrast in an image is increased by making the bright pixels brighter and the dark pixels darker. An example of a contrast manipulation technique is contrast stretching. Normally, the output device (e.g., color monitor) is capable of displaying 256 levels. However, the image data may consist of a smaller range of DN's. Figure 3.1(a) shows a histogram of a hypothetical gray scale or one-band satellite image. A histogram shows the distribution and frequencies of the DN's in an image. In this case, pixels only have DN's in the range 32 to 96. If we display this image as it is, only the gray levels from 32 to 96 will be used. We are not taking advantage of the full capability of the display device (Figure 3.1(a)).

We will have more contrast among the pixels if we avail of the full color range of our computer monitor (256 gray levels) by doing a linear stretch. Here, the lowest DN of the raw image, 32 here, will be assigned to the lowest DN possible in the display device (i.e., zero). The highest DN, 96 here, will be assigned to the highest DN possible (i.e., 255). The raw DN's in between will be stretched linearly. The result is an image with a better contrast than the one without the stretch (Figure 3.1(b)).

There are other stretches, like in Figure 3.1(c), which aims to emphasize certain features of the image. Here, the analyst is interested in the brighter pixels (48 to 96). In this case, pixels with DN's from 32 to 47 are virtually "washed away" from the image.

There are myriad of other special stretches designed for specific applications (ERDAS Field Guide, 1997). Examples are the histogram-equalized, Gaussian, standard deviation, and gamma stretches.

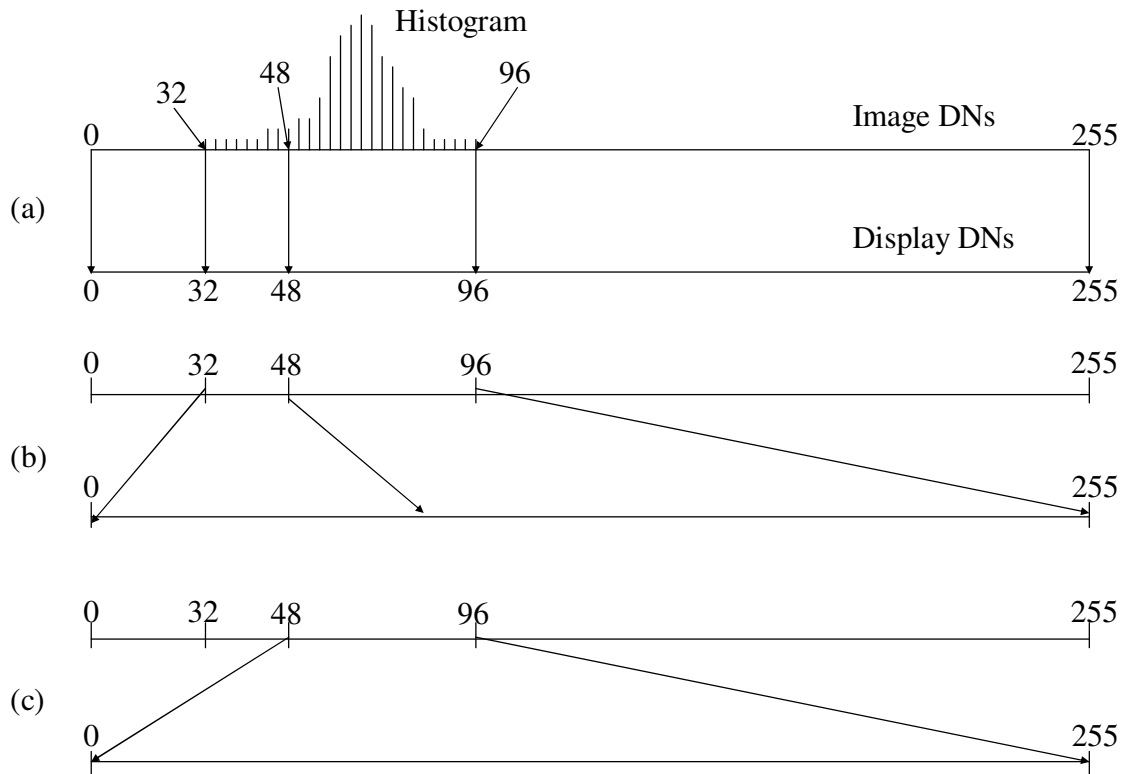


Figure 3.1: Principle of contrast stretch enhancement

3.2.2 Spatial Feature Manipulation

We apply spatial feature manipulation methods if we need to emphasize or deemphasize certain spatial features in our image. One technique is convolution. Unlike contrast stretching, the new DN in the enhanced image is affected by the DNs of the surrounding pixels. A moving window that holds an array of coefficients or weighting

factors is designated. Such arrays are called kernels. They are usually an odd number of pixels (e.g., 3 x 3, 5 x 5). This kernel is moved throughout the original image. Then, each coefficient in the kernel is multiplied by the corresponding DN in the original image. The sum of these products is the new DN at the center of the kernel in the enhanced (convoluted) image. The window is moved until all the pixels are considered, except at the edges where the original DNs are retained.

The convolution process in Figure 3.2 stresses the “smooth” areas in an image. Examples of these are extensive agricultural fields or deep water bodies where the gray levels gradually change over numerous pixels. Consequently, this process also deemphasizes the “rough” areas, for example, across roads, where gray levels vary abruptly over a few pixels. The effect of convolution is dependent upon the size of the kernel and the coefficients. In Figure 3.2, more smoothing will occur if the kernel is 5 x 5, rather than 3 x 3. The effect of applying the kernel in Figure 3.3 is to detect line features like roads and rivers (Richards, 1986).

1/9	1/9	1/9
1/9	1/9	1/9
1/9	1/9	1/9

(a) Kernel

29	29	30
30	31	32
29	29	31

(b) Original image DNs

	30	

(c) Convoluted image DN

$$\text{Convolution} = 1/9 (29) + 1/9 (29) + 1/9 (30) + 1/9 (30) + 1/9 (31) + 1/9 (32) + 1/9 (29) + 1/9 (29) + 1/9 (31) = 30$$

Figure 3.2: Concept of convolution

-1	0	+1
-1	0	+1
-1	0	+1

Figure 3.3: Kernel that detects vertical line features

3.2.3 Multi-image Manipulation

Multi-image manipulation considers pixels in other bands to compute for the new DNs in the enhanced image. For example, the tasseled cap transformation (Crist and Cicone, 1984) results in six components that are just linear combinations of the DNs in the raw bands of the raw TM image. Table 3.1 shows the transformation used in ERDAS Imagine 8.7 (ERDAS Field Guide, 1997). The “brightness” component displays the variation in the reflectance of soil. Orthogonal to the “brightness” component, the “greenness” component is highly related to the quantity of green vegetation. Moisture in the canopy and soil is accentuated by the “wetness” component. Less studied is the “haze” component which is named as such because of its large coefficient in the blue band. The “fifth” and the “sixth” components are created to complete the transformation.

3.3 Image Classification

The aim of image classification is to group all pixels in an image into categories, for example, land use or land cover classes. This is possible because each pixel exhibits a pattern of digital numbers (DNs) for the group of bands included in the classification. Let us use, for example, Landsat TM bands blue, green, red, and near infrared for

classification. A pixel may have a DN of 5 in the blue band, 11 in the green band, 7 in the red band, and 0 in the near infrared band. These DNs together (5, 11, 7, 0) compose the spectral pattern of that pixel. Each pixel has a pattern. All the pixels in one land cover category have similar patterns. Therefore, if we know the pattern of each land cover class, then we can allocate all the pixels in their respective land cover classes. This can be done automatically using standard statistical algorithms (Lillesand and Kiefer, 1994).

There are two general approaches to image classification. When the analyst has previous knowledge about the study area, he utilizes the supervised classification method. Otherwise, the unsupervised classification scheme is more appropriate (Richards, 1986).

Table 3.1: Tasseled cap transformation

Component	Transformed Digital Number
Brightness	0.3037 (Blue band) + 0.2793 (Green band) + 0.4743 (Red band) + 0.5585 (NIR band) + 0.5082 (MIR band 5) + 0.1863 (MIR band 7)
Greenness	- 0.2848 (Blue band) - 0.2435 (Green band) - 0.5436 (Red band) + 0.7243 (NIR band) + 0.0840 (MIR band 5) - 0.1800 (MIR band 7)
Wetness	0.1509 (Blue band) + 0.1973 (Green band) + 0.3279 (Red band) + 0.3406 (NIR band) - 0.7112 (MIR band 5) - 0.4572 (MIR band 7)
Haze	0.8832 (Blue band) - 0.0819 (Green band) - 0.4580 (Red band) - 0.0032 (NIR band) - 0.0563 (MIR band 5) + 0.0130 (MIR band 7)
Fifth	0.0573 (Blue band) - 0.0260 (Green band) + 0.0335 (Red band) - 0.1943 (NIR band) + 0.4766 (MIR band 5) - 0.8545 (MIR band 7)
Sixth	0.1238 (Blue band) - 0.9038 (Green band) + 0.4041 (Red band) + 0.0573 (NIR band) - 0.0261 (MIR band 5) + 0.0240 (MIR band 7)

(from ERDAS Field Guide, 1997)

3.3.1 Supervised Classification

There are three basic steps in supervised classification. These are the training, classification, and output stages. In the training stage, we find the pattern for each class and describe it using statistical descriptors. In the classification stage, each unknown pixel is classified to its most likely class. This is according to the decision rule established by the algorithm based on the statistical descriptors. The result, a land use or land cover map, for example, is then presented in the output stage.

3.3.1.1 Training Stage

In the training stage, we select pixels of known types to “train” our algorithm. These training pixels are just a small fraction of the image that we need to classify (e.g., 10%). A collection of pixels belonging to one class is called a training site or a training area. The statistical descriptors for each category are computed in different ways depending on the algorithm.

In Figure 3.4, these training pixels are plotted in a scatter diagram or scatter plot. They are plotted according to their digital numbers in Band 1 and Band 2. Although the pixels in one class do not have the same exact pattern (i.e., exactly the same DN for Band 1 and Band 2), they exhibit a natural centralizing tendency. This is apparent in the clustering of the pixels belonging to one class. Suppose we are using only these two bands for classification. Then the pattern for each pixel will consist only of two DNs, that for Band 1, and the other for Band 2. The patterns of all the pixels in one class are the

basis of the statistical descriptors for that class. Analysts generally employ more than two bands for classification, but the principle is the same.

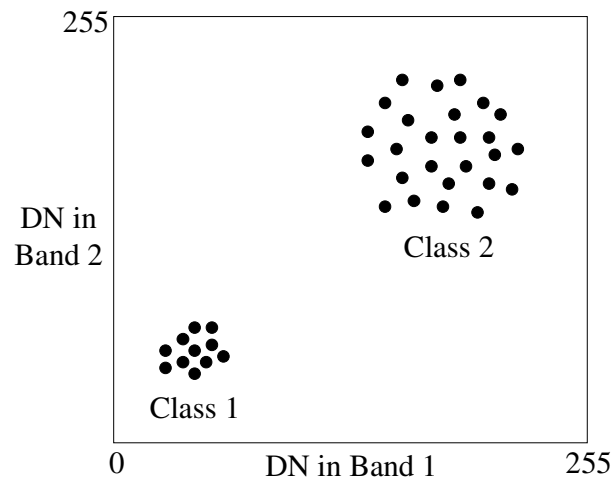


Figure 3.4: Pixel observations from training areas

Training pixels can be delineated interactively using a computer monitor and mouse. They are usually defined in the form of polygons. Frequently, image enhancement techniques are employed so that the analyst can distinguish clearly among the classes. Care must be taken so as not to get sample pixels from edges as this may not constitute one class. At this point, it is necessary to make a distinction between spectral class and information class. A group of pixels with very similar spectral response (i.e., similar patterns of DN's) belong to the same spectral class. An information class is what interests the analyst. This is a more meaningful class that is relevant to the analyst's particular application. For example, deep, clear water will appear dark blue in an infrared image, while turbid water will appear bright blue. This means that they have different sets

of DNs and therefore they are not in the same spectral class. The analyst, however, may not need to distinguish among water types. Instead, he just needs to delineate the water bodies in his study area. Therefore, he should use a training area in the turbid water class, and also in the deep, clear water class. Then he will just combine these two spectral classes into one information class (i.e., water) later. In short, he must take into account the spectral variability of the information class (Lillesand and Kiefer, 1994).

The following sections will discuss the three main statistical classifiers for supervised classification approach. These are the parallelepiped, minimum distance to means, and maximum likelihood classifiers.

3.3.1.2 Parallelepiped Classification

In the parallelepiped classification strategy (Figure 3.5), the classes are “enclosed” by a box or a parallelepiped in multidimensional space. The statistical descriptors are the two sets of digital numbers defining the classes (i.e., two DNs in Band 1, two DNs in Band 2). During classification, an unknown pixel will be associated with the parallelepiped where it falls.

This classifier is the simplest to apply, and requires less computing time. Hence, it is often utilized for a first pass, broad classification. It works for a non-normal distribution and takes into account the spread of the data. However, there may be overlaps and unclassified pixels since some pixels may not fall inside any of the parallelepipeds. The result may also be difficult to interpret (ERDAS Field Guide, 1997)

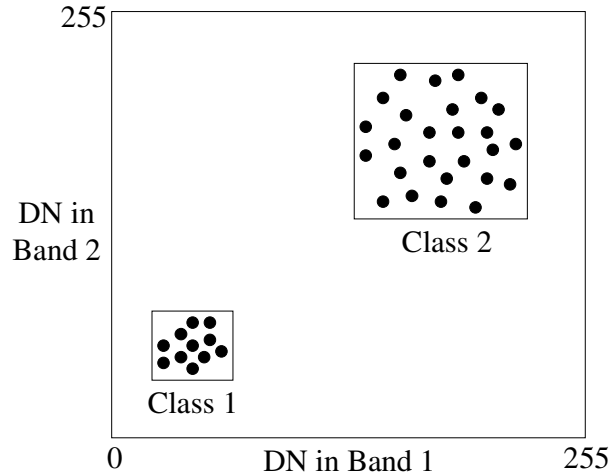


Figure 3.5: Parallelepiped classification scheme

3.3.1.3 Minimum Distance to Means Classification

The pattern that an individual pixel exhibits is associated with a pixel vector x in multi-spectral space. If K pixel vectors are plotted in space, the average location of these pixels is called the mean pixel vector m defined as

$$m = \frac{1}{K} \sum_{j=1}^K x_j \quad (3.3)$$

In the minimum distance to means classifier, the statistical descriptor for each class is its mean pixel vector. This is specified by the diamond mark in the center of every class (Figure 3.6). The Euclidean distance between the value of the unknown pixel and a class mean vector is computed. The unknown pixel is assigned to that class nearest to that pixel.

There are advantages to using this classifier. Except for parallelepiped, this has the fastest decision equations to compute. In this method, variability is not taken into account, which can present both advantages and drawbacks. Because of this characteristic, there are no unclassified pixels. However, an unknown pixel can be incorrectly assigned to a “nearer” class, but it may actually belong to a “farther” class that has a greater variability (ERDAS Field Guide, 1997). This is especially a problem with urban areas.

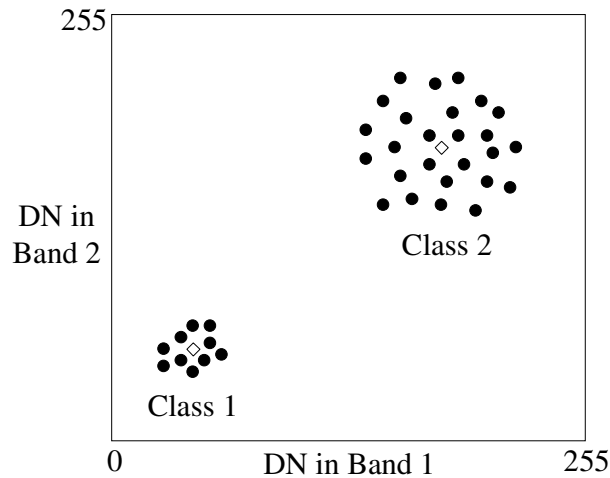


Figure 3.6: Minimum distance to means classification scheme

3.3.1.4 Maximum Likelihood Classification

This classifier not only considers the mean vector of the pixels in one class, but also takes into account the spread or variability of these pixels in multispectral space. This parameter is quantified by the covariance matrix C_x , defined as

$$C_x = \frac{1}{K-1} \sum_{j=1}^K (x_j - m)(x_j - m)^t \quad (3.4)$$

In the maximum likelihood classification, the mean vector and the covariance matrix are computed for each class. With these two parameters, we can calculate the statistical probability of a pixel x being a member of a specific land cover class ω_i . Simply,

$$x \in \omega_i \quad \text{if } g_i(x) > g_j(x) \quad \text{for all } j \neq i$$

which means that the pixel at vector location x belongs to class ω_i if the value of the discriminant function associated with class ω_i is greater than those of other classes. This function is defined as

$$g_i(x) = -\ln|C_i| - (x - m_i)^t C_i^{-1} (x - m_i) \quad (3.5)$$

If the pixels follow a normal or Gaussian distribution in multispectral space, then the maximum likelihood classifier is the most accurate because it considers the most variables in computation. It takes into account the variability of classes by utilizing the covariance matrix. However, if the pixels are characterized by non-normality, then this classifier will not work well. As the equation is extensive, the calculations will require more computing resources. Computation time is proportional to the number of input bands. This classifier also has a tendency to overclassify signatures with high values in the covariance matrix. This is true if there is a large dispersion of the pixels in the training set (ERDAS Field Guide, 1997).

3.3.1.5 The Jeffries-Matusita (J-M) Distance

There are separability measures that quantify how well we can separate spectral classes from each other. A spectral class is associated with a probability density function. The Jeffries-Matusita distance (Richards, 1986) between a pair (classes i and j) of probability density functions (associated with one band or several bands) for normally distributed classes is

$$J_{ij} = 2(1 - e^{-\alpha}) \quad (3.6)$$

where

$$\alpha = \frac{1}{8}(m_i - m_j)^t \left\{ \frac{C_i + C_j}{2} \right\}^{-1} (m_i - m_j) + \frac{1}{2} \ln \left\{ \frac{(C_i + C_j)^{1/2}}{|C_i|^{1/2} |C_j|^{1/2}} \right\} \quad (3.7)$$

The Jeffries-Matusita distance, also called the Bhattacharyya distance, is usually utilized to determine which band or combination of bands will give maximum separability. For example, we want to know which subset of bands from the six reflective bands of Landsat ETM+ will provide the highest separation between classes. Also, a project normally requires the separation of more than two spectral classes. In this case, all the pairwise J-M distances are calculated, and an average J-M distance can be determined. That subset of bands with the highest average J-M distance is usually chosen for classification. The selection may also be based on the best minimum J-M distance.

3.3.2 Unsupervised Classification

In unsupervised classification, there is no attempt to train the algorithm or to supervise the classification process. The algorithm will find the natural spectral groupings of pixels. As we have seen, these are called spectral classes or clusters. The number of clusters is specified by the analyst. After the clusters have been identified, the analyst will group these spectral classes into information classes. He may go to the field and determine the actual types of the spectral classes. He can also interpret aerial photographs or use other ancillary or reference data (Richards, 1986).

There are many clustering methods available. Here, we discuss only one example, the ISODATA (Iterative Self-Organizing Data Analysis Technique) (Richards, 1986). This clustering strategy categorizes pixels the same way the minimum distance to means classifier does. In Figure 3.7, nine pixels are plotted in a two-band scatter diagram. The analyst initially specifies two arbitrary clusters with centers at m_1 and m_2 . Then, the distance between a pixel and m_1 and m_2 will be computed. If it is nearer to m_1 , then the pixel is assigned to cluster 1. Otherwise, it is assigned to cluster 2. This will be done for all the other eight pixels. To determine the quality of the clustering procedure, the distances of the pixels to their respective mean vectors are squared and then added together. This summation is called the sum of squared error (SSE). If it is small, then the distances of pixels to mean vectors are small, and the clustering is judged favorably.

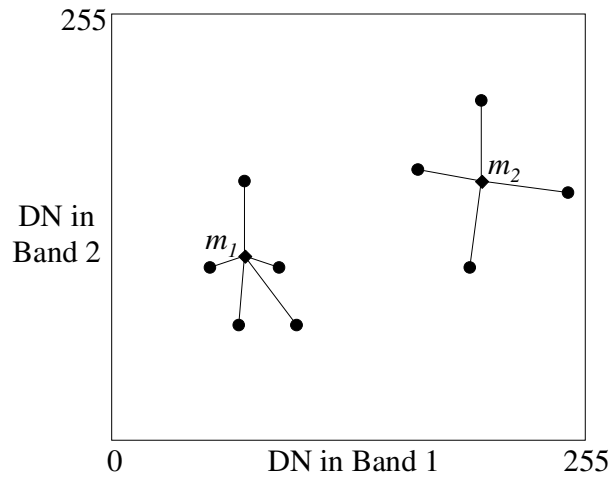
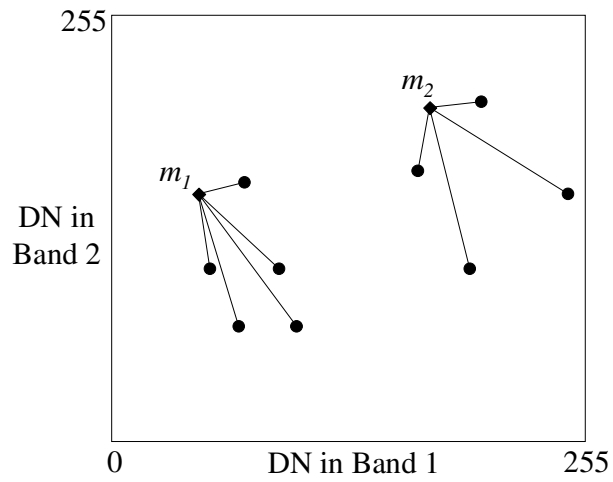
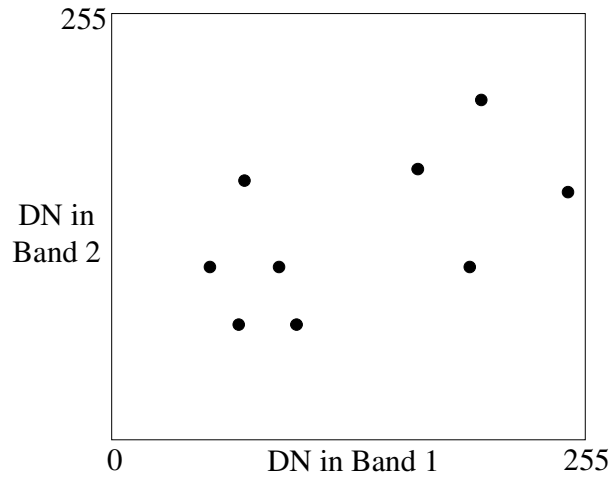


Figure 3.7: Clustering by the ISODATA method

Next, the mean vectors of cluster 1 and cluster 2 will be computed. So that now, the positions of m_1 and m_2 have migrated within these pixels. A new assignment will then occur based on these new mean vectors m_1 and m_2 . Again, the nine pixels will be assigned to the nearest candidate cluster. This procedure will be repeated until the predefined analyst-specified SSE has been reached.

This unsupervised classification strategy has advantages and drawbacks. Since it is iterative, clustering is not biased to the upper or lower pixels in the image. If the number of iterations is sufficient, then this procedure works well no matter where the initial cluster centers are located. The main drawback is the long computing time. Also, since it considers only the spectral characteristics of the pixels, spatial homogeneity is not considered (ERDAS Field Guide, 1997).

3.3.3 Accuracy Assessment

A prospective user of a map produced from satellite imagery usually needs to know about the quality of information shown by the map. Hence, a digital map generated from image processing techniques is evaluated for its accuracy. Accuracy assessment begins with acquiring or making a reference image. Compilation from various sources is not unusual for creating the reference image. Examples are aerial photographs or field work. The reference data are called ground truth. This reference image is then compared to the automatically classified image. Ideally, all the pixels in the image should be assessed (Janssen and Van der Wel, 1994). Most of the time, however, this is not possible because of cost or physical restraint.

The confusion matrix (also called error matrix or contingency table) (Lillesand and Kiefer, 1994) is the most widely used technique to assess the accuracy of a classified image. Although Foody (2002) identified some flaws in using the confusion matrix, such as problems with mixed pixels and image registration, the confusion matrix is still an acceptable measure to assess accuracy.

Figure 3.8 is a schematic representation of a confusion matrix (Foody, 2002). There are n randomly selected pixels involved. The known types (columns) are compared to the results of the classification (rows). The pixels that are correctly classified are located along the major diagonal of the matrix.

All non-diagonal elements of the matrix denote either errors of omission or commission. Nondiagonal column elements represent errors of omission. This means that a pixel has been omitted from its correct class. Conversely, an error of commission is done when a pixel is included in a class when it should not have been. These are represented by the nondiagonal row elements of the matrix.

Other metrics can be calculated from the confusion matrix. The overall accuracy is computed by dividing the total number of correctly classified pixels (i.e., the sum of the elements along the diagonal) by the total number of test pixels n . If we divide the number of correctly classified pixels in each class by the number of test pixels utilized in that class (the column total), the result is called the producer's accuracy. This parameter indicates how well test pixels of that particular category are classified. User's accuracies are similarly computed but using the number of pixels classified as belonging to that class (the row total). This value represents commission error. It is associated with the

probability that a pixel classified into a given class represents that class on the ground in reality (Story and Congalton, 1986). The kappa coefficient includes the effect of chance in the accuracy of the classification (Lillesand and Kiefer, 1994).

		Reference					Σ
		A	B	C	D		
Classification	A	n_{AA}	n_{AB}	n_{AC}	n_{AD}	n_{A+}	
	B	n_{BA}	n_{BB}	n_{BC}	n_{BD}	n_{B+}	
	C	n_{CA}	n_{CB}	n_{CC}	n_{CD}	n_{C+}	
	D	n_{DA}	n_{DB}	n_{DC}	n_{DD}	n_{D+}	
	Σ	n_{+A}	n_{+B}	n_{+C}	n_{+D}	n	

$$\text{Overall Accuracy} = \frac{\sum_{k=1}^q n_{kk}}{n}$$

$$\text{Producer's Accuracy} = \frac{n_{ii}}{n_{+i}}$$

$$\text{User's Accuracy} = \frac{n_{ii}}{n_{i+}}$$

$$\text{Kappa coefficient} = \frac{n \sum_{k=1}^q n_{kk} - \sum_{k=1}^q n_{k+} n_{+k}}{n^2 - \sum_{k=1}^q n_{k+} n_{+k}}$$

Figure 3.8: Confusion matrix (from Foody, 2002)

3.4 References

Crist, E.P. and Cicone, R.C. (1984) A physically-based transformation of Thematic Mapper data- The TM tasseled cap. *IEEE Transactions on Geoscience and Remote Sensing*, 22 (3): 256-263.

ERDAS Field Guide, 4th Edition (1997) Erdas, Inc., Atlanta, Georgia.

Foody, G.M. (2002) Status of land cover classification accuracy assessment. *Remote Sensing of Environment*, 80 (1): 185-201.

Janssen, L.L.F. and Van der Wel, F.J.M. (1994) Accuracy assessment of satellite derived land-cover data: A review. *Photogrammetric Engineering and Remote Sensing*, 60 (4): 419-426.

Lillesand, T.M. and Kiefer, R.W. (1994) *Remote Sensing and Image Interpretation, 3rd Edition*, John Wiley & Sons, Inc., U.S.A.

Richards, J.A. (1986) *Remote Sensing Digital Image Analysis: An Introduction*, Springer-Verlag, Germany.

Story, M. and Congalton, R.G. (1986) Accuracy assessment: A user's perspective. *Photogrammetric Engineering and Remote Sensing*, 52 (3): 397-399.

Chapter 4

Geographic Information Systems

4.1 Definitions

A geographic information system (GIS) can be regarded as a set of tools to analyze spatial data. By spatial, we mean the space around us, where we live and function (Clarke, 2001). Specifically, a GIS is an automated system that can capture, store, retrieve, analyze, and display spatial data (Clarke, 1995) from actual surroundings for a particular objective (Burrough, 1989).

A data layer portrays one theme (Figure 4.1). Entities such as points, lines, polygons, and surfaces are encoded on a data layer (Star and Estes, 1990). A stormwater runoff sampling station illustrates the concept of a point entity. A road is an example of a line entity. A land use category qualifies as a polygon entity. While elevation data can be regarded as a surface entity. These entities are associated with spatial data which are their location in a two-dimensional space. The spatial data of a point entity are its x and y coordinates. Entities also possess non-spatial features called attributes. For instance, for a point entity depicting a stormwater runoff sampling station, its attribute data can include its name, the sampling frequency, its associated land use type, and so on.

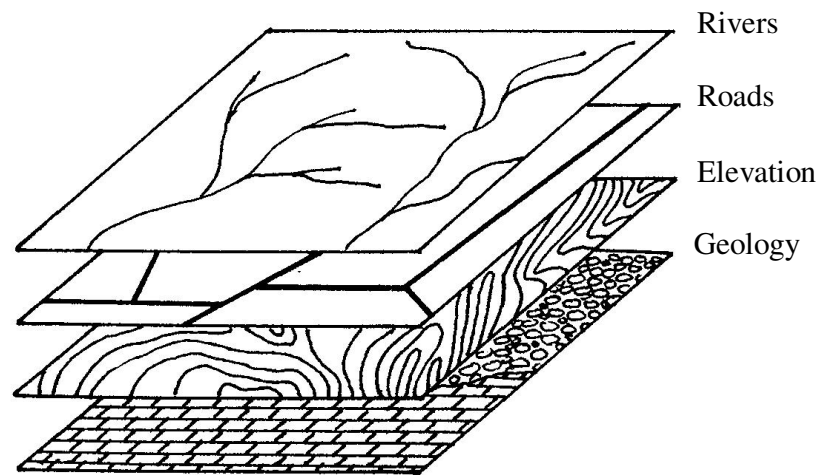


Figure 4.1: Examples of data layers in a GIS (from Abellera, 1997)

4.2 Data Structures

We can organize spatial and non-spatial information about these entities by means of a raster or a vector data structure (Star and Estes, 1990). In a raster structure, data are placed in a square or rectangular array which contains pixels or cells. A satellite image, for instance, has a raster structure. The resolution describes the quantitative relationship of the individual pixel, usually a square, to the ground surface it represents. Row and column coordinates mark the position of entities in the array. There is a way to relate these arbitrary locations to actual geographic coordinates like latitude and longitude, or Northing and Easting.

In a vector data structure, the location of entities is demarcated by x and y coordinates. These values can be true geographic positions or arbitrarily chosen (Figure 4.2). A pair of x and y coordinates is associated with a point. Several pairs of x and y

coordinates describe a line. A polygon is characterized by separate pairs of x and y coordinates, where the first pair is exactly the same as the last pair.

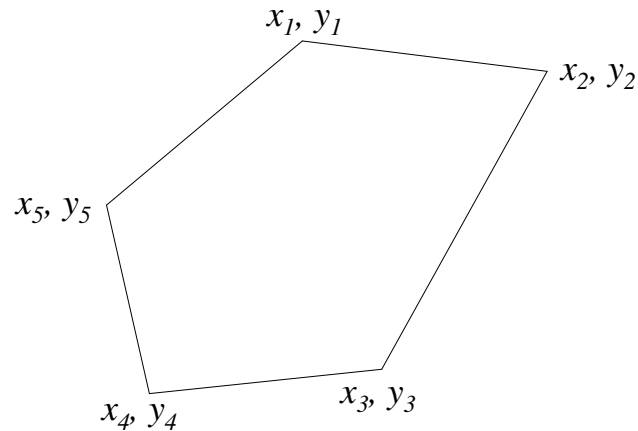


Figure 4.2: Vector data structure

Selection of data structure is contingent upon project objectives and application. Spatial analysis that requires overlay tasks can be easily handled with a raster structure because of its simple data organization. Raster structure is usually preferred, for example, for investigations involving remotely sensed images, but a great deal of storage space is sometimes necessary. Also, the resulting hard copy maps do not produce high quality graphics. Where precise locations are required, the vector structure is the more reasonable and suitable choice. Examples are in network analysis like utility mapping or transport connection. There is no requirement for large storage space due to the complex structure of vector-based systems. With this structure, accurate and attractive maps can be made (Burrough, 1989).

4.3 Data Conversion

Data conversion or preprocessing includes procedures to change data into a format that is suitable for a particular GIS project (Star and Estes, 1990). For instance, in a study involving a satellite image that requires overlaying with ancillary vector data, the vector data must be converted to its raster equivalent. This is demonstrated in Figure 4.3 where a vector line entity is merely overlain on the raster array. Pixels crossed by the line are assigned the attribute of that line.

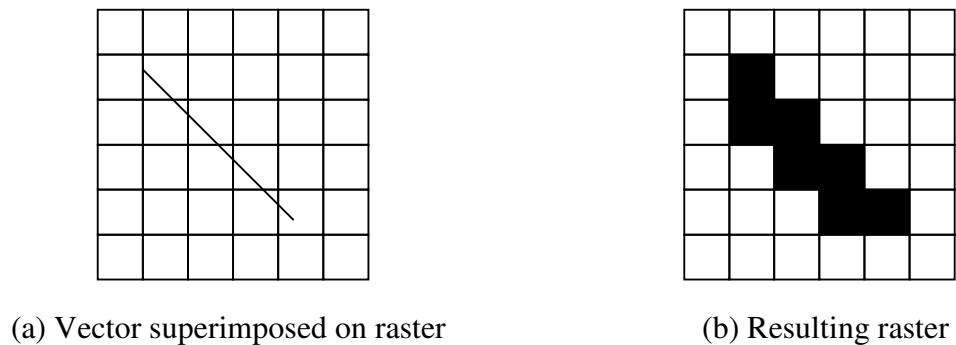


Figure 4.3: Vector to raster conversion of line entity

Format conversion procedures aim to transform material into a form that can be processed automatically. Digitizing is one way to convert analogue data to digital format by means of a digitizer (Figure 4.4). The graphic data is put on a surface that can be as small as one square foot or as large as 20 square feet. The analyst traces the features (point, line, polygon) using a cursor. When he clicks on it, the electronics in the digitizing tablet system changes the position of the cursor to a signal readable by the computer. The resulting data are in vector form.

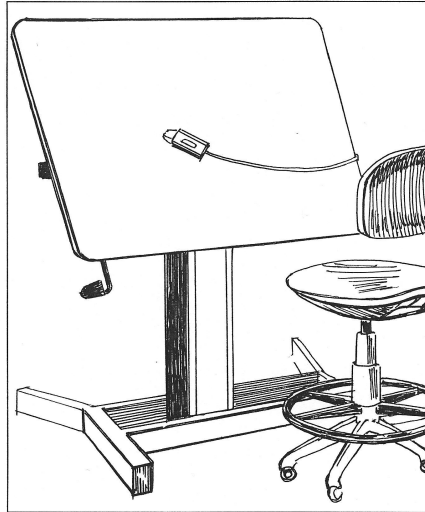


Figure 4.4: Digitizer (illustrated by Robustiano L. Abellera)

Figure 4.5 displays a scanner. Here, a map is passed through a system with units called charged coupled devices that detect reflected light emitted by the drawings. The reflected light in analog form is then converted to its digital counterpart. The output is a raster image that shows pixel values proportional to the reflectance of the map features.

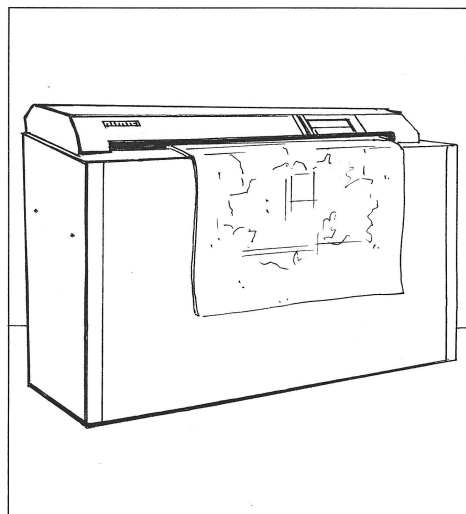


Figure 4.5: Scanner (illustrated by Robustiano L. Abellera)

4.4 Spatial Manipulation and Analysis

The real strength of GIS is its ability to perform spatial manipulation and analysis. The geographic properties of size, shape, scale, distribution, pattern contiguity, neighborhood, and orientation can be used to find the relationships among geographic features (Clarke, 2001). The following sections describe some of GIS's capabilities (Star and Estes, 1990).

4.4.1 Reclassification

Oftentimes, the original data are not relevant to the GIS analyst. It may be necessary to reclassify data so that information is suitable for a particular application. For example, land use data from public records may be too specific to be used for stormwater management applications. Hence, some classes have to be aggregated into categories relevant for stormwater modeling.

When dealing with many data layers, the overlay procedure is generally utilized. Addition, subtraction, multiplication, division, and other mathematical or statistical relationships can be applied to pixels in corresponding positions or globally in order to obtain the required conditions. In this case, we have reclassified and combined layers into a single layer that is relevant to our objectives. It is more direct to do this in raster than in vector data layer due to the one-to-one pixel correspondence in raster format.

4.4.2 Interpolation

Geographic data are usually measured only at some locations. Physical restraints or cost oftentimes make observations at many positions difficult or even impossible. When represented in a GIS layer, these values present an irregular pattern. Rainfall and elevation are some examples. It may be necessary to know the values at points where observations are not taken. The surface describing the geographic data can even be utilized for spatial modeling. Several techniques for interpolating, like kriging, have been well-studied. The fundamental concept is that the effect of neighboring data points on an unknown point is more than the effect of points that are farther away.

4.4.3 Connectivity Operations

In proximity or buffer procedures, areas adjacent to specific conditions or activities are delineated. These areas of interest are called buffer zones. This concept is also applicable to locations that should be avoided. These GIS operations are particularly applicable in site selection projects. For instance, planning for the construction of a landfill involves the identification of locations near major roads, but relatively far from residential areas. In this case, the roads are represented by one data layer, and residential areas are depicted by another data layer. After the buffer zones have been mapped, the two layers are overlain to show locations satisfying the two criteria.

4.4.4 Neighborhood Operations

Convolution, discussed in Chapter 3, is a technique based on the original values of neighboring pixels. The first kernel discussed in that chapter is also called a low pass filter. In GIS, it is generally applied to remove or reduce noise in the data layer. In processing satellite images, classified data usually show a salt and pepper appearance. The low pass filter can be used to remove these speckles. A tool that can also perform a similar task is the majority filter (Figure 4.6). Here, a kernel is superimposed on each pixel in the original image. The kernel can be of different sizes (e.g., 3 x 3, 5 x 5). The majority value in that window is determined. This majority value replaces the value in the original image. Figure 4.7 is an example of applying a 3 x 3 majority filter.

4.4.5 Measurement

Computation of distances, areas, volumes, direction and other quantities is a straightforward procedure in GIS. For example, calculation of areas of polygons in a raster layer is a direct operation if the pixel resolution is given. Open land, for example, is composed of 1,000 pixels in an image. These pixels represent 90 hectares on the earth's surface if the pixel resolution is 30 meters. We can also count specific objects in a particular region. For example, we can count the number of vegetation pixels in a training area designated as single-family residential area.

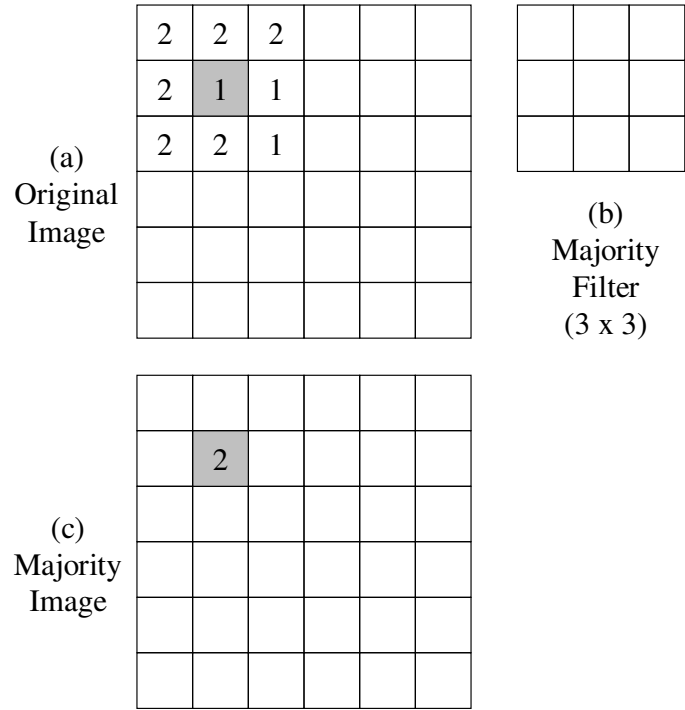


Figure 4.6: Creating a majority image

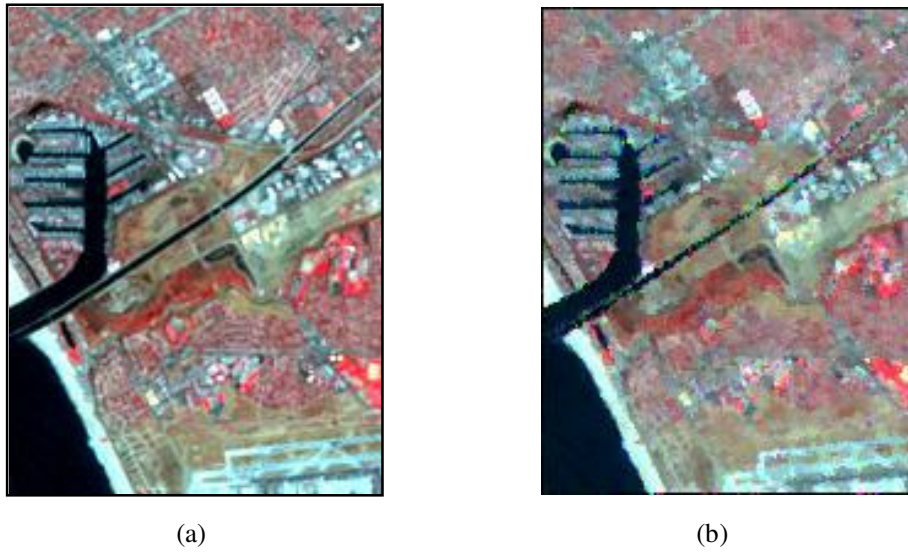


Figure 4.7: Original image (a), and image (b) resulting from the application of a 3 x 3 majority filter

4.4.6 Statistical Analysis

Basic and sometimes sophisticated statistical procedures are available in GIS. Descriptive statistics like the mean, median, and variance of the values in a class or data layer can be calculated. In addition, histograms can be displayed on a table or graphically. The histogram of a dataset shows how the values are divided into classes. We can determine, for example, how many pixels have been classified into the single-family residential category. We can also compare pixels in their corresponding locations. In correlation, we try to see if the value of pixels in one image will predict the values of corresponding pixels in another image. If they do, the two images have high correlation. In cross-tabulations, attribute values are compared one by one. Assembling the error matrix involves a cross-tabulation procedure.

4.5 References

Abellera, L.V. (1997) *Mapping Philippine Tarsier Habitat Using Image Processing (IP) and Geographic Information Systems (GIS) Techniques*, Master's Thesis, University of the Philippines, Diliman, Quezon City, Philippines.

Burrough, P.A. (1989) *Principles of Geographical Information Systems*, Oxford University Press, New York.

Clarke, K.C. (1995) *Analytical and Computer Cartography, 2nd Edition*, Prentice-Hall, Inc., Upper Saddle River, New Jersey.

Clarke, K.C. (2001) *Getting Started with Geographic Information Systems, 3rd Edition*, Prentice-Hall, Inc., Upper Saddle River, New Jersey.

Star, J. and Estes, J. (1990) *Geographic Information Systems: An Introduction*, Prentice-Hall, Inc. A Division of Simon and Schuster, New Jersey.

Chapter 5

Knowledge-Based Classification

5.1 Definitions

A knowledge-based system performs a task by applying rules of thumb, called heuristics, to a symbolic representation of knowledge, instead of using mostly statistical (e.g., maximum likelihood) or algorithmic (e.g., artificial neural network) methods. A knowledge-based system is sometimes regarded to be synonymous to an expert system, but the former, strictly speaking, is more general (Jackson, 1999). Also using heuristics and symbolic logic, an expert system is a computer program that applies human knowledge in a particular area of expertise to solve problems or give advice (Awad, 1996; Jackson, 1999). Both are fields in artificial intelligence.

In remote sensing, knowledge-based classification specifically refers to techniques where thematic or geometric data are included in the classification process. This is done when it is difficult or insufficient to recognize classes only on the basis of spectral characteristics. It is knowledge-based because this approach must acquire knowledge about the relationships between classes and the various ancillary sources (Skidmore, 1989). If there is no definite association between classes and ancillary data, then a knowledge-based approach will not work (Middelkoop and Janssen, 1991). An

artificial neural network, for example, is not knowledge-based because it is a black box and cannot explain the correlation between classes and ancillary data.

In a knowledge-based system, representation of knowledge is explicit. This provides benefits because artificial expertise is stable, consistent, and inexpensive. It can also be transferred and documented without difficulty. In contrast, human expertise is changeable and costly. It is likely to be lost. It is also hard to transfer and document. (Waterman, 1986). Goodenough (1986) lists further advantages of explicit knowledge. It can be utilized to record generalizations permanently. It can be easily changed to rectify mistakes or to adopt another point of view. It can be used in myriad of situations even if it is not complete or absolutely correct. However, knowledge-based systems require specific instructions and do not have the inspiration of human experts (Awad, 1996).

5.2 Components of a Knowledge-Based System

A knowledge-based system has four components: knowledge base, inference engine, justifier/scheduler, and user interface (Awad, 1996). The knowledge base is the heart of a knowledge-based system. It is a collection of facts, rules, and procedures arranged into models. Knowledge can be acquired from GIS layers (e.g., digital elevation model, geology, hydrology), analogue or paper maps, or socioeconomic data in tabular or digital form. There is also the written literature. Experts can be interviewed. Field work can be carried out. The knowledge engineer translates the knowledge into a format that can be understood and manipulated in the computer. As the knowledge acquisition is a difficult and time-consuming stage, there is a tendency to automate the knowledge-

acquisition process (Huang and Jensen, 1997) especially with the accessibility of GIS layers in the internet.

The inference engine is the brain of a knowledge-based system. Here, rules are examined and combined with new facts in the knowledge base to generate inferences and produce solutions. The justifier explains the line of reasoning of the system to the user. The scheduler (also called rule interpreter) is that element of the inference engine which coordinates and controls the sequencing of the rules. The user interface facilitates communication between the system and its user. Everything that a user sees and interacts with on the computer screen is associated with the user interface.

A knowledge-based system can be constructed using any standard programming language. However, there are special commercial software packages called shells which can be immediately used without programming (Awad, 1996). A shell is a complete knowledge-based system that lacks knowledge. The user provides the knowledge, and the system instantly becomes operational.

Once an assembly of knowledge has been acquired, the next step is to find ways to represent it. Knowledge representation is a collection of facts, rules, or procedures portrayed in a knowledge base (Awad, 1996). Common strategies for representing knowledge include rules, semantic nets, frames, and decision trees. A rule (also called production rule) is a provisional statement that instigates an action if a particular condition is true. This is expressed as an “IF (premise)... THEN (conclusion)” statement. One example is “If the digital number in the near infrared band is less than 32,

then assign the pixel to the water category.” A knowledge-based system based on production rules is called a rule-based system.

A semantic network or net provides a graphical method to portray descriptive or declarative knowledge. The net describes the associations that relate objects, called nodes. Each node represents a fact or idea. Arcs are lines that connect the nodes to show their relationship. Nodes and arcs together form a semantic net. In short, a semantic network is just a network of concepts and relationships. Figure 5.1 is an example of a semantic network.

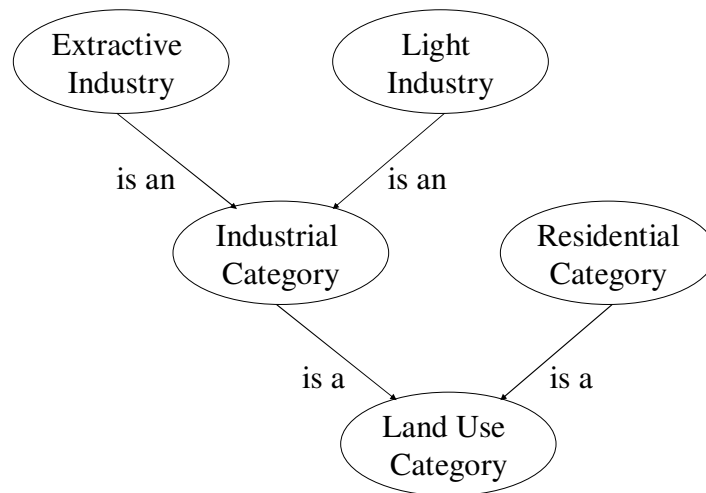


Figure 5.1: An example of a semantic net

A frame organizes knowledge through past experience. It combines declarative and operational knowledge. The two elements of a frame are the slot and the facet. A slot is a certain object being described or a property of an entity (light industrial in Table 5.1). A facet (e.g., 107 hectares) is a value of a slot (e.g., area). When all slots are occupied with values, an instance of a frame is generated or instantiated.

Table 5.1: An example of a frame

Object: Light Industrial	
<i>Slot</i>	<i>Facet</i>
Area	107 hectares
Impervious Surface Area	91%
Runoff Coefficient	0.74

A decision tree is a hierarchically organized semantic network. It consists of nodes depicting goals and links that designate decisions or outcomes. In Figure 5.2, a pixel is subjected to the first condition. If condition 1 is satisfied, then the pixel is assigned to class 1. Otherwise, the pixel is examined for condition 2. If that condition is true, then the pixel is tested for another condition. This procedure continues until the pixel has been assigned a class.

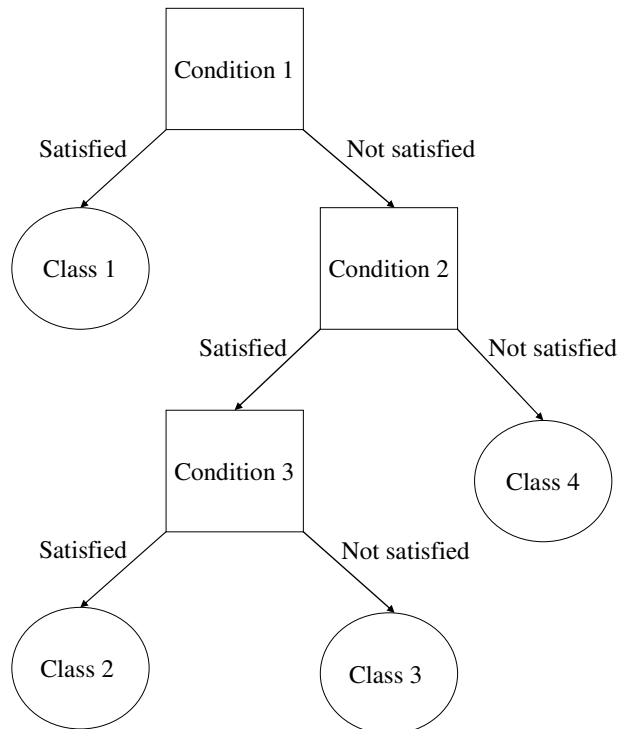


Figure 5.2: An example of a decision tree

5.3 Knowledge Acquisition

One of the issues in building a knowledge-based system is in knowledge acquisition. The common method of obtaining knowledge to build a knowledge base involves human experts and knowledge engineers. Bratko *et al.* (1989) identifies reasons why this is an arduous task. First, it takes a long period of time to engage the expert and the knowledge engineer. Second, experts find it hard to phrase precisely their knowledge in a form compatible to a computer application. For knowledge to be useful, it must be correct, unambiguous, and complete. Several remote sensing practitioners have expressed dismay because of the difficulties encountered in building knowledge bases (Argialas and Harlow, 1990; Kontoes *et al.*, 1993).

Because of this, there is a tendency in the artificial intelligence community to automate the knowledge-acquisition process. This is a field called machine learning. However, the application is not usually in remote sensing image analysis combined with GIS data. Two of the few who tried machine learning are Huang and Jensen (1997). They attempted to automate the knowledge acquisition process by using the GIS layers of soil, slope, digital elevation model, and texture. They used the inductive learning algorithm called C4.5. They found that the automatically generated production rules are of good quality but not significantly better than those acquired by conventional methods.

5.4 Knowledge Representation

After knowledge is obtained, the knowledge engineer decides how to represent them. Production rules are widely employed for knowledge representation. Investigations

made by Nazif and Levine (1984), Wharton (1987), and Ton *et al.* (1991) are just some of them. This is because rules are easy to understand. It is also easy to document an expert's experience and wisdom. Adding, removing, or changing a module does not affect other modules in the system. This characteristic is called modularity. Rule-based systems are also flexible. However, rules are expressed at a fine level of detail, and therefore may be difficult to form. Also, only limited knowledge per rule can be made (Awad, 1996). Rules are usually transformed into a decision tree.

Some researchers like Niemann *et al.* (1990), Liedtke *et al.* (1997) and Tonjes *et al.* (1999) preferred to use semantic nets for their application. This method has many advantages. It is characterized by deductive reasoning. This is associated with the concept of inheritance, where instances in one category are assumed to have all the characteristics of the more general categories of which they are members. The semantic net shows meaningful associations definitely and evidently. The hierarchy of relationships is followed without difficulty. It is flexible because new nodes can be added to a definition when necessary. There are drawbacks, however. First, it is an incomplete knowledge representation. It does not support operational knowledge. The net may be manipulated to produce invalid inferences. The definition of a node may be misleading. There are no standards that exist about the definition of nodes. Lastly, procedural knowledge may be difficult to represent as sequence and time are not obviously depicted (Awad, 1996).

Frames have been used by McKeown (1987) and Wu *et al.* (1988). This strategy has been employed because it provides invariable representation schemes and combines declarative and operational knowledge. It is concerned with hierarchical knowledge and

is characterized by modularity. It explicates inferences and identifies missing values. However, because of its higher level of complexity, it is slower than the other methods. Furthermore, it makes inference and explanation difficult (Awad, 1996).

There are efforts to implement uncertain knowledge by using certainty factors (Desachy *et al.*, 1988), the Dempster-Shafer theory (Shrinivasan and Richards, 1990), and even a neural network (Hepner *et al.*, 1990). Alternative representations are also suggested for a specific application. Middelkoop and Janssen (1991), for example, found that Markov chains and probabilistic transition matrices were the most appropriate representation schemes for their study involving temporal relationships.

Others devise representation methods that address the issues of data format, data accuracy, and system communication in a knowledge-based system integrating remote sensing data and GIS (Wang, 1991). Since remote sensing data are raster-based, and GIS data may be vector-based, format conversion may be necessary. Conversion between these two structures can produce positional errors and may take a long time. Also, accuracy assessment is performed by means of the confusion matrix for remote sensing data, while GIS operators utilize error models to assess their quality. These methods are incompatible. Finally, there is a semantic mismatch in communication between an expert system and a GIS database. To alleviate some of these problems, Wang (1991) has proposed three new techniques: relational-linear quadtree, fuzzy representation method, and communication subschema.

5.5 Approaches to Knowledge-Based Classification

There are two general approaches in implementing knowledge-based classification systems. These are evidential and hierarchical approaches. In evidential methods, measures of the relative mass of evidence are acquired to support opposing hypotheses (Goldberg *et al.*, 1985; Lee *et al.*, 1987). The hypothesis (e.g., land-cover class assignment) with the highest evidence mass is chosen. Hierarchical techniques, on the other hand (e.g., decision tree) eliminate alternative hypotheses during inference until only one hypothesis is left. Conceptually, categories are represented as leaves of bi- or multinary trees, with decision rules applied at each node to stop or continue on a decision course (Swain and Hauska, 1977; Ferrante *et al.*, 1984). Usually, a study will take one approach and not the other. However, Bolstad and Lillesand (1992) were able to combine both evidential and hierarchical strategies in their study involving a Landsat TM image, and GIS layers of soil texture, and topographic position.

Knowledge-based systems especially work well with the incorporation of ancillary data, particularly when they are in GIS format. McKeown (1987) developed an entirely integrated knowledge-based/GIS system (called MAPS) that merge remote sensing imagery, GIS data (e.g., terrain), and other non-map information (e.g., three-dimensional features like bridges and buildings). It was a big, complex system that tried to solve deficiencies in user interfaces, data representation, and its utilization. Goodenough *et al.* (1987) developed a similar system called the Analyst Advisor and the Map Image Congruency Evaluation (MICE) advisor. Others use ancillary/GIS data for specific purposes. For example, Middelkoop and Janssen (1991) constructed their

knowledge base from temporal relationships between classes and ancillary data. They gained knowledge about crop rotations. While Swain (1978), and Strahler (1980) worked on multi-season images.

Rules have been developed based on the spatial characteristics of an image. Researchers have segmented an image and calculated spatial attributes on the segments. Common attributes are area, perimeter, compactness ($\text{area}/\text{perimeter}^2$), degree of texture (roughness or smoothness), and minimum bounding rectangle (Gonzalez and Wintz, 1987; Patterson, 1990). Many studies have incorporated spatial information this way (Nagao and Matsuyama, 1980; Goodenough *et al.*, 1987; Civco, 1989; Mehldau and Schowengerdt, 1990; Johnsson, 1994). A few researchers try to get more information just from the spectral characteristics of the image. Wharton (1987), for example, built knowledge based on color and contrast of a high-resolution (5 meter) image. The rules were assembled from visual interpretation of the Thematic Mapper Simulator data. However, his method did not work well for a 30-meter resolution Landsat TM data. He concluded that the method was sensitive to the purity or homogeneity of the pixel. Another group of scientists, Ferrante *et al.* (1984) developed the multispectral image analysis system (MSIAS). This system incorporated rules on the basis of the appearance of surface features as viewed by a specific sensor under certain imaging conditions. The system did not work well because the rule-based configuration cannot recover from decision errors. Also, the spectral characteristics of neighboring pixels were not taken into account. This implies that knowledge-based systems are not especially applicable where only spectral information is considered.

5.6 References

- Argialas, D. and Harlow, C. (1990) Computational image interpretation models: An overview and perspective. *Photogrammetric Engineering and Remote Sensing*, 56 (6): 871-886.
- Awad, E.M. (1996) *Building Expert Systems: Principles, Procedures, and Applications*, West Publishing Company, St. Paul, Minnesota.
- Bolstad, P.V. and Lillesand, T.M. (1992) Rule-based classification models: Flexible integration of satellite imagery and thematic spatial data. *Photogrammetric Engineering and Remote Sensing*, 58 (7): 965-971.
- Bratko, I., Kononenko, I., Lavrac, N., Mozetic, I., and Roskar, E. (1989) Automatic synthesis of knowledge: Ljubljana research. In *Machine and Human Learning* (Y. Kodratoff and A. Hutchinson, Eds.), GP Publishing, Inc., Columbia, Maryland, pp. 25-33.
- Civco, D. (1989) Knowledge-based land use and land cover mapping. In *Proceedings ASPRS/ACSM Annual Convention, 2-7 April, Baltimore*, pp. 276-289.
- Desachy, J., Debord, P., and Castan, S. (1988) An expert system for satellite image interpretation and GIS based on problem solving. In *ISPRS Proceedings, Kyoto, Comm. 4/5, Vol 27, B4*.
- Ferrante, R.D., Carlotto, M.J., Pomarede, J., and Baim, P.W. (1984) Multi-spectral image analysis system. In *Proceedings of the 1st Conference on Artificial Intelligence Applications*, pp. 357-363.
- Goldberg, M., Goodenough, D.G., Alvo, M., and Karma, G.M. (1985) A hierarchical expert system for updating forestry maps with Landsat data. In *Proceedings IEEE*, Vol. 73, pp. 1054-1063.
- Gonzalez, R. and Wintz, P. (1987) *Digital Image Processing, 2nd Edition*, Addison-Wesley, Reading, Massachusetts.
- Goodenough, D.G. (1986) A hierarchical expert system. Presentation made to NASA/GSFC, May 1.
- Goodenough, D., Goldberg, M., Plunkett, G., and Zelek, J. (1987) An expert system for remote sensing. *IEEE Transactions on Geoscience and Remote Sensing*, GE-25 (3): 349-359.

- Hepner, G.F., Logan, T., Ritter, N., and Bryant, N. (1990) Artificial neural network classification using a minimal training set: Comparison to conventional supervised classification. *Photogrammetric Engineering and Remote Sensing*, 56 (4): 469-473.
- Huang, X. and Jensen, J.R. (1997) A machine-learning approach to automated knowledge-base building for remote sensing image analysis with GIS data. *Photogrammetric Engineering and Remote Sensing*, 63 (10): 1185-1194.
- Jackson, P. (1999) *Introduction to Expert Systems, 3rd Edition*, Addison-Wesley, U.S.A.
- Johnsson, K. (1994) Segment-based land-use classification from SPOT satellite data. *Photogrammetric Engineering and Remote Sensing*, 60 (1): 47-53.
- Kontoes, C., Wilkinson, G., Burrill, A., Goffredo, S., and Megier, J. (1993) An experimental system from the integration of GIS data in knowledge-based image analysis for remote sensing of agriculture. *International Journal of Geographical Information Systems*, 7 (3): 247-262.
- Lee, T., Richards, J.A., and Swain, P.H. (1987) Probabilistic and evidential approaches for multisource data analysis. *IEEE Transactions on Geoscience and Remote Sensing*, GE-25 (3): 283-293.
- Liedtke, C.E., Buckner, J., Grau, O., Grove, S., and Tonjes, R. (1997) AIDA: A system for the knowledge based interpretation of remote sensing data. In *Proceedings of the 3rd International Airborne Remote Sensing Conference and Exhibition*, July, Copenhagen, Denmark, pp. 313-320.
- McKeown, D.M. (1987) The role of artificial intelligence in the integration of remotely sensed data with geographic information systems. *IEEE Transactions on Geoscience and Remote Sensing*, GE-25: 330-348.
- Mehldau, G. and Schowengerdt, R. (1990) A C-extension for rule-based image classification systems. *Photogrammetric Engineering and Remote Sensing*, 56 (6) 887-892.
- Middelkoop, H. and Janssen, L.L.F. (1991) Implementation of temporal relationships in knowledge based classification of satellite images. *Photogrammetric Engineering and Remote Sensing*, 57 (7): 937-945.
- Nagao, M. and Matsuyama, T. (1980) *A Structural Analysis of Complex Aerial Photographs*, Plenum Press, New York.
- Nazif, A.M. and Levine, M.D. (1984) Low level image segmentation: An expert system. *IEEE Transactions on Pattern Analysis and Machine Intelligence*, PAMI-6: 555-577.

- Niemann, H., Sagerer, G., Schroder, S., and Kummert, F. (1990) ERNEST: A semantic network system for pattern understanding. *IEEE Transactions on Pattern Analysis and Machine Intelligence*, 12 (9): 883-905.
- Patterson, D. (1990) *Introduction to Artificial Intelligence and Expert Systems*, Prentice Hall International, New Jersey.
- Shrinivasan, A. and Richards, J.A. (1990) Knowledge-based techniques for multi-source classification. *International Journal of Remote Sensing*, 11 (3): 505-525.
- Skidmore, A.K. (1989) An expert system classifies eucalypt forest types using Thematic Mapper data and a digital terrain model. *Photogrammetric Engineering and Remote Sensing*, 55 (1): 133-146.
- Strahler, A.H. (1980) The use of prior probabilities in maximum likelihood classification of remotely sensed data. *Remote Sensing of Environment*, 10: 135-163.
- Swain, P.H. (1978) Bayesian classification in a time-varying environment. *IEEE Transactions on Systems, Man and Cybernetics*, SMC-8 (12): 879-883.
- Swain, P.H. and Hauska, H. (1977) Decision tree classifier: Design and potential. *IEEE Transactions on Geoscience and Remote Sensing*, 15 (3): 142-147.
- Ton, J., Sticklen, J., and Jain, A.K. (1991) Knowledge-based segmentation of Landsat images. *IEEE Transactions on Geoscience and Remote Sensing*, 29: 222-232
- Tonjes, R., Growe, S., Buckner, J., and Liedtke, C.E. (1999) Knowledge-based interpretation of remote sensing images using semantic nets. *Photogrammetric Engineering and Remote Sensing*, 65 (7): 811-821.
- Wang, F. (1991) Integrating GIS's and remote sensing image analysis systems by unifying knowledge representation schemes. *IEEE Transactions on Geoscience and Remote Sensing*, 29 (4): 656-664.
- Waterman, D.A. (1986) *A Guide to Expert Systems*, Addison-Wesley, Reading, Massachusetts.
- Wharton, S.W. (1987) A spectral knowledge-based approach for urban land-cover discrimination. *IEEE Transactions on Geoscience and Remote Sensing*, GE-25: 272-282.
- Wu, J.K., Cheng, D.S., Wang, W.T., and Cai, D.L. (1988) Model based remotely sensed imagery interpretation. *International Journal of Remote Sensing*, 9 (8): 1347-1356.

Chapter 6

Application of Satellite Data for Stormwater Modeling

6.1 Introduction

Stormwater models are used to quantify and hopefully solve environmental problems associated with runoff. A stormwater model simulates the motion of stormwater and transported materials through a drainage basin (Nix, 1994). Stormwater runoff is an environmental system that is not well-understood. Numerous factors influence runoff. Examples are topography, precipitation characteristics, and human activities. Because of this, data input and parameter acquisition is a tedious and time-consuming process in stormwater modeling.

Hydrologic variables for stormwater modeling are usually obtained through traditional methodologies such as stream gauging, field surveys, and aerial photo-interpretation. With the advent of space technologies, satellite data have become a more convenient alternative to these customary procedures. The most common hydrologic variables derived from satellite data are land use/land cover, imperviousness, and elevation. Other parameters include rainfall, snow cover, and soil types. There are many advantages to using satellite data. They are generally less costly and quicker to acquire and interpret than aerial photographs. They also cover extensive areas. Because satellite

imagery is captured regularly, the same area can be observed over time. Almost all parts of the world are covered by satellites in many resolutions (e.g., 20 meters for SPOT, 30 meters for Landsat) and in several operating modes (e.g., Synthetic Aperture Radar, Thematic Mapper). Furthermore, the satellite imagery's digital format can be directly studied with innumerable image processing programs. The processed image can also be incorporated in a geographic database. Moreover, the raster-based format satellite data are compatible with GIS-based hydrologic modeling software packages.

There are three watershed scales in stormwater modeling according to Schultz (1994). Micro-scale ranges from 1 sq cm to 1 sq km of watershed area. Meso-scale ranges from 1 sq km to 100,000 sq km, while macro-scale varies from 100,000 sq km up to global scale. Because of their spatial resolution, satellite data and Geographic Information Systems (GIS) techniques are specifically appropriate for meso-scale modeling. In general, rivers drain catchments that are of meso-scale type. Most stormwater models were associated with the lumped system until the mid-1960s. The distributed system models appeared when satellite data, digital elevation model (DEM), and GIS tools became available. These technologies are able to incorporate the spatial aspect of hydrologic processes. Lumped models cannot predict the hydrologic consequences of land use changes, but distributed models have this capability because they use distributed elements in space.

6.2 Land Use/Land Cover

A critical input parameter to any stormwater model is land use and/or land cover. Individual land use classes determine the rate of pollutant generation in a piece of land. For example, Stenstrom *et al.* (1984) found that oil and grease have high concentrations in commercial properties and parking areas. Indeed, stormwater models are applied to identify problem land uses and help designate appropriate mitigation measures. Land uses are commonly delineated from aerial photographs and/or field surveys. These procedures are long, tedious, and expensive. When the first Landsat satellite was launched in 1972, scientists immediately realized that satellite images had the potential to rapidly map land uses. They can also cover extensive areas. The first sensor to be launched was the Multispectral Scanner (MSS) that produced an image format with a coarse resolution of 80 meters.

With the low resolution of Landsat MSS covering the Upper Anacostia River basin in the suburbs of Washington, D.C., Ragan and Jackson (1980) recognized that they would not be able to represent all the land use categories required by the stormwater model SCS (Soil Conservation Service). This model accepted land use and soil type as major input parameters. To be able to run this model with satellite data, they developed an alternative set of land use classes identifiable in the Landsat MSS image. Computer aided study of the MSS was backed up by limited manual practices. With these land uses, they calculated runoff curve numbers that were still adequate to the overall operation of the SCS model. They found that values of runoff discharge predicted from aerial

photograph-derived land uses were nearly identical to those computed from MSS-extracted land uses.

Cermak *et al.* (1979) also developed their own classification technique and tested it using the Crow Creek watershed near Davenport, Iowa, and in Walnut Creek watershed near Austin, Texas. Again, they modified the land use categories to reflect the level of detail recognizable in the Landsat MSS. The classification was evaluated by means of an error matrix before the land uses were applied to the stormwater model HEC (Hydrologic Engineering Center). Discharge frequency curves (discharge vs. recurrence interval) based on Landsat MSS resembled those based on conventional land uses. These curves were critical information in flood monitoring and estimation of damage.

Although earlier researchers were successful in producing satisfactory model results even with the coarse resolution of Landsat MSS, scientists tend to use higher resolution images as they become available. The Thematic Mapper (TM) imagery immediately became popular when the TM sensor was added to the Landsat program. The 30-meter resolution imagery significantly increased the number of objects that can be identified in the satellite image. France also launched its own satellite producing SPOT multispectral imagery with 20-meter resolution. The satellite also has a panchromatic mode producing 10-meter resolution imagery. In some cases, these images are replacing aerial photographs for stormwater applications.

A Landsat TM image, a SPOT panchromatic image, and two types of scanned aerial photographs were compared by Ventura and Harris (1994) to determine if more land use categories would produce more accurate values of pollutant loadings. They

extracted land uses in the city of Beaver Dam, in Dodge County, Wisconsin, using unsupervised and supervised classification strategies and manual air photo interpretation. Error matrices were calculated before the land uses were applied in the stormwater model SLAMM (Source Loading and Management Model). As expected, more land use categories were resolved in the higher resolution images. Yet, the input of more specific land uses did not produce higher accuracy in the estimates of pollutant loadings of lead, copper, zinc, cadmium, phosphorus, and suspended sediment.

Harris and Ventura (1995) made analogous conclusions for the same study area when they tried to increase the land use class specificity of the Landsat TM by adding ancillary data. First they classified the Landsat TM image with the maximum likelihood approach. Thereafter, they manipulated zoning and housing density information to correct regions of confusion. They had four classifications: TM only; TM and zoning; TM, zoning, and housing; and zoning only. The four classifications had different class specificities. The classification with the TM image produced the fewest categories. Classifications were also analyzed using error matrices. However, again using SLAMM, they found that more classes did not produce significant differences in model results of pollutant loadings.

Later studies considered satellite imagery as their main source of land cover/land use data. This is probably because their study areas were more extensive. In this case, obtaining land uses from aerial photographs and/or field surveys can be impractical. It is also possible that image processing software has become more reliable and easier to use. Computer hardware and satellite data may have also become more accessible.

Mattikalli *et al.* (1996) worked on historical land use data that covered the River Glen catchment in eastern England. Aside from satellite images that included Landsat TM, they also added maps and aerial photos for several dates from the 1931 to 1989 period. Because these formats were different from each other, they developed a new methodology that combined land use data in raster and vector formats. With land use as the main input component, they utilized the SCS model to compute for river discharge and the export coefficient model to predict nitrogen loading. The simulated values were comparable to their measured counterparts. Because of the large amount of data involved, the model was run in a GIS environment.

Efforts in enhancing the efficiency and accuracy of the land use classification process continued. Ning *et al.* (2002) developed a novel and rapid way for land-use identification from SPOT imagery using 3S technologies in the ERDAS Imagine and Arc View environments. They investigated the Kao-Ping River basin in southern Taiwan. With GIS, GPS (Global Positioning System), and the GWLF (Generalized Watershed Loading Functions) model, they calculated the pollutant loadings of total phosphorus (TP) and total nitrogen (TN). They found that there was a relationship between the TP and TN loadings with the rainfall amount over the seasons.

Not only Landsat and SPOT images are used in stormwater modeling, but other images as well. Dayawansa (1997) evaluated IRS LISS II imagery covering the Nilambe sub-catchment in the central portion of Sri Lanka. Land use was acquired from a supervised classification of this imagery. With GIS tools and the AGNPS (Agricultural Non-Point Sources) model, amounts of soil erosion, sediment yield, and pollutant

loadings of nitrogen, phosphorus, and chemical oxygen demand (COD) were computed. A best management practice called SALT (Sloping Agricultural Land Technology) was also tested. In SALT, crops were cultivated along the contours of sloping agricultural grounds, and sediments were trapped by hedgerows. This practice controlled erosion. Model simulation indicated that SALT could minimize erosion and limit the production of sediment, nutrient, and COD.

In a related inquiry, Tripathi *et al.* (2003) also acquired land use/land cover from the supervised classification of IRS-1B (LISS II) imagery. GIS was likewise employed to generate the other watershed characteristics such as soil and slope. Based on statistical analyses of simulated and measured values, they concluded that SWAT (Soil and Water Assessment Tool) could precisely simulate runoff, sediment yield, and nutrient losses (organic nitrogen, phosphorus, nitrate nitrogen, and soluble phosphorus). Model results enabled them to prioritize erosion-prone sub-watersheds in the Nagwan basin in Bihar, India.

Although many researchers have applied the standard statistical practices for land cover classification, other scientists have considered more sophisticated schemes. Artificial intelligence techniques were tried by Ha *et al.* (2003) to classify land use/land cover in an area around Chongju city, situated in the middle of Korea. They applied both the RBF-NN (radial-basis-function neural network) and the ANN (artificial neural network) on fused Landsat TM and KOMPSAT panchromatic imageries. Classification was evaluated by means of an error matrix. With SWMM (Storm Water Management Model), they predicted the values of stormwater runoff quantity and biochemical oxygen

demand (BOD). The predicted runoff, peak time, and pollutant emissions changed significantly with respect to the classification accuracy and percentile unit load used.

6.3 Impervious Surface

Another important model parameter for stormwater modeling is imperviousness. An impervious surface, such as pavement and rooftops, prevents water from infiltrating the soil. Imperviousness determines the amount of rainfall that becomes runoff in a parcel of land. Therefore, the total amount of impervious surface in a watershed directly relates to the runoff rates and volumes. This information is important, for example, to calculate the size of storage necessary for flood control.

In the early days of the Landsat program, where the satellite image was captured by the Multispectral Scanner (MSS) with a low resolution of 80 meters, imperviousness was obtained by delineating the land uses in the study area, and then assigning an average imperviousness for each land use class. For example, commercial land use may be assigned 92% imperviousness. There were significant savings in labor, time, and money when satellite data were tried instead of aerial photographs and/or field surveys. Ragan and Jackson (1975) found that about 94 man-days were necessary to finish the land use classification using 1:4,800 aerial photographs. But it took fewer than 4 man-days to reach the same goal using Landsat MSS. They discovered that overall imperviousness from the aerial photos and Landsat MSS were in close agreement. The dollar value of Landsat MSS was even quantified by Jackson and Ragan (1977) using Bayesian Decision Theory. For flood control, they needed imperviousness to compute for optimal depth of

detention storage. They concluded that Landsat MSS was a cost-effective source for calculating impervious cover based on land use.

Jackson *et al.* (1977) also analyzed Landsat MSS to indirectly calculate impervious surface from land uses. They needed this variable to run STORM (Storage Treatment Overflow Runoff Model) to enable them to know the most cost-effective option for flood control in the Fourmile Run watershed in the suburbs of Washington, D.C. They were considering channelization work or storage. Discharge, hydrographs, and flood frequency curves were simulated. These model outputs resembled their observed equivalents. Individual figures varied slightly, but versions of STORM showed the same decision about flood control management whether they used aerial photographs or Landsat MSS. Since the satellite image was less expensive than aerial photos, they concluded that it was the more reasonable source to delineate impervious cover.

With the advent of high resolution imagery, scientists are already able to map imperviousness directly from satellite imagery. Morgan *et al.* (1993) performed supervised and unsupervised classification on a SPOT, 10-meter panchromatic imagery to quantify overall impervious cover in an urban watershed in Dallas, Texas. For the manual mode, they worked on aerial photographs. Runoff volumes from USGS stream gauge station were compared to the runoff volumes computed using imperviousness from satellite data. The results were remarkably similar.

Investigators have attempted to use even higher resolution images. Thomas *et al.* (2003) worked on a one-meter resolution image captured by the ADAR 5500 digital multispectral scanner. They applied three different ways to map impervious cover in the

city of Scottsdale, Arizona for runoff estimation. In the first approach, supervised and unsupervised statistical classification schemes were combined. In the second procedure, the misclassifications in the first methodology were corrected by means of ancillary data. The last system made use of a classification tree that was based on image segmentation. They produced error matrices, both the regular and fuzzy types. They concluded that high-resolution imagery interpretation required the combination of spectral response with ancillary information such as shape, texture, and context.

6.4 Other Hydrologic Parameters

Land use and/or land cover and imperviousness are the most common hydrologic parameters derived from satellite data. But there are additional variables of recent interest. Elevation is one of these. A depiction of the earth's surface by a grid of elevation values is called a digital elevation model (DEM). A DEM is routinely manipulated for delineating the drainage system in a watershed. DEMs are frequently produced from aerial photographs and field surveys. However, DEMs can also come from SPOT stereoscopic image pairs (Wharton, 1994). Muller *et al.* (2000) digitized a JERS-1 radar imagery to produce an outline of the whole drainage network of the Amazon basin.

Other drainage variables that can be estimated reasonably from satellite images are descriptors of the watershed such as channel length, channel junctions, and basin areas. Wharton (1994) suggested the use of satellite data to calculate drainage network indices. These indices are important because they describe the relationship of the basin characteristics with the runoff generated. An example of a drainage network index is

drainage density. This is defined as the total stream length divided by the basin area. Manual procedures for calculating indices like this are difficult, time-consuming, and laborious. Wharton (1994) reasoned that these indices could be computed easily and rapidly with high resolution images (e.g., 5-meter resolution). In low resolution images, smaller streams that equally contribute to drainage characteristics cannot be detected.

Snow cover can be delineated from satellite images, too. Sensoy *et al.* (2003) analyzed NOAA AVHRR images to determine the percentages of snow-covered area for the three elevation zones in the Upper Karasu Basin in Turkey. Using HEC-1 that interfaced with WMS (Watershed Modeling System), NOAA AVHRR and ground-truth data were incorporated to determine the snow water equivalent of the snow-covered areas. After the potential meltwater was converted to its real volume, they produced runoff simulation from both snowmelt and rainfall. They noted that calculated and observed hydrographs were similar.

Rainfall is a required variable in any stormwater model. It is routinely collected from rain gauge measurements. However, in developing nations, rainfall is measured in only a few watersheds. Hence, Tripathi *et al.* (2004) used the stormwater model SWAT to generate rainfall in Nagwan watershed in India. As usual, land use/land cover was needed, and it was produced from the supervised classification of IRS-1B (LISS II) satellite data. The classification was assessed using an error matrix and the kappa coefficient. A GIS was used to manage the large amounts of data stored and manipulated. With the model-generated rainfall, surface runoff and sediment yield were computed. The simulated monthly rainfall, runoff, and sediment yield estimates were comparable to their

corresponding observed values. Hence, they concluded that SWAT could be applied to develop a management strategy for lands susceptible to erosion.

In the investigation of Sharma and Singh (1995), not only the land use/land cover was mapped from Landsat TM image, but also landform, drainage, and soil in the three watersheds within the Bandi river basin in India. The raw image was enhanced by principal components analysis and a high pass filter. Both raw and digitally enhanced images were visually interpreted because different landforms specifically did not have individual, distinctive spectral signatures. The computer processing was also supported by limited ground truth. The model ANSWERS (Areal Non-point Source Watershed Environment Response Simulation) predicted the hydrographs and sediment graphs. When compared to their actual equivalents, the model results were within acceptable limits. However, the model underpredicted the total soil loss, the important variable needed for erosion control. Sharma and Singh (1995) asserted that the manual approaches were necessary because of limited human expertise in digital image processing in Third World countries like India.

All of the inquiries previously discussed indirectly estimated final model outputs such as runoff volumes, hydrographs, and pollutant loadings. However, Park and Stenstrom (2004) were able to directly map the qualitative descriptions of pollutant loadings using Bayesian Networks in the Santa Monica Bay area in Los Angeles, California. Using the spectral response of earth surface features and positional ancillary data, they learned the specific pollutants that had high, medium, and low concentrations on particular land uses. For example, open land use had low emissions of COD (chemical

oxygen demand), BOD₅ (biochemical oxygen demand), TKN (total Kjeldahl nitrogen), NO_{2&3} (nitrite and nitrate), TP (total phosphorus), and SP (soluble phosphorus). On the other hand, the transportation category had high emissions of COD, BOD₅, TKN, and TP.

6.5 Discussion

The choice of ground resolution of satellite data is probably the most important concern of the stormwater modeler. The resolution is associated with the amount of detail that can be resolved in an image. The advent of space technologies initially prompted scientists to identify land uses from satellite imagery. In the past, scientists had little selection of images. The Landsat MSS with an 80-meter resolution was the most commonly analyzed. Scientists created various ways to get the level of detail required by their modeling objectives. Because a coarse resolution image cannot describe all the land use classes specified by the conventional practice, they developed alternative sets of categories identifiable in the satellite data. They concluded that low resolution images (e.g., Landsat MSS) could be used with their stormwater models with acceptable accuracy. Simulated runoff volumes, hydrographs, and pollutant loadings, for example, were in close agreement to their actual counterparts. Recently, however, there has been an increase in the capture of higher resolution satellite imagery (e.g., Landsat TM). Yet, having an enhanced specificity of land use classes does not necessarily increase the accuracy of the model results. Even broad categories of land cover can be utilized without significantly deteriorating the operation of stormwater models.

Generally, for urbanized areas, higher resolution images may be more appropriate as the land cover structure is complex. For rural and agricultural areas, lower resolution images may be sufficient because of their homogeneous composition. Lower resolution satellite data may be less expensive because they can cover larger areas. However, even a homogeneous area may require many land cover classes, depending on the application. If more land cover classes are needed, then a higher resolution image may be more useful. A system should be developed that will quantify the trade-off between accuracy and cost.

Higher resolution imagery is probably applicable in detecting impervious areas. Impervious surfaces, like roads and rooftops, are usually narrower than the ground resolution of most satellite data. Therefore, ground resolution that approaches the size of impervious surfaces will be the most beneficial. However, the cost of acquisition, storage, and processing of a high resolution image is much more than that of a low resolution image. Hence, high resolution images should not be evaluated for one-time application but should also be considered for other purposes. In this case, using the high resolution image can be cost-effective.

Objectives of the modeling effort vary. In agricultural areas, land parcels susceptible to erosion are identified and prioritized. While in urban areas, flooding and pollution of the receiving water body are the important concerns. Because rural and agricultural areas have a homogeneous land cover structure, there is a tendency to use the established statistical classifiers to depict land cover. On the other hand, in urban areas, it is usual to have more than one land cover in a particular pixel. Land covers here are mixed, and that pixel is usually called a “mixel”. More sophisticated strategies such as

artificial neural networks can be successful in delineating urban land uses. Yet, many studies merely utilized the standard classifiers for land use classification. The most popular scheme is the maximum likelihood, a supervised classification method. It should be noted that land use/land cover is just one input variable to stormwater models. If more sophisticated means are attempted just for the land use classification stage alone, then the entire stormwater modeling process will probably become more tedious.

Some researchers assess the accuracy of the land use classification first before applying it to the model, while others do not. Earlier researchers did not assess land use classification procedure by means of the error matrix or confusion matrix, which is the standard tool of the remote sensing community. In the past, the tendency was to validate the overall results of the model by means of runoff volumes, hydrographs, or pollutant loadings. Now, researchers are inclined to do both. But overall, they are successful whether they assess the accuracy of the satellite data first, or validate only the final model outputs, or do both. However, it should be remembered that satellite data are just one input element in the model. Each of the other parameters like stream length and slope, for example, has its measure of accuracy. This aspect of the modeling activity is not discussed in the studies.

Stormwater modelers follow the progress in the computing technologies. In the early investigations, scientists made their own in-house programs and techniques that were simple and easy to use and implement. Remote sensing or pattern recognition knowledge was not required. Most of them worked only on raw satellite images. Some still had a manual component in their procedures. But now, with the availability of image

processing software, modelers just use the proven methods of these programs. Images are routinely enhanced first before being classified. For example, principal components analysis or high pass filtering are employed as preliminary steps to maximize the amount of relevant information that can be extracted from an image.

At first, only the established stormwater models are analyzed (e.g., SCS, HEC-1). With the advent of GIS technology, these stormwater models are immediately linked with GIS. There is hardly any stormwater modeling activity which does not use GIS at present. GIS is either completely or partly integrated with the stormwater model. Computer systems have become more sophisticated, more powerful, and faster. They are able to process large amounts of data in less time. Vector to raster conversion and vice-versa are easy to do. Storage of large dataset is no longer an impediment. However, retrieval of useful information from myriad of dataset is still hard to do. This becomes a more difficult issue when using high resolution images.

Personnel expertise is not an issue now because training in remote sensing and GIS is highly accessible in the United States. Knowledge of GIS and remote sensing is required in most modeling efforts, especially in large areas. There are lots of programs offering short courses in GIS and remote sensing. Some companies, like ESRI for example, are even offering online courses.

6.6 Summary and Conclusions

The use of satellite data provides a cost-effective alternative to standard ways of hydrologic parameter acquisition. Still, there are issues to consider in this endeavor such

as ground resolution of satellite data, methods of stormwater model validation, classification accuracy assessment, personnel expertise, and cost.

Satellite data are reasonable sources of input parameters in stormwater modeling. As space and computing technologies advance, there will be more opportunities for stormwater modelers to find more effective and efficient ways to estimate hydrologic components. Having an ungauged watershed, or having few rain gauges, for example, should not be an impediment in operating a stormwater model with acceptable accuracy, if equivalent data can be acquired from the processing of satellite images.

6.7 References

- Cermak, R.J., Feldman, A., and Webb, R.P. (1979) Hydrologic land use classification using Landsat. In *Satellite Hydrology* (M. Deutsch, D.R. Wiesnet, and A. Rango, Eds.), American Water Resources Association, Minneapolis, Minnesota, pp. 262-269.
- Dayawansa, N.D.K. (1997) Identification of non-point source pollution risk using GIS and remote sensing techniques. In *Proceedings of the 18th Asian Conference on Remote Sensing*, 20-24 October, Malaysia <<http://www.gisdevelopment.net/aars/acrs/1997/ps1/ps2019.shtml>>, accessed on 2 Sept. 2004.
- Ha, S.R., Park, S.Y., and Park, D.H. (2003) Estimation of urban runoff and water quality using remote sensing and artificial intelligence. *Water Science and Technology*, 47 (7-8): 319-325.
- Harris, P.M. and Ventura, S.J. (1995) The integration of geographic data with remotely sensed imagery to improve classification in an urban area. *Photogrammetric Engineering and Remote Sensing*, 61 (8): 993-998.
- Jackson, T.J. and Ragan R.M. (1977) Value of Landsat in urban water resources planning. *Journal of the Water Resources Planning and Management Division*, 103 (WR1): 33-46.
- Jackson, T.J., Ragan, R.M., and Fitch, W.N (1977) Test of Landsat-based urban hydrologic modeling. *Journal of the Water Resources Planning and Management Division*, 103 (WR1): 141-158.
- Mattikalli, N.M., Devereux, B.J., and Richards, K.S. (1996) Prediction of river discharge and surface water quality using an integrated geographical information system approach. *International Journal of Remote Sensing*, 17 (4): 683-701.
- Morgan, K.M., Newland, L.W., Weber, E., and Busbey, A.B. (1993) Using SPOT satellite data to map impervious cover for urban runoff predictions. *Toxicological and Environmental Chemistry*, 40: 11-16.
- Muller, F., Cochonneau, G., Guyot, J.L., and Seyler, F. (2000) Watershed extraction using together DEM and drainage network: Application to the whole Amazonian basin. In *Proceedings of the 4th International Conference on Integrating GIS and Environmental Modeling (GIS/EM4)*, 2-8 September, Banff, Alberta, Canada, in CD-ROM.
- Ning, S.K., Jeng, K.Y., and Chang, N.B. (2002) Evaluation of non-point sources pollution impacts by integrated 3s information technologies and GWLF modelling. *Water Science and Technology*, 46 (6-7): 217-224.

- Nix, S.J. (1994) *Urban Stormwater Modeling and Simulation*, Lewis Publishers, Boca Raton, Florida.
- Park, M.H. and Stenstrom, M.K. (2004) A new classification system for urban stormwater pollutant loading: A case study in the Santa Monica Bay area. In *Proceedings of the IWA Diffuse Pollution Conference*, 24-29 October, Kyoto, Japan, Paper 2-E-IV-4.
- Ragan, R.M. and Jackson T.J. (1975) Use of satellite data in urban hydrologic models. *Journal of the Hydraulics Division-ASCE*, 101 (12): 1469-1475.
- Ragan, R.M. and Jackson, T.J. (1980) Runoff synthesis using Landsat and SCS model. *Journal of the Hydraulics Division-ASCE*, 106 (5): 667-678.
- Schultz, G.A. (1994) Mesoscale modeling of runoff and water balances using remote-sensing and other GIS data. *Hydrological Sciences Journal-Journal Des Sciences Hydrologiques*, 39 (2): 121-142.
- Sensoy, A., Tekeli, A.E., Sorman, A.A., and Sorman, A.U. (2003) Simulation of event-based snowmelt runoff hydrographs based on snow depletion curves and the degree-day method. *Canadian Journal of Remote Sensing*, 29 (6): 693-700.
- Sharma, K.D. and Singh, S. (1995) Satellite remote-sensing for soil-erosion modeling using the ANSWERS model. *Hydrological Sciences Journal-Journal Des Sciences Hydrologiques*, 40 (2): 259-272.
- Stenstrom, M.K., Silverman, G.S., and Bursztynsky, T.A. (1984) Oil and grease in urban stormwaters. *Journal of Environmental Engineering*, 110 (1): 58-72.
- Thomas, N., Hendrix, C., and Congalton, R.G. (2003) A comparison of urban mapping methods using high-resolution digital imagery. *Photogrammetric Engineering and Remote Sensing*, 69 (9): 963-972.
- Tripathi, M.P., Panda, R.K., and Raghuwanshi, N.S. (2003) Identification and prioritisation of critical sub-watersheds for soil conservation management using the SWAT model. *Biosystems Engineering*, 85 (3): 365-379.
- Tripathi, M.P., Panda, R.K., Raghuwanshi, N.S., and Singh, R. (2004) Hydrological modelling of a small watershed using generated rainfall in the soil and water assessment tool model. *Hydrological Processes*, 18 (10): 1811-1821.
- Ventura, S.J. and Harris, P. (1994) A comparison of classification techniques and data sources for urban land use mapping. *Geocarto International*, 3: 5-14.

Wharton, G. (1994) Progress in the use of drainage network indexes for rainfall-runoff modeling and runoff prediction. *Progress in Physical Geography*, 18 (4): 539-557.

Chapter 7

Land Use Classification Using Satellite Data: New Approaches

7.1 Introduction

Land use is a necessary input parameter for stormwater models. It is used to estimate the imperviousness of surface areas. Each type of land parcel is impervious to rainfall to some extent. Commercial business districts, for instance, are highly impervious because most of the land surface is paved or has structures on it. Open land, on the other hand, has very little impervious surface, and water will directly infiltrate the ground. Therefore, more runoff will be generated in a land parcel that has more impervious surface. The category of land use also determines the nature and quantity of pollutants produced by a parcel of land. For example, oil and grease concentrations are higher in runoff from commercial properties and parking areas than in residential areas (Stenstrom *et al.*, 1984). Generally, land use categories are manually delineated from aerial photographs and field work data. However, land use classifications can be obtained more efficiently by digital processing of satellite imagery.

Remote sensing scientists often interchange the terms “land use” and “land cover”. Their denotations, however, are distinct (Donnay *et al.*, 2001). Land cover is the physical material present on the surface of a land parcel (e.g., grass, water). Land use, on

the other hand, refers to the human activity associated with that land parcel (e.g., residential, industrial). Both land cover (physical component of the land parcel) and land use (economic component) data are important for stormwater modeling. The results of modeling aid in the selection of best management practices.

The traditional or conventional classifiers (parallelepiped, minimum distance to means, maximum likelihood, clustering) have limitations that reduce the correctness of land use/land cover classification. This inspires researchers to devise new strategies to improve the efficiency and accuracy of the classification process. To determine the performance of their proposed approach, investigators compare their methods with these standard classifiers. In particular, the maximum likelihood classifier is the most widely used because of its well-developed theoretical base, facility of automation, and reliable track record (Swain and Davis, 1978; Richards, 1986; Lillesand and Kiefer, 1994). Many have utilized the confusion matrix for accuracy assessment and the common measures derived from it (e.g., overall accuracy). But other metrics are also available. For example, Cohen's kappa coefficient is often employed to accommodate for the effects of chance that a pixel has been classified into its correct land cover category (Foody, 2002). In the literature, there are many ways that researchers try to refine the accuracy of the classification process. Only a small fraction of these are explored here.

7.2 Incorporation of Ancillary Data

Ancillary data, usually in GIS format, can be incorporated before, during, and after classification (Hutchinson, 1982). They are called stratification, classifier

operations, and post-classification sorting respectively. In stratification, the most common technique, the image is divided into smaller regions to enhance the homogeneity of the data to be classified. Then, relevant properties of the land use categories are derived. For instance, the image may be segmented based on the density of the built-up areas (Michalak, 1993).

In classifier operations, the decision rules of the statistical classifiers are adjusted to reflect the areal combination of the known land use classes by specifying prior probabilities (Gorte and Stein, 1998; McIver and Friedl, 2002). Another technique is to treat the ancillary data as another band in the classification. Elumnoh and Shrestha (2000) combined a digital elevation model with the spectral bands using ISODATA. In post-classification sorting, similar land use classes with different spectral responses are merged based on the additional data. Harris and Ventura (1995), for example, took advantage of available zoning and housing density data to correct regions of confusion.

7.3 Contextual Classifiers

The standard classification strategies are point or pixel specific classifiers. Here, the pixels are classified independently of the classifications of the neighboring pixels. It has long been acknowledged that adjacent pixels may have similar land cover classes. Contextual classification is employed when neighboring pixels are taken into account during the classification process (Richards, 1986). For example, Barnsley and Barr (1996) developed a two-stage classification system, the first of which involved the standard per-pixel classification of the image into broad land cover classes. In the second

stage, they passed a kernel across the image which took into account both the frequency and the spatial arrangement of the pixels. Wharton (1982) recognized that urban land use classes have different amounts of the same land cover components. For example, there are more pavement and roof components in a commercial district than in a single-family residential area. This observation was his basis for his two-stage cluster analysis procedure. Other contextual classifiers were developed by Gurney (1983), Mohn *et al.* (1987), Carlotto (1998), and Sharma and Sarkar (1998).

7.4 Neural Networks

A neural network is an information system of interconnected elements called neurons (Awad, 1996). In Figure 7.1, neurons measure the inputs, calculate their weights, total the weighted inputs, and compare this value to a threshold. If this value is larger than the threshold, the neurons fire (output). Otherwise, it produces no signal. When the network alters the weights and changes its activity based on the inputs, learning has taken place. Back propagation involves adjusting the weights by backing up from the output.

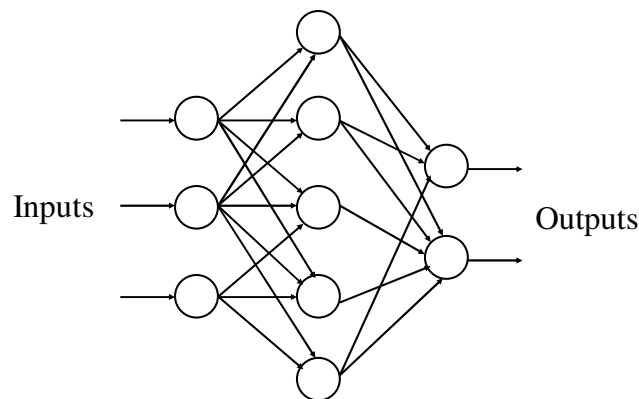


Figure 7.1: An example of a neural network

Neural network classifiers have many advantages over statistical techniques (Ji, 2000). First, there is no assumption about the distribution of the data (e.g., Gaussian). Second, it can form generalizations even in noisy environments. And third, it is capable of learning complex patterns. However, there are disadvantages (Awad, 1996). They may not be able to provide accurate answers. Learning is difficult and processing is time-consuming. They are a black box; they do not have explanatory abilities like a knowledge-based system. A big network is also required for complex problems. Despite these apparent drawbacks, it is found that accuracy increased when neural networks are applied.

In a neural network, the inputs are the individual digital numbers. Ancillary data can also be added to the pattern of the pixels. The outputs are the land use/land cover categories of the pixels. Lee (2003) utilized not only the spectral characteristics of the image, but also included the pixel locations as inputs to his neural networks. Sometimes, the number of nodes can be huge. Kanellopoulos *et al.* (1992) trained a 98-node network to identify 20 land cover classes. There are many other studies that have used neural networks and obtained improved classification results (Chen *et al.*, 1995; Foody *et al.*, 1995; Gong *et al.*, 1996; Paola and Schowengerdt, 1997; Ji, 2000).

7.5 Fuzzy Classifiers

So far, we have discussed only per-pixel classification, in which a pixel can only have one and only one category. These are called hard classifiers. In urban regions, a pixel in reality may have more than one category because of the heterogeneity of the land

cover composing that pixel. We call this a mixed pixel. Presence of these pixels in an urban setting prompted the development of soft or fuzzy classifiers. This term stems from the fact that a pixel does not belong fully to one class but it has different degrees of membership in several classes. The mixed pixel problem is more pronounced in lower resolution data. In fuzzy classification, or pixel unmixing, the proportion of the land cover classes from a mixed pixel is calculated (Eastman and Laney, 2002). Fuzzy classifiers are especially applicable if areas of individual categories are needed, for example, the total area of impervious surface in a watershed. Wang (1990) devised an algorithm similar to maximum likelihood except that he replaced the mean vectors and the covariance matrix with their fuzzy equivalents. Foody and Cox (1994), Warner and Shank (1997), and Eastman and Laney (2002) proved that classification accuracy improved with this method.

7.6 Knowledge-Based Systems

In a knowledge-based system, tasks are completed by the application of rules to a symbolic depiction of knowledge (Jackson, 1999). Here, thematic or geometric data are incorporated in the classification. This method is applied when spectral characteristics alone cannot provide sufficient information to identify classes of interest. One group called hierarchical strategies excludes optional classes during classification until only one category is left (Figure 7.2). Land use/cover types are portrayed as leaves of bi- or multinary trees. The decision course is halted or resumed depending on the rules applied at every node (Swain and Hauska, 1977; Ferrante *et al.*, 1984). Johnsson and Kanonier

(1991) segmented a classified image based on their spectral properties. Then, they calculated the size, perimeter, and shape of the segments. In effect, their rules were based both on spectral and spatial properties of the image.

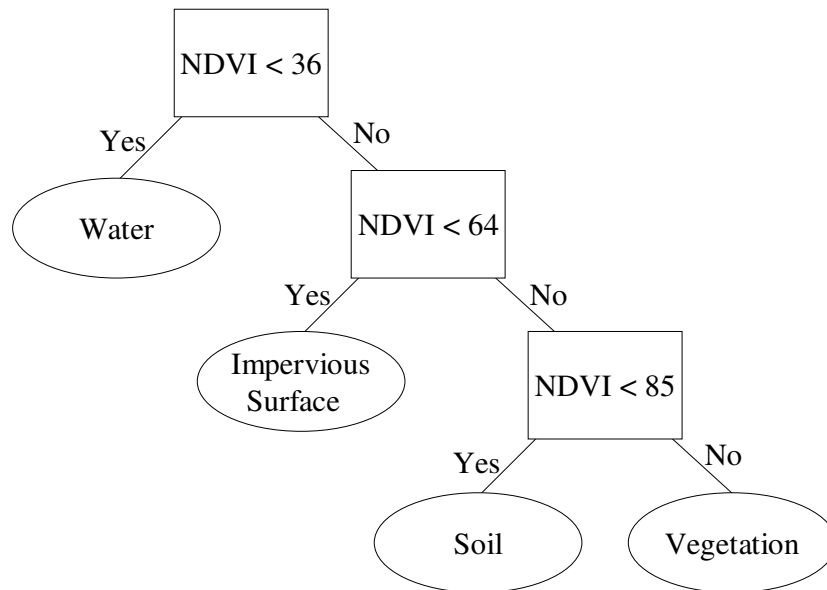


Figure 7.2: An example of a decision tree

7.7 Discussion

Numerous scientists in different disciplines (e.g., geography, computer science, electrical engineering) have exerted much effort to improve the land use classification process. However, the ultimate goal of many of these investigations is the classification procedure itself. There are some studies that analyzed satellite data specifically to provide inputs to their stormwater models. Examples that extracted mainly land use classes are

investigations by Cermak *et al.* (1979), Ragan and Jackson (1980), and Harris and Ventura (1995).

More engineers and planners should consider utilizing satellite data for their stormwater modeling efforts. However, there are issues to be addressed. First, the level of detail must be appropriate for a specific study area. For example, some land use classification studies can identify up to Anderson level III. However, in stormwater modeling, Anderson level II is often sufficient even for a highly urbanized city like Los Angeles. The level of detail is also associated with the ground resolution of the satellite data. For instance, a high resolution IKONOS image will definitely resolve more objects. A decision should be made if the accuracy achievable is indeed necessary because using this image has disadvantages such as expense and large storage space. Second, the categories of land use must be relevant to the study area. For example, “transportation” may be a relevant land use category in Los Angeles where wide freeways are prevalent, but it may not be a useful land use class in a small city in Kansas. Lastly, the performance of the classification procedure should be assessed. One way is to apply the accuracy assessment tool (i.e., error/confusion matrix) of the remote sensing community. But we can also evaluate the results of the stormwater modeling itself. The modeling outputs can be runoff volumes, hydrographs, or pollutant loadings. We can compare the outputs that used satellite data to those that utilized traditional methods (e.g., stream gauging). By addressing these issues, satellite data can be applied in stormwater management in the best possible way.

7.8 References

- Awad, E.M. (1996) *Building Expert Systems: Principles, Procedures, and Applications*, West Publishing Company, St. Paul, Minnesota.
- Barnsley, M.J. and Barr, S.L. (1996) Inferring urban land use from satellite sensor images using kernel-based spatial reclassification. *Photogrammetric Engineering and Remote Sensing*, 62 (8): 949-958.
- Carlotto, M.J. (1998) Spectral shape classification of Landsat Thematic Mapper imagery. *Photogrammetric Engineering and Remote Sensing*, 64 (9): 905-913.
- Cermak, R.J., Feldman, A., and Webb, R.P. (1979) Hydrologic land use classification using Landsat. In *Satellite Hydrology* (M. Deutsch, D.R. Wiesnet, and A. Rango, Eds.), American Water Resources Association, Minneapolis, Minnesota, pp. 262-269.
- Chen, K.S., Tzeng, Y.C., Chen, C.F., and Kao, W.L. (1995) Land-cover classification of multispectral imagery using a dynamic learning neural network. *Photogrammetric Engineering and Remote Sensing*, 61 (4): 403-408.
- Donnay, J.P., Barnsley, M.J., and Longley, P.A. (Eds.) (2001) *Remote Sensing and Urban Analysis*, Taylor and Francis, London, England.
- Eastman, J.R. and Laney, R.M. (2002) Bayesian soft classification for sub-pixel analysis: A critical evaluation. *Photogrammetric Engineering and Remote Sensing*, 68 (11): 1149-1154.
- Elumnoh, A. and Shrestah, R.P. (2000) Application of DEM data to Landsat image classification: Evaluation in a tropical wet-dry landscape of Thailand. *Photogrammetric Engineering and Remote Sensing*, 66 (3): 297-304.
- Ferrante, R.D., Carlotto, M.J., Pomarede, J., and Baim, P.W. (1984) Multi-spectral image analysis system. In *Proceedings of the 1st Conference on Artificial Intelligence Applications*, pp. 357-363.
- Foody, G.M. (2002) Status of land cover classification accuracy assessment. *Remote Sensing of Environment*, 80 (1): 185-201.
- Foody, G.M. and Cox, D.P. (1994) Sub-pixel land cover composition estimation using a linear mixture model and fuzzy membership functions. *International Journal of Remote Sensing*, 15 (3): 619-631.

- Foody, G.M., McCulloch, M.B., and Yates, W.B. (1995) Classification of remotely sensed data by an artificial neural network: Issues related to training data characteristics. *Photogrammetric Engineering and Remote Sensing*, 61 (4): 391-401.
- Gong, P., Pu, R., and Chen, J. (1996) Mapping ecological land systems and classification uncertainties from digital elevation and forest-cover data using neural networks. *Photogrammetric Engineering and Remote Sensing*, 62 (11): 1249-1260.
- Gorte, B. and Stein, A. (1998) Bayesian classification and class area estimation of satellite images using stratification. *IEEE Transactions on Geoscience and Remote Sensing*, 36 (3): 803-812.
- Gurney, C.M. (1983) The use of contextual information in the classification of remotely sensed data. *Photogrammetric Engineering and Remote Sensing*, 49 (1): 55-64.
- Harris, P.M. and Ventura, S.J. (1995) The integration of geographic data with remotely sensed imagery to improve classification in an urban area. *Photogrammetric Engineering and Remote Sensing*, 61 (8): 993-998.
- Hutchinson, C.F. (1982) Techniques for combining Landsat and ancillary data for digital classification improvement. *Photogrammetric Engineering and Remote Sensing*, 48: 123-130.
- Jackson, P. (1999) *Introduction to Expert Systems, 3rd Edition*, Addison-Wesley, U.S.A.
- Ji, C.Y. (2000) Land-use classification of remotely sensed data using Kohonen self-organizing feature map neural networks. *Photogrammetric Engineering and Remote Sensing*, 66 (12): 1451-1460.
- Johnsson, K. and Kanonier, J. (1991) Knowledge based land-use classification. In *Proceedings of the International Geoscience and Remote Sensing Symposium IGARSS '91*, 3-6 June, Espoo, Finland, pp. 1847-1850.
- Kanellopoulos, I., Varfis, A., Wilkinson, G.G., and Megier, J. (1992) Land-cover discrimination in SPOT HRV imagery using an artificial neural network- A 20-class experiment. *International Journal of Remote Sensing*, 13 (5): 917-924.
- Lee, H.H. (2003) *Data Mining of Remote Sensed Data for Stormwater Systems*, Ph.D. Dissertation, University of California, Los Angeles, U.S.A.
- Lillesand, T.M. and Kiefer, R.W. (1994) *Remote Sensing and Image Interpretation, 3rd Edition*, John Wiley & Sons, Inc., U.S.A.

- McIver, D.K. and Friedl, M.A. (2002) Using prior probabilities in decision-tree classification of remotely sensed data. *Remote Sensing of Environment*, 81: 253-261.
- Michalak, W.Z. (1993) GIS in land use change analysis: Integration of remotely sensed data into GIS. *Applied Geography*, 13: 28-44.
- Mohn, E., Hjort, N.L., and Storvik, G.O. (1987) A simulation study of some contextual classification methods for remotely sensed data. *IEEE Transactions on Geoscience and Remote Sensing*, GE-25 (6): 796-804.
- Paola, J.D. and Schowengerdt, R.A. (1997) The effect of neural-network structure on a multispectral land-use/land-cover classification. *Photogrammetric Engineering and Remote Sensing*, 63 (5): 535-544.
- Ragan, R.M. and Jackson, T.J. (1980) Runoff synthesis using Landsat and SCS model. *Journal of the Hydraulics Division-ASCE*, 106 (5): 667-678.
- Richards, J.A. (1986) *Remote Sensing Digital Image Analysis: An Introduction*, Springer-Verlag, Germany.
- Sharma, K.M.S. and Sarkar, A. (1998) A modified contextual classification technique for remote sensing data. *Photogrammetric Engineering and Remote Sensing*, 64 (4): 273-280.
- Stenstrom, M.K., Silverman, G.S., and Bursztynsky, T.A. (1984) Oil and grease in urban stormwaters. *Journal of Environmental Engineering*, 110 (1): 58-72.
- Swain, P.H. and Davis, S.M. (Eds.) (1978) *Remote Sensing: The Quantitative Approach*, McGraw-Hill, Inc., U.S.A.
- Swain, P.H. and Hauska, H. (1977) Decision tree classifier: Design and potential. *IEEE Transactions on Geoscience and Remote Sensing*, 15 (3): 142-147.
- Wang, F. (1990) Fuzzy supervised classification of remote sensing images. *International Transactions on Geoscience and Remote Sensing*, 28 (2): 194-201.
- Warner, T.A. and Shank, M. (1997) An evaluation of the potential for fuzzy classification of multispectral data using artificial neural networks. *Photogrammetric Engineering and Remote Sensing*, 63 (11) 1285-1294.
- Wharton, S.W. (1982) A contextual classification method for recognizing land use patterns in high resolution remotely sensed data. *Pattern Recognition*, 15 (4): 317-324.

Chapter 8

Impervious Surface Detection from Satellite Data

8.1 Introduction

Stormwater management is concerned with regulating runoff. Increased amounts of runoff can cause flooding, erosion, and habitat destruction. A stormwater model is the tool that helps planners and engineers estimate runoff rates and volumes. An important stormwater model parameter directly related to runoff is imperviousness. Impervious areas prevent water from infiltrating the soil. Hence, a watershed that has much impervious surface generates a large amount of runoff which can cause a great deal of damage especially when discharged in a short period of time. The conventional ways of delineating imperviousness is through the use of aerial photographs, field surveys, and existing analogue maps. These techniques are tedious and time-consuming. A faster way to map imperviousness is by satellite image processing. Satellite data are easily obtained, able to cover large areas, and compatible with most hydrologic modeling software packages.

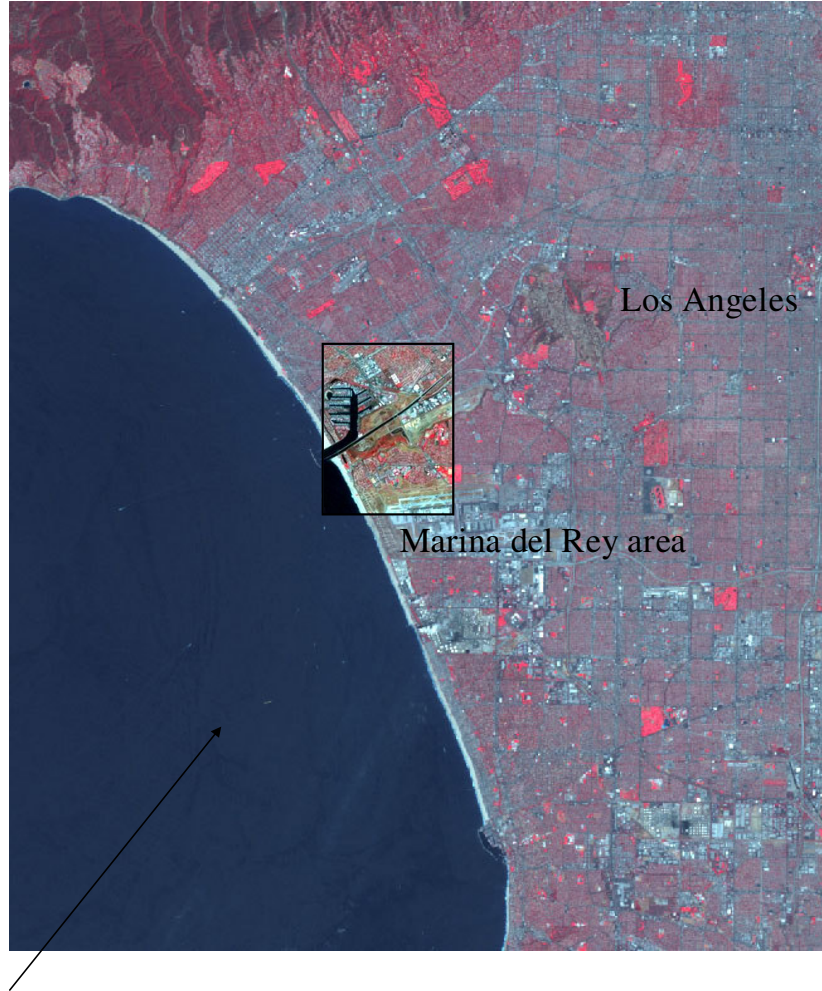
The objective of this study is to distinguish pervious and impervious areas in a satellite image of a highly urbanized part of Los Angeles, the Marina del Rey area (Figure 8.1). It is a part of the Santa Monica Bay watershed, and has an area of 24.7 sq

km. The study area covers the Ballona Wetlands a large portion of which is currently being developed, which will increase the impervious surfaces in the area.

We propose the use of knowledge-based systems in classifying land cover. A knowledge-based system applies rules to a symbolic depiction of knowledge to complete a task (Jackson, 1999). This is in contrast with statistical (e.g., maximum likelihood) or algorithmic (e.g., neural network) techniques. Knowledge is in the form of spectral data but usually ancillary data are also added, such as elevation, housing density, or zoning information. As such, knowledge-based classification commonly employs a geographic information system (GIS), which is a powerful tool that can obtain, store, recover, analyze, and display spatial data (Clarke, 1995). Many studies have shown that classification based on knowledge can help increase the accuracy of the land cover classification process (Johnsson and Kanonier, 1991; Middelkoop and Janssen, 1991).

8.2 Data, Materials, and Software

The study area is a subset from a Landsat ETM+ scene (path 41, row 36) acquired on August 11, 2002 (Figure 8.2). The exact limits are from 33°56'40" to 33°59'42" North latitude and from 118°24'42" to 118°27'32" West longitude. There are six reflective bands of data including the blue, green, red, near infrared (NIR), and the two mid-infrared bands (MIR5 and MIR7). Their characteristics are shown in Table 8.1 The image was rectified to UTM, Zone 11 (North) with the WGS 84 spheroid. Each square pixel's side is equivalent to 28.5 meters on the ground. The image was downloaded from the University of California, Los Angeles (UCLA) GIS Database.



Pacific Ocean

Figure 8.1: Vicinity map of the study area



0 1 km

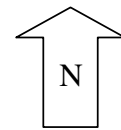


Figure 8.2: Black and white reproduction of infrared color image of the study area

Table 8.1: Raw image characteristics

Band	Wavelength (μm)	Spectral Location	Maximum	Minimum	Mean	SD
1	0.450- 0.515	Blue	255	74	111	17
2	0.525- 0.605	Green	255	50	93	20
3	0.63-0.69	Red	255	34	99	28
4	0.75-0.90	NIR	155	13	58	18
5	1.55-1.75	MIR	255	3	93	37
7	2.09-2.35	MIR	255	0	73	30

NIR = Near-infrared

MIR = Mid-infrared

SD = Standard deviation

To check the accuracy of the classification process, the study area was visited on October 12, 2003. During the field visit, the following materials were referred to: Thomas Guide (2004), a topographic map with a scale of 1:24,000, and an earlier version (1993) of the SCAG (Southern California Association of Governments) land use map printed in hard-copy. Photographs of the selected sites visited were taken. Aerial photos acquired in year 2000 with a resolution of one meter were later consulted to identify the classes of the test pixels that were used for accuracy assessment.

To calculate the overall imperviousness in the study area, a land use digital map published by SCAG was downloaded from the UCLA GIS Database. It was in vector format and then converted to its raster equivalent using ArcGIS 9.0. It is georeferenced to the same projection as the satellite image, UTM, Zone 11 (North). However, it is referenced to another spheroid, GRS 1980, but this was not an issue, as we were dealing with a small study area. The SCAG land use map was compiled using digital aerial

imagery acquired in year 2000. Percentages of imperviousness for specific types of land uses are available from the Los Angeles County Department of Public Works (LACDPW).

The image processing and GIS software used was ERDAS Imagine 8.7. This application package has a knowledge-based classification system, and lets the knowledge engineer assemble the knowledge base to fill the empty shell. There is a feature called spatial modeler where the knowledge engineer can make models the outputs of which can be incorporated in the knowledge base.

8.3 Methodology

8.3.1 Calculation of the Jeffries-Matusita Distances

To determine if classes of interest can be distinguished in a satellite image, there are separability measures available to know how unique the spectral signatures are. One of these is the Jeffries-Matusita (J-M) distance (Richards, 1986), although there are others. We selected training areas on classes of interest on an NDVI image (defined in the next page). This transformed image is shown in Figure 8.3. Each training area was associated with the signature of a particular class. From that group of pixels, means and covariances were calculated. With these two parameters, the J-M distances were computed. In ERDAS Imagine, a J-M distance of zero means that the classes cannot be separated in that particular image or combination of images, and a J-M distance of 1414 signifies that the two classes are completely separable. The land cover classes we

designated were water, impervious surface, soil, vegetation, and beach. Soil could mean bare soil or soil with sparse vegetation.

We calculated the J-M distances for the six raw bands and also for the following transformed images. The following equations define each pixel value in the transformed images. In these equations, the name of the band corresponds to the DN value in that band.

$$\text{Normalized Difference Vegetation Index (NDVI)} = \frac{(\text{NIR band} - \text{red band})}{(\text{NIR band} + \text{red band})} \quad (8.1)$$

$$\text{IR/R} = \text{NIR band} / \text{red band} \quad (8.2)$$

$$\text{SQRT (IR/R)} = (\text{NIR band} / \text{red band})^{1/2} \quad (8.3)$$

$$\text{Vegetation Index} = \text{NIR band} - \text{red band} \quad (8.4)$$

$$\text{Transformed NDVI (TNDVI)} = \frac{((\text{NIR band} - \text{red band}) / (\text{NIR band} + \text{red band})) + 0.5}{1}^{1/2} \quad (8.5)$$

At first, only the five initial classes were considered for the calculation of J-M distances. However, during the initial classifications, we found that the impervious surfaces among the residential areas were misclassified. We concluded that this class had a distinct spectral signature, and hence was designated as another class. The training areas are shown in Figure 8.4.



0 1 km

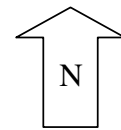


Figure 8.3: Normalized Difference Vegetation Index (NDVI) image

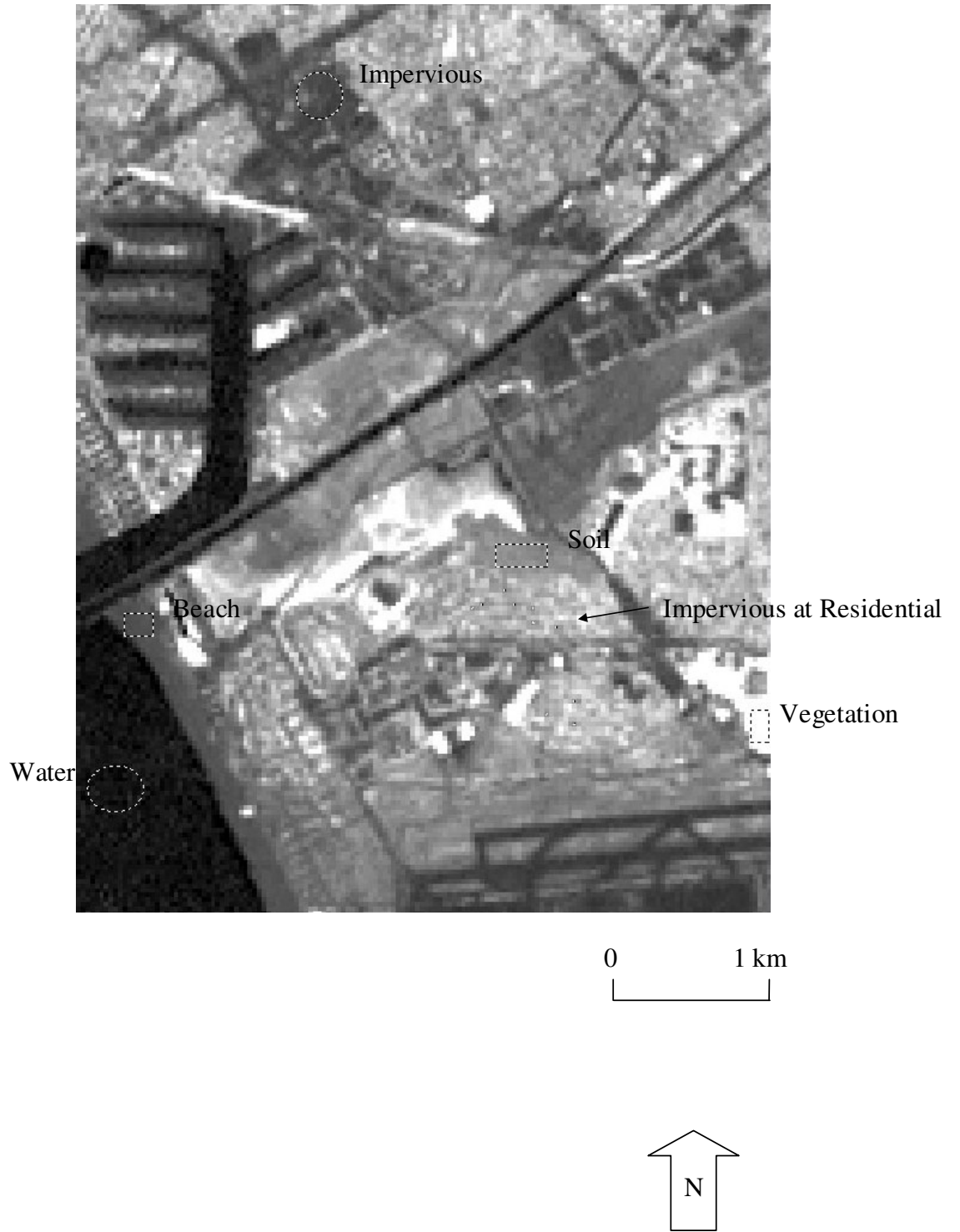


Figure 8.4: Training areas on NDVI image

Table 8.2 shows the J-M distances for the six classes using the NDVI image. Similar tables were made for the other transformed images. However, for the raw image, the J-M distances were calculated using different combinations of bands. The number of bands could also be selected. Using only one band showed lower J-M distances, and using all the six bands showed higher J-M distances. This meant that the more bands were selected, the more separable classes became. Table 8.3 shows the J-M distances when all six raw bands were considered.

Table 8.2: Jeffries-Matusita distances for the NDVI image

	Water	Imper- vious	Soil	Vege- tation	Beach	IAR
Water	0	1382	1414	1414	1413	1414
Impervious	1382	0	1401	1414	433	1393
Soil	1414	1401	0	1412	1414	170
Vegetation	1414	1414	1412	0	1414	1412
Beach	1413	433	1414	1414	0	1414
IAR	1414	1393	170	1412	1414	0

IAR = Impervious Surface at Residential

Table 8.3: Jeffries-Matusita distances for the raw image (6 bands)

	Water	Imper- vious	Soil	Vege- tation	Beach	IAR
Water	0	1414	1414	1414	1414	1414
Impervious	1414	0	1414	1414	1411	1412
Soil	1414	1414	0	1414	1414	1414
Vegetation	1414	1414	1414	0	1414	1414
Beach	1414	1411	1414	1414	0	1414
IAR	1414	1412	1414	1414	1414	0

IAR = Impervious Surface at Residential

8.3.2 Knowledge-Based Classification

Among the transformed images, the NDVI image generally showed the best separability values. Therefore, we chose this image to make rules for classification. The J-M distances using the NDVI image indicated that most classes should be highly separable except for the impervious-beach pair and the soil-impervious at residential pair. From training areas and from observations of random pixels, it was found that the range of the NDVI values could be generally divided among the four classes. Water's NDVI values ranged from 0 to less than 36, impervious surface's values were from 36 to less than 64, soil, from 64 to less than 85, and vegetation, from 85 to 255. As indicated by the J-M distance of 433, impervious surface and beach cannot be separated because their NDVI values overlap. Indeed, the NDVI values for beach ranged from 45 to 51. They had similar values except that beach had a narrower range. An initial classification using only the NDVI values above totally excluded beach. This also misclassified the impervious surfaces among the residential areas to soil, as predicted by the low J-M distance of 170.

To solve these initial misclassifications, we considered the raw image, and noted that the J-M distance between impervious surface and beach is 1411 (Table 8.3), which meant they were highly separable but not totally using the six raw bands. From the statistics of the training areas, we noted the range of DNs covering beach in each raw band and incorporated them in the knowledge base. We also noted that the J-M distance between soil and impervious surface among residential in the raw image is 1414. So a similar task was performed to recover the misclassified impervious surfaces among the residential areas.

The result of this first classification (Figure 8.5) had several impervious surface pixels misclassified to beach. We knew that beach could be found only near the ocean, and not inland. Therefore, for the second classification, we separated the ocean using standard GIS tools such as clumping and recoding. At first, we made a buffer zone of just five pixels (142.5 m) from the ocean, and made a rule stating that if a pixel was classified as beach but outside the buffer zone, then the classifier should reassign the pixel to impervious surface. However, this rule reassigned correctly classified beach pixels to impervious surface. Therefore, we increased the buffer distance to 30 pixels (855 m), and this solved the problem. Figure 8.6 shows the classification procedure.

The second classification was then refined by using another ancillary data, in this case the location of pixels relative to each other. First, we created a majority image using standard GIS neighborhood tools. A 3 x 3 filter was superimposed at each pixel. Whatever the majority value was for that group of nine pixels, would replace the value in the center pixel. Next, we looked at the second classification image. We considered each pixel, and observed its neighbors in the north, east, west, and south directions (Figure 8.7). If the pixel's class, for example, soil, was the same as its neighbor's class in the north, there was a high probability that the pixel under consideration also belonged to the soil class. Indeed, we designated that if at least three of its neighbors were of the same class, then we retained the class of that pixel. If not, it would be replaced by the class in the majority image. Figure 8.8 shows the third classification described above.

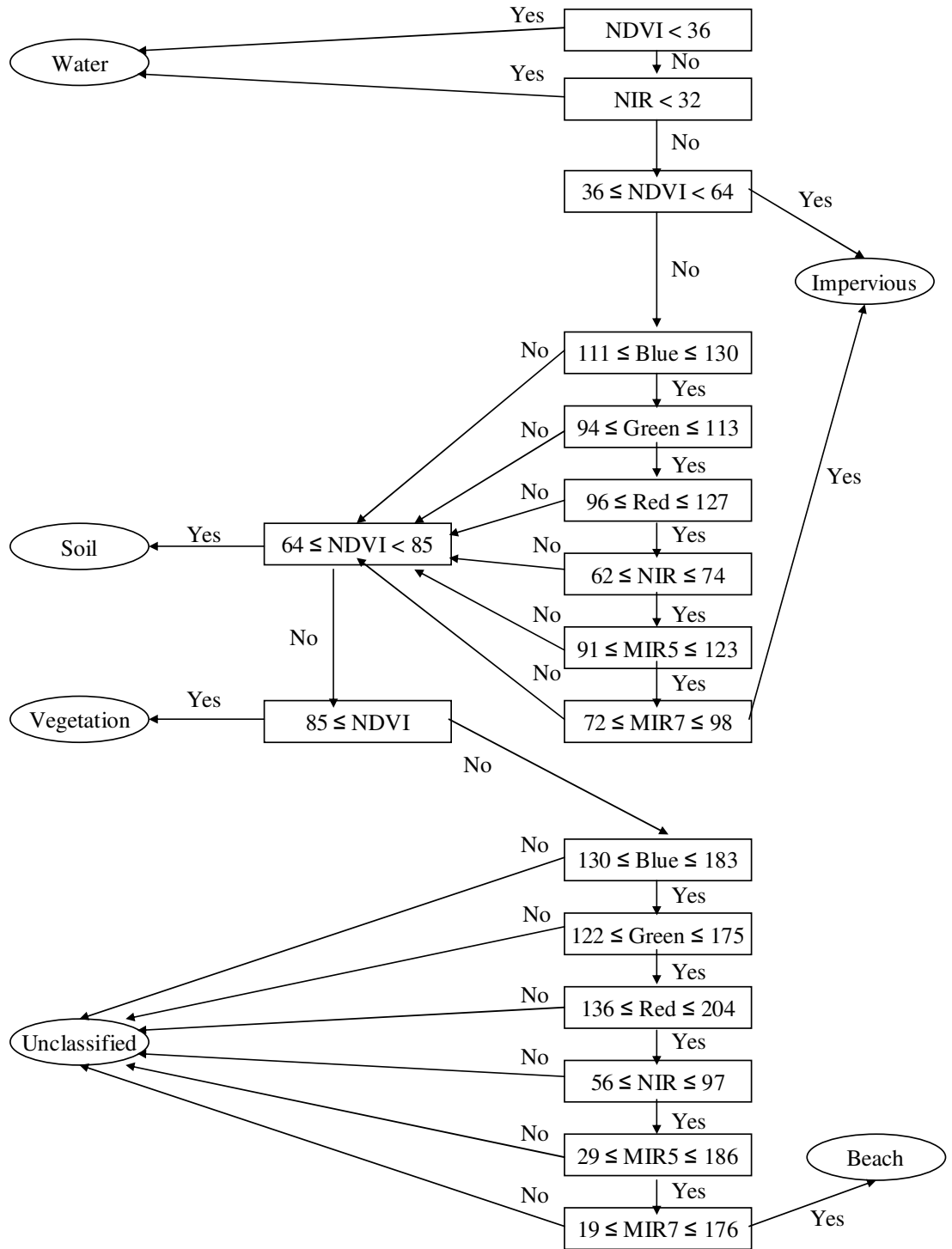


Figure 8.5: Knowledge base with spectral data

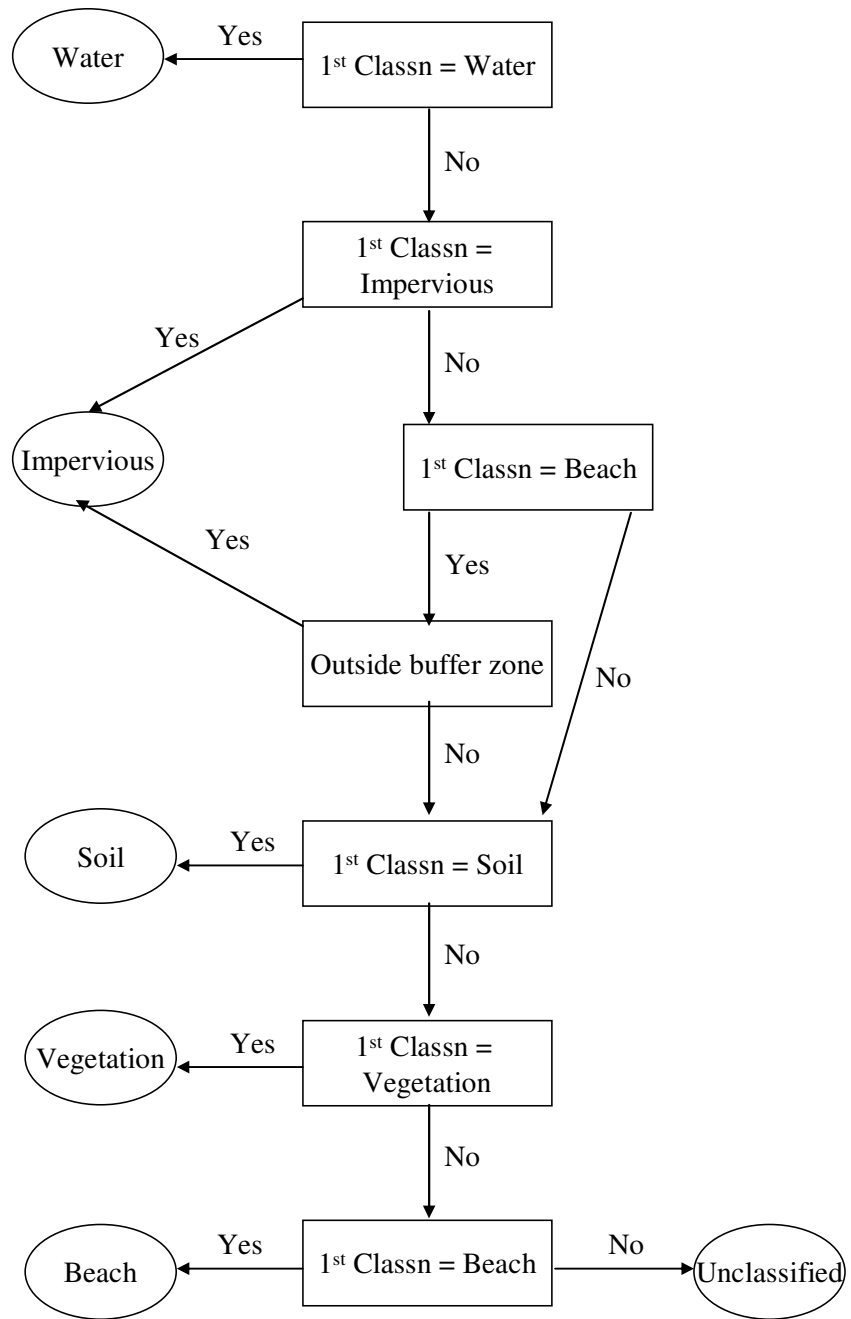


Figure 8.6: Knowledge base with spectral data and buffer zone

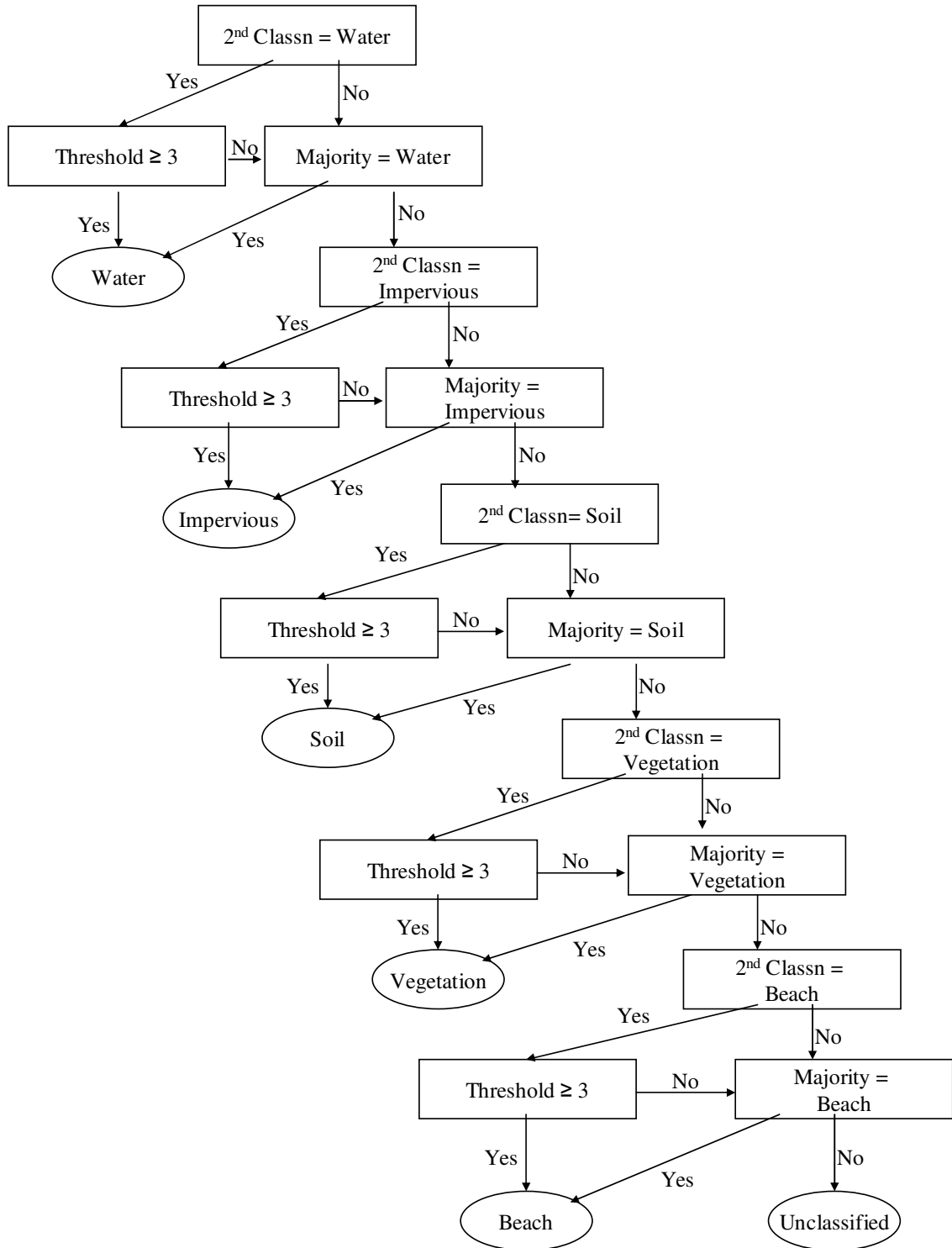


Figure 8.8: Knowledge base with spectral data, buffer zone, and neighborhood information

In knowledge-based classification, a pixel is subjected to a series of rules, and is assigned a class when a set of criteria have been met. Sequencing of the rules is important because only one rule can be fired at one time. Once a pixel is assigned to a class, it can no longer be considered for other classes. However, confidences can be changed such that rules with higher confidences are fired first before rules with lower confidences. In our classifications, there were many refinements applied to the rules. For example, using only the NDVI image, we saw that the water was not continuous in the Ballona Creek and in the inner waters. But using only the NIR band left some of the pixels unclassified in the area where the beach met the ocean. Therefore, we decided to use both NDVI and NIR rules to avoid unclassified pixels and at the same time, made the water body as continuous as possible. Also, although the beach looked homogeneous, we actually selected a training area which was not representative of the spectral variability of the entire beach area. Therefore, we took note of the raw DN values in the initial misclassifications (to impervious surface), and modified the rules in the two mid-infrared bands.

8.3.3 Maximum Likelihood Classification

We also performed a maximum likelihood (MXL) classification (Richards, 1986) using the same training areas used to compute the J-M distances. We applied MXL on the raw and NDVI images. The MXL classification is a standard statistical classifier usually employed to compare with new, proposed classification techniques. It is the most common method to classify land use and land cover. All standard image processing

software packages usually have this tool. In maximum likelihood classification, the mean and the covariance matrix of the group of pixels in the selected training areas are computed. Based on these values, the probability of a pixel being classified to a specific category is calculated, and it is assigned to the class where the likelihood is highest. The success of the MXL procedure depends on the correct selection of training areas.

8.3.4 Calculation of Overall Imperviousness

The original SCAG land use digital map was in vector format, and was rasterized using ArcGIS 9.0. The map initially had 48 classes, which were regrouped to seven classes (Table 8.4) that were relevant in the calculation of the imperviousness of the study area. Table 8.5 shows the seven classes and their associated imperviousness. Figure 8.9 shows the modified SCAG land use map. To compute for the imperviousness, we multiplied the percent imperviousness by the area, and then added the entire impervious surface. The overall imperviousness in the study area is 10.2 sq km. For the classified images, overall imperviousness was estimated by multiplying the total number of impervious pixels by 28.5 m twice.

Table 8.4: Aggregation of original SCAG classes to categories relevant to stormwater modeling

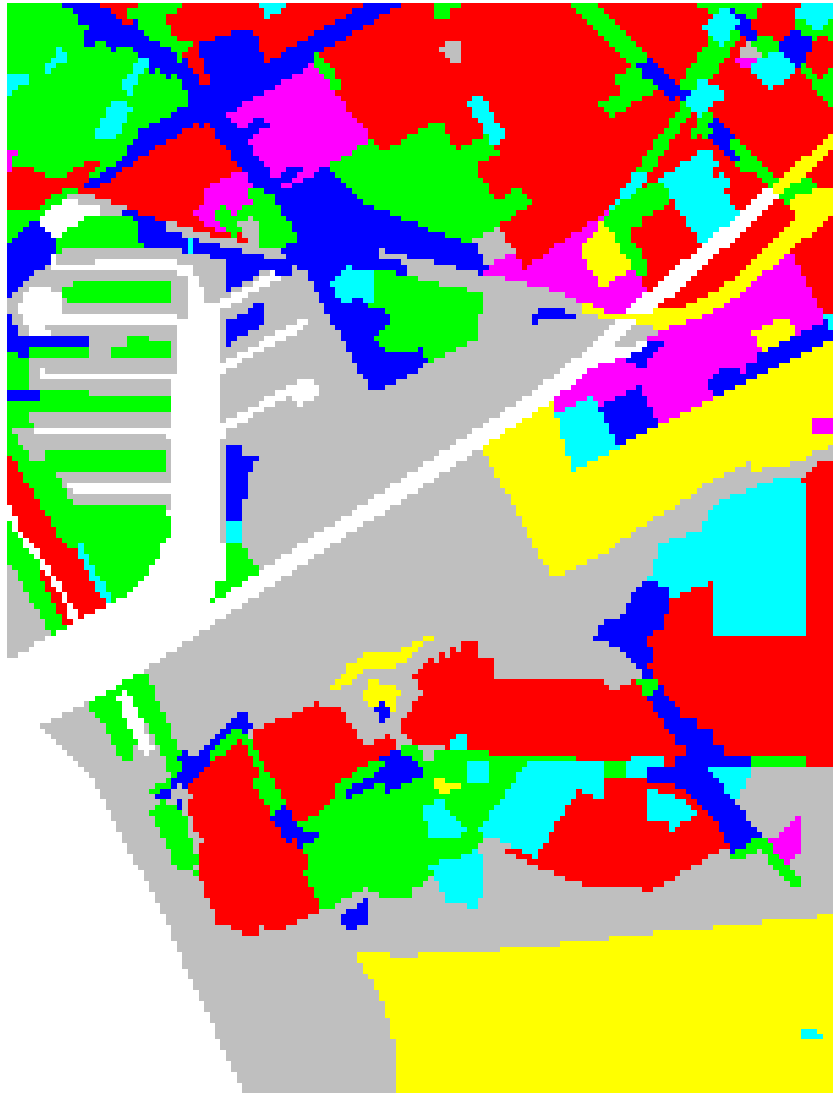
Original SCAG Class	New Class
High Density Single Family Residential	Single-Family
Duplexes Triplexes and 2 or 3 Unit Condos and Town	Multi-Family
Low-Rise Apartments Condominiums and Townhouses	
Medium-Rise Apartments and Condominiums	
High-Rise Apartments and Condominiums	
Mixed Residential	
Low- and Medium-Rise Major Office Use	Commercial
High-Rise Major Office Use	
Regional Shopping Mall	
Retail Centers Non-Strip Contiguous Interconnected	
Modern Strip Development	
Older Strip Development	
Commercial Storage	
Commercial Recreation	
Hotels and Motels	
Attended Pay Public Parking Facilities	
Government Offices	Public
Police and Sheriff Stations	
Fire Stations	
Major Medical Health Care Facilities	
Religious Facilities	
Other Public Facilities	
Non-Attended Public Parking Facilities	
Other Special Use Facilities	
Elementary Schools	
Junior or Intermediate High Schools	
Senior High Schools	
Colleges and Universities	Light Industrial
Manufacturing Assembly and Industrial Services	
Research and Development	
Wholesaling and Warehousing	
Mixed Commercial and Industrial	

Table 8.4 (Cont.): Aggregation of original SCAG classes to categories relevant to stormwater modeling

Original SCAG Class	New Class
Airports	Other Urban
Freeways and Major Roads	
Communication Facilities	
Electrical Power Facilities	
Natural Gas and Petroleum Facilities	
Improved Flood Waterways and Structures	
Maintenance Yards	
Under Construction	
Golf Courses	Open
Local Park Developed	
Wildlife Preserves and Sanctuaries	
Beach Parks	
Other Open Space and Recreation	
Vacant Undifferentiated	
Marina Water Facilities	

Table 8.5: Overall imperviousness determined from SCAG and LACDPW

Land Use Class	Number of Pixels	Area (sq km)	Percent Imperviousness	Impervious Area (sq km)
Single-Family	6,306	5.1	0.42	2.2
Multiple-Family	3,746	3.0	0.68	2.1
Commercial	2,186	1.8	0.92	1.6
Public	1,566	1.3	0.80	1.0
Light Industrial	1,096	0.9	0.91	0.8
Other Urban	3,888	3.2	0.80	2.5
Open	11,612	9.4	0	0
Total	30,400	24.7		10.2



- Single-Family
- Multiple-Family
- Commercial
- Public
- Light Industrial
- Other Urban
- Open

0 1 km

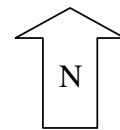


Figure 8.9: SCAG land use map (48 classes aggregated to 7 classes)

8.3.5 Accuracy Assessment

To test the initial rules, a few pixels were chosen for accuracy assessment. The program has a random number generator. At least 50 pixels were needed for each class (Congalton, 1991), and 250 pixels were initially selected (5 classes x 50 pixels). We found that beach was poorly represented so we added 30 more pixels. However, not exactly 50 pixels were assigned to each class. The random number generator worked on an image which was classified by ISODATA (Iterative Self-Organizing Data Analysis Technique) with 14 clusters. In essence, the ISODATA tool groups pixels according to the similarity of their DN's in all the bands (Richards, 1986). We believed there were 14 spectral classes present in the image which could be merged to define the five major classes we have designated. Next, we added more points to reflect the areal distribution of the five classes. In this case, biases could be avoided because the number of test pixels in a class was proportional to their corresponding area in a preliminary classification. The total number of test pixels was 1,040, which represented 3.4% of the entire study area. Table 8.6 shows how the test pixels were distributed among the land cover classes. Finally, we generated the error matrices for all classifications (Table 8.7-8.11).

Table 8.6: Distribution of test pixels

Class	Number of Test Pixels	Percentage of Total
Water	104	10.0
Impervious	286	27.5
Soil	324	31.2
Vegetation	276	26.5
Beach	50	4.8
Total	1,040	100

Table 8.7: Error matrix (using raw & NDVI images)

		Reference					
		Water	Imper- vious	Soil	Vege- tation	Beach	Row Total
Classification	Water	106	6	0	1	3	116
	Impervious	2	312	13	9	1	337
	Soil	2	41	174	11	0	228
	Vegetation	0	14	13	251	1	279
	Beach	0	25	1	0	54	80
	Column Total	110	398	201	272	59	1040
Producer's Accuracy				User's Accuracy			
Water	=	96.4%	Water	=	91.4%		
Impervious	=	78.4%	Impervious	=	92.6%		
Soil	=	86.6%	Soil	=	76.3%		
Vegetation	=	92.3%	Vegetation	=	90.0%		
Beach	=	91.5%	Beach	=	67.5%		
Overall Accuracy = 86.2%							

Table 8.8: Error matrix (using raw & NDVI images, & buffer zone)

		Reference					
		Water	Imper- vious	Soil	Vege- tation	Beach	Row Total
Classification	Water	106	6	0	1	3	116
	Impervious	2	342	13	9	1	367
	Soil	2	36	174	11	0	223
	Vegetation	0	13	13	251	1	278
	Beach	0	1	1	0	54	56
	Column Total	110	398	201	272	59	1,040
Producer's Accuracy				User's Accuracy			
Water	=	96.4%	Water	=	91.4%		
Impervious	=	85.9%	Impervious	=	93.2%		
Soil	=	86.6%	Soil	=	78.0%		
Vegetation	=	92.3%	Vegetation	=	90.3%		
Beach	=	91.5%	Beach	=	96.4%		
Overall Accuracy = 89.1%							

Table 8.9: Error matrix (using raw & NDVI images, buffer zone, & neighborhood info.)

		Reference					
		Water	Imper- vious	Soil	Vege- tation	Beach	Row Total
Classification	Water	104	8	0	1	3	116
	Impervious	3	323	23	11	1	361
	Soil	3	44	161	15	0	223
	Vegetation	0	22	16	245	1	284
	Beach	0	1	1	0	53	55
	Unclassified	0	0	0	0	1	1
	Column Total	110	398	201	272	59	1040
Producer's Accuracy				User's Accuracy			
Water	=	94.5%	Water	=	89.6%		
Impervious	=	81.2%	Impervious	=	89.5%		
Soil	=	80.1%	Soil	=	72.2%		
Vegetation	=	90.1%	Vegetation	=	86.3%		
Beach	=	89.8%	Beach	=	96.4%		
Overall Accuracy = 85.2%							

Table 8.10: Error matrix (using MXL on raw image)

		Reference					
		Water	Imper- vious	Soil	Vege- tation	Beach	Row Total
Classification	Water	78	0	0	0	0	78
	Impervious	32	391	114	180	4	721
	Soil	0	3	65	6	0	74
	Vegetation	0	1	22	86	1	110
	Beach	0	3	0	0	54	57
	Column Total	110	398	201	272	59	1040
Producer's Accuracy				User's Accuracy			
Water	=	70.9%	Water	=	100.0%		
Impervious	=	98.2%	Impervious	=	54.2%		
Soil	=	32.3%	Soil	=	87.8%		
Vegetation	=	31.6%	Vegetation	=	78.2%		
Beach	=	91.5%	Beach	=	94.7%		
Overall Accuracy = 64.8%							

Table 8.11: Error matrix (using MXL on NDVI image)

		Reference					
		Water	Imper- vious	Soil	Vege- tation	Beach	Row Total
Classification	Water	90	1	0	0	6	97
	Impervious	19	306	133	54	9	521
	Soil	0	43	65	40	0	148
	Vegetation	0	6	3	178	1	188
	Beach	1	42	0	0	42	85
	Unclassified	0	0	0	0	1	1
	Column Total	110	398	201	272	59	1040
Producer's Accuracy				User's Accuracy			
Water	=	81.8%		Water	=	92.8%	
Impervious	=	76.9%		Impervious	=	58.7%	
Soil	=	32.3%		Soil	=	43.9%	
Vegetation	=	65.4%		Vegetation	=	94.7%	
Beach	=	71.2%		Beach	=	49.4%	
Overall Accuracy = 65.5%							

8.4 Results and Discussion

Table 8.8 shows the error matrix for the second classification image, which is the best classified image. The values in the diagonal are the number of pixels correctly identified. For example, there were 106 water pixels in the group of test pixels which were correctly classified as water pixels in the classification. Off-diagonal values represent erroneous classifications. For example, there were six pixels that were classified as water but were impervious surface in reality. The overall accuracy is the sum of the correctly classified pixels divided by the total number of test pixels. We see that the classification is satisfactory, with a high accuracy of 89.1%. Just by looking at the

producer's and user's accuracy, we find that all the land cover classes were classified well. We consider the impervious surface because this is the class that we must locate. The producer's accuracy is 85.9%, which means that the producer of the classification (i.e., the knowledge engineer) classified the image well. 85.9% of the impervious surface in the study area has been classified as such. The user who visits the field and goes to a specific area classified as impervious surface has a 93.2% (user's accuracy) chance that the area is actually impervious. Even if considering only the impervious class, this is a fairly good classification. Generally, an 85% or higher accuracy is considered satisfactory.

Table 8.12 compares the three knowledge-based (KBS) systems and the two MXL classifications. The overall accuracy is fairly high for all the three KBS classifications. The addition of the buffer distance from the ocean increased the accuracy by 2.9%. However, the addition of neighborhood information did not necessarily increase the overall accuracy. However, the overall imperviousness increased with the subsequent addition of ancillary data. We suspect that not all impervious surfaces in the residential areas were detected. This will require a refinement of the rules. The producer's accuracy of just 78.4% in the first classification is due to the fact that large areas of impervious surfaces were classified to beach. We see a large improvement to a producer's accuracy of 85.9% when the buffer distance was applied. However, using neighborhood functions, the producer's accuracy dropped to 81.2%. This is probably due to many impervious pixels being filtered out by the model. To solve this problem, we can vary the threshold,

or even apply the threshold only to some classes. All the user's accuracies are generally good.

Table 8.12: Comparison of classifications

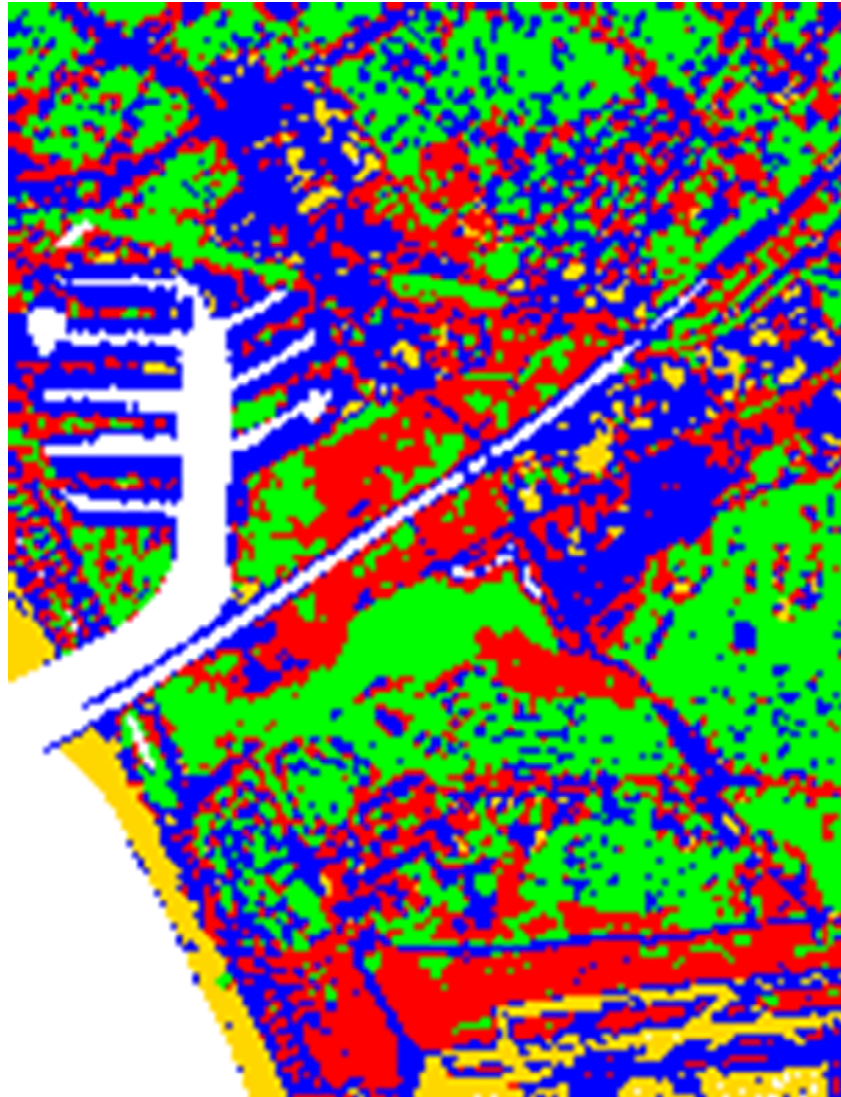
Parameter	KBS- Raw & NDVI	KBS- Raw & NDVI, Buffer	KBS- Raw & NDVI, Buffer, Neighbor- hood	MXL- Raw	MXL- NDVI
Overall Accuracy	86.2%	89.1%	85.2%	64.8%	65.5%
Producer's Accuracy (Impervious)	78.4%	85.9%	81.2%	98.2%	76.9%
User's Accuracy (Impervious)	92.6%	93.2%	89.5%	54.2%	58.7%
Overall Imperviousness	7.5 sq km	8.4 sq km	8.5 sq km	17.0 sq km	10.6 sq km
Error Rate on Overall Imperviousness	-26.5%	-17.6%	-16.7%	+66.7%	+3.9%

Regarding the MXL classifications, we see that the overall classification is poor (64.8% and 65.5%). Although the J-M distances showed high separability, it is possible that the complete variability of classes were not taken into account. In addition, the J-M distances were low between the impervious-beach pair and soil-impervious at residential pair. So these low accuracies are not a surprise. For the MXL classifications on the raw image, although the producer's accuracy is high (98.2%), only 54.2% of these areas are actually impervious surfaces in the ground. The classifier produced more impervious areas that was why it overestimated the actual overall imperviousness (66.7% error rate).

For the MXL classification on the NDVI image, the overall imperviousness of 10.6 sq km is close to the value from public records (10.2 sq km). However, since the producer's and user's accuracies are low, it is doubtful that the impervious surfaces were classified to their correct locations. Using only the raw and NDVI images individually, we see that the overall classification is far less satisfactory than those achieved by the knowledge-based classifications, which utilized both sets of images. Figures 8.10 to 8.14 display the classified images.

8.5 Conclusions

Because different materials on the earth's surface reflect radiation in various amounts, they can be distinguished from satellite images. Impervious surfaces have components distinct from other land cover such as vegetation or soil. Therefore, satellite imagery is a good alternative to manual methods for mapping impervious surfaces. If spectral signatures overlap, ancillary data can be incorporated to increase the accuracy of the classification process. Knowledge-based systems and GIS are tools that can accommodate both spectral information and ancillary data. The advantage of these methods is that the knowledge engineer can interact with the knowledge base and modify it until an acceptable classification has been achieved.



0 1 km

-  Impervious Surface
-  Water
-  Soil
-  Vegetation
-  Beach

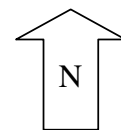
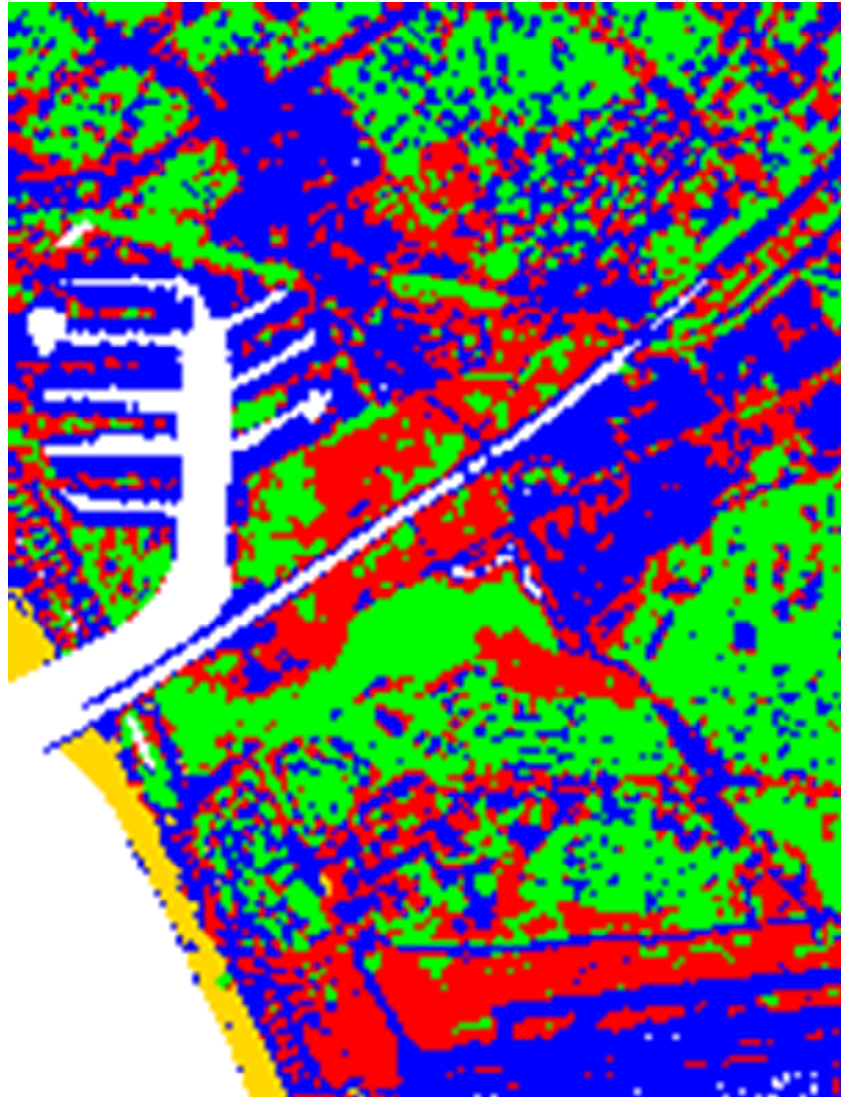


Figure 8.10: Knowledge-based classification with spectral data

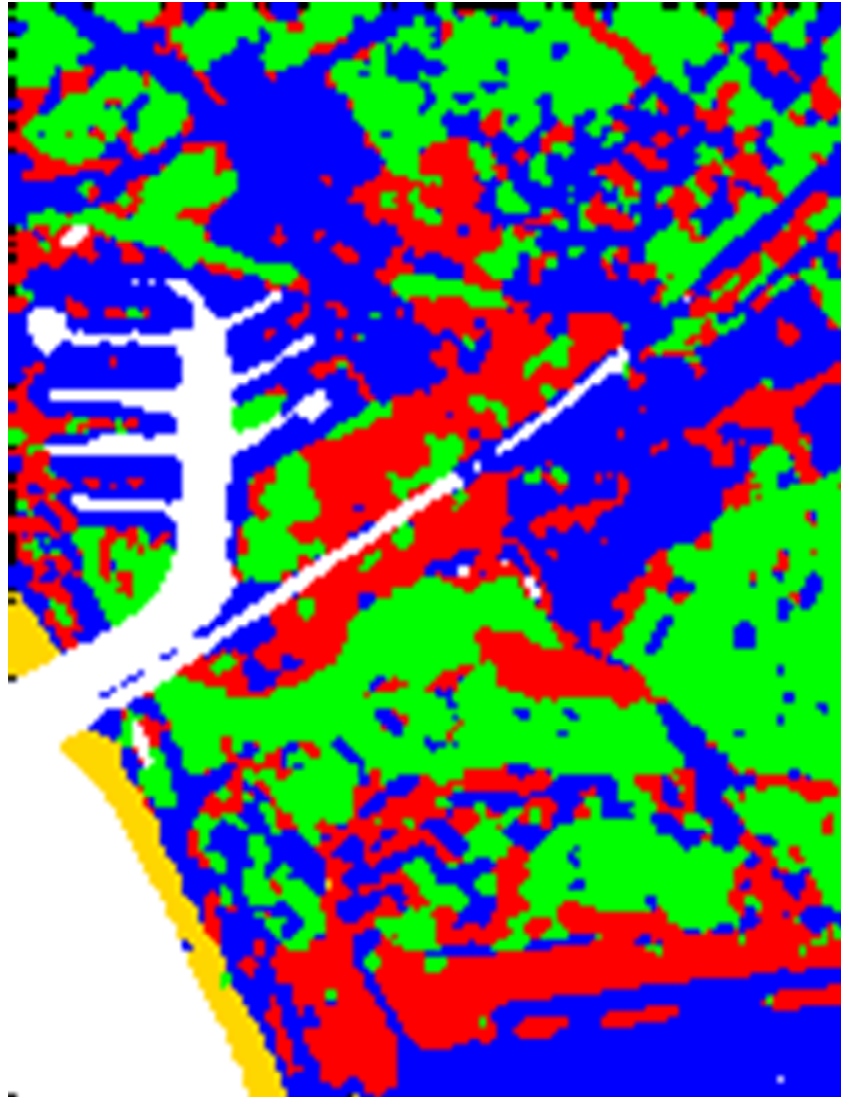


0 1 km

-  Impervious Surface
-  Water
-  Soil
-  Vegetation
-  Beach



Figure 8.11: Knowledge-based classification with spectral data and buffer zone



0 1 km

-  Impervious Surface
-  Water
-  Soil
-  Vegetation
-  Beach

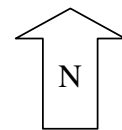
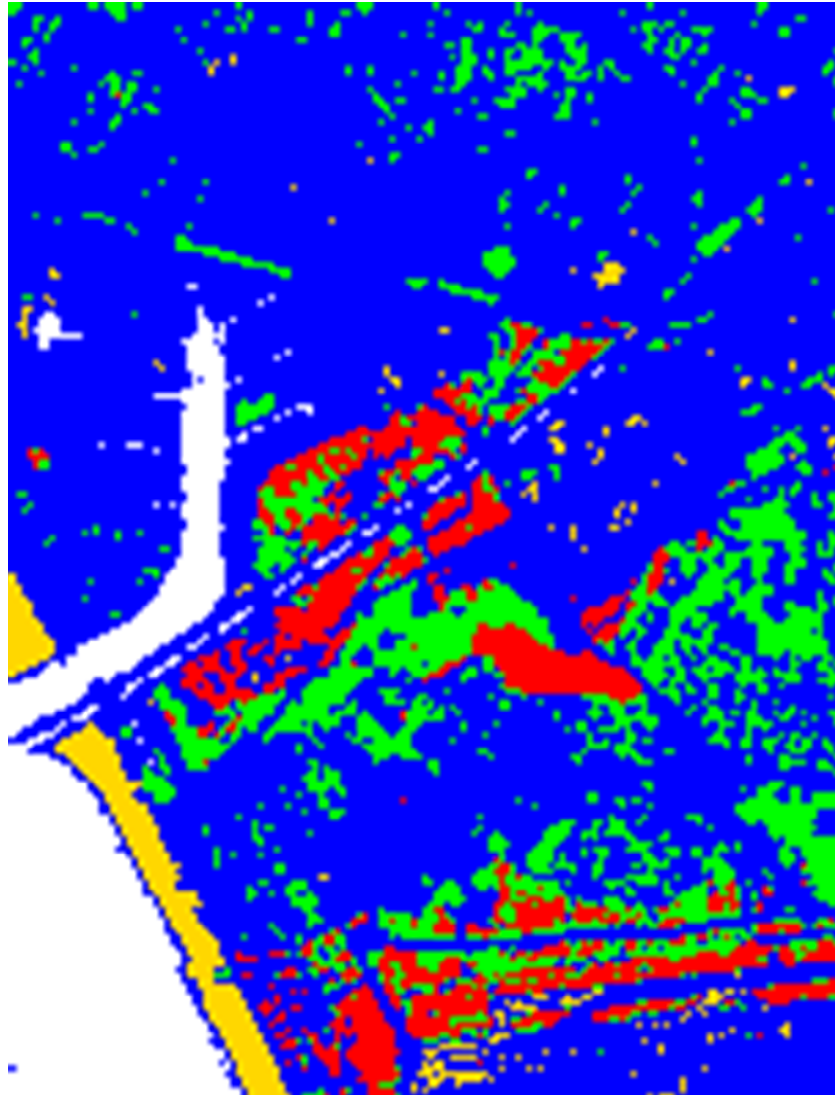


Figure 8.12: Knowledge-based classification with spectral data, buffer zone, and neighborhood information



0 1 km

-  Impervious Surface
-  Water
-  Soil
-  Vegetation
-  Beach

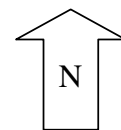
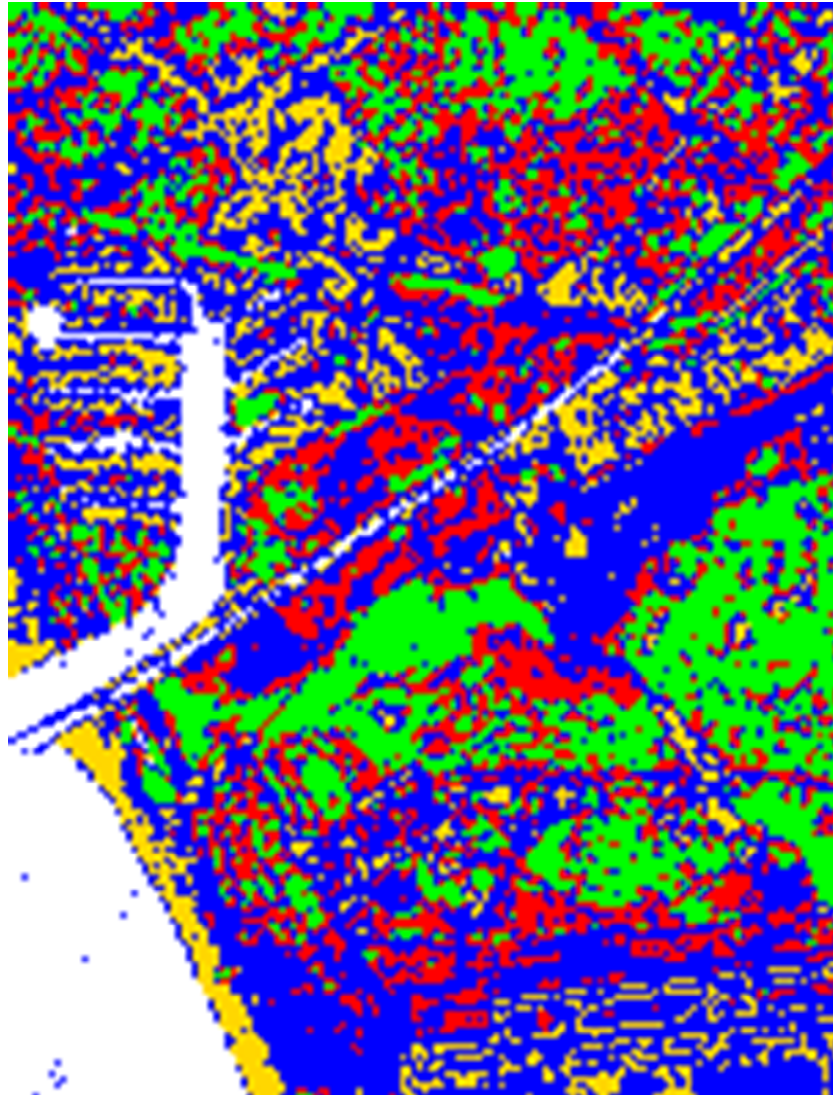


Figure 8.13: Maximum likelihood classification on raw image



0 1 km

-  Impervious Surface
-  Water
-  Soil
-  Vegetation
-  Beach

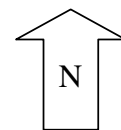


Figure 8.14: Maximum likelihood classification on NDVI image

8.6 References

Clarke, K.C. (1995) *Analytical and Computer Cartography, 2nd Edition*, Prentice-Hall, Inc., Upper Saddle River, New Jersey.

Congalton, R.G. (1991) A review of assessing the accuracy of classifications of remotely sensed data. *Remote Sensing of Environment*, 37 (1) 35-46.

Jackson, P. (1999) *Introduction to Expert Systems, 3rd Edition*, Addison-Wesley, U.S.A.

Johnsson, K. and Kanonier, J. (1991) Knowledge based land-use classification. In *Proceedings of the International Geoscience and Remote Sensing Symposium IGARSS '91*, 3-6 June, Espoo, Finland, pp. 1847-1850.

Middelkoop, H. and Janssen, L.L.F. (1991) Implementation of temporal relationships in knowledge based classification of satellite images. *Photogrammetric Engineering and Remote Sensing*, 57 (7) 937-945.

Richards, J.A. (1986) *Remote Sensing Digital Image Analysis: An Introduction*, Springer-Verlag, Germany.

Chapter 9

Estimation of Pollutant Loadings from Satellite Data

9.1 Introduction

Stormwater is a significant source of nonpoint pollution because it contains many toxic contaminants. Stormwater runoff can carry and distribute sediment, nutrients, oxygen-demanding organics, toxic substances, and pathogens to drainage systems and watercourses. Being able to identify land parcels with high stormwater pollutant emissions allows policy makers to prioritize specific areas in the watershed for the implementation of best management practices (BMPs). The amounts and types of pollutants generated are closely associated with land use. Hence, pollutant loadings are normally estimated from land use maps. These maps are usually assembled from aerial photography and field visits, which are tedious and time-consuming methods. In addition, land use data from public records, such as tax collection databases, are often poorly defined or categorized for environmental purposes. Levels of pollutant loadings can actually be estimated from remotely-sensed data because they are closely associated with land cover, unlike land use which has an economic component. Different types of land cover have distinct spectral signatures which enable them to be identified from satellite imagery.

9.2 Data, Materials, and Software

The goal of this investigation is to identify areas that show various pollution levels directly from remotely sensed data. The six water quality parameters considered were total suspended solids (TSS), biochemical oxygen demand (BOD5), total phosphorus (Total P), total Kjeldahl nitrogen (TKN), copper (Cu), and oil and grease (O & G). The study area selected was Marina del Rey and its vicinity described in Chapter 8. Data, materials, and software have also been discussed in that chapter. Event mean concentrations of pollutants were obtained from Stenstrom and Strecker (1993).

9.3 Methodology

9.3.1 Calculation of Pollutant Loadings

When it rains, not all water seeps to the ground. Because of impervious surfaces, some of the water becomes runoff and reaches a water body. The relationship of rainfall to runoff is:

$$RC = \text{runoff}/\text{rainfall} \quad (9.1)$$

where RC = runoff coefficient

It has been observed that RC is highly correlated with the amount of impervious surface.

An example of this relationship is:

$$RC = (0.7)I + 0.1 \quad (9.2)$$

where I = fraction of impervious surface of a land parcel

Imperviousness I depends on the type of land use. Hence RC can be calculated for different kinds of land use. Table 9.1 shows the runoff coefficient, calculated from equation (9.2) for the various land use types found in the Santa Monica Bay watershed.

Table 9.1: Land use characteristics

Land Use	Impervious Surface Area (I)	Runoff Coefficient (RC)
Single-Family	0.42	0.39
Multiple-Family	0.68	0.58
Commercial	0.92	0.74
Public	0.80	0.66
Light Industrial	0.91	0.74
Other Urban	0.80	0.66
Open	0	0.10

(from Wong *et al.*, 1997)

For a specific storm, the volume of water produced by rainfall is:

$$TVR = (A)(RF) \quad (9.3)$$

where TVR = total volume of water produced from rainfall in a single storm event

A = drainage area

RF = rainfall

However, only a fraction of this water becomes runoff, and its total volume is

$$RV = (RC)(A)(RF) \quad (9.4)$$

where RV = runoff volume/storm event

Usually, we have several storm events in a year. So the annual volume of runoff is

$$RVA = (RV)(NSTORM) \quad (9.5)$$

where RVA = total volume of runoff/year

NSTORM = total number of storms/year

Knowing the total volume of runoff and the event mean concentration of a particular pollutant gives us the pollutant loadings per year. In equation form, this is:

$$PL = (RVA)(EMC) \quad (9.6)$$

where PL = pollutant loadings/year

EMC = event mean concentration of a pollutant (mg/L)

In (9.6), RVA can be substituted by (9.5)

$$PL = (RV)(NSTORM)(EMC) \quad (9.7)$$

In (9.7), RV can be substituted by (9.4)

$$PL = (RC)(A)(RF)(NSTORM)(EMC) \quad (9.8)$$

We can calculate the pollutant loading for a unit area (a pixel whose size is 28.5 m x 28.5 m) and a unit rainfall of 10 mm. Wong *et al.* (1997) reported 16 storms per year in this watershed. If we substitute these values in (9.8), we get:

$$PL = (RC)(28.5 \text{ m})(28.5 \text{ m})(10 \text{ mm})(16 \text{ storms/year})(EMC) \quad (9.9)$$

which can be simplified to

$$PL = \mu(RC)(EMC) \quad (9.10)$$

where μ = product of the constants and conversion factors.

The above equation is valid only for a small area where it can be assumed that the rainfall is the same for all pixels, the number of storms is the same for all pixels, and all the water drains to the same water body. Table 9.2 shows the annual loadings for the six pollutants according to land use. Park and Stenstrom (2004) computed polluted loadings using a similar equation.

Table 9.2: Pollutant concentrations and annual loadings

Land Use	TSS		BOD5		Total P		TKN		Cu		O & G	
	C	L ₁	C	L ₁	C	L ₂	C	L ₁	C	L ₂	C	L ₁
SF	290	14.70	17	0.86	0.85	43.08	4.3	0.22	0.095	4.82	3	0.15
MF	210	15.83	15	1.13	0.62	46.73	2.4	0.18	0.100	7.54	22	1.66
Co	180	17.31	14	1.35	0.43	41.35	2.0	0.19	0.072	6.92	22	2.12
P	180	15.44	14	1.20	0.43	36.88	2.0	0.17	0.072	6.18	22	1.89
LI	180	17.31	14	1.35	0.43	41.35	2.0	0.19	0.072	6.92	22	2.12
OU	210	18.01	15	1.29	0.62	53.18	2.4	0.20	0.100	8.58	22	1.89
O	490	6.37	2	0.02	0.52	6.76	2.8	0.04	0.055	0.71	0	0

SF = Single-Family

MF = Multiple-Family

Co = Commercial

P = Public

LI = Light Industrial

OU = Other Urban

O = Open

C = Event mean concentration (mg/L) (from Stenstrom and Strecker, 1993)

L₁ = Loadings (kg/yr)

L₂ = Loadings (g/yr)

9.3.2 Knowledge-Based Classification

Our next task was to determine the pollution levels for each contaminant. We designated these levels as high, medium, and low loading. For TSS, because open land is mostly soil, it has the highest concentration of 490 mg/L. A fairly high concentration of TSS is also generated by single-family residential (at 290 mg/L) because of the presence of lawns. However, we found that open land has a low loading of only 6.37 kg/yr. For single-family, the loading is very similar to those of the other classes, although the concentration is higher. This is because the rest of the classes have higher runoff coefficients. Therefore, for TSS, we designated two classes: low loading for open areas (6.37 kg/yr), and high loading for the non-open areas (14.70 - 18.01 kg/yr). We observed

the same for BOD5, Total P, and TKN. For copper, we observed that open land has a low loading of 0.71 g/yr, single-family has a medium loading of 4.82 g/yr, and the rest of the classes have a high loading (6.18 - 8.58 g/yr). For oil and grease, we grouped open (no loading) and single family (0.15 kg/yr) as low loading and the rest as high loading (1.66 to 2.12 kg/yr). Oil and grease have high concentrations in parking lots which can be found mostly in commercial and light industrial areas (Stenstrom *et al.*, 1984). Table 9.3 shows the individual or range of values for the different pollution levels. Averages, whenever applicable, were also computed.

Table 9.3: Range and average loadings for the different pollution levels

Pollutant	High Loading-Range	High Loading-Average	Medium Loading-Range	Medium Loading-Average	Low Loading-Range	Low Loading-Average
TSS	14.70-18.01	16.43	-	-	6.37	6.37
BOD5	0.86-1.35	1.20	-	-	0.02	0.02
Total P	36.88-53.18	43.76	-	-	6.76	6.76
TKN	0.17-0.22	0.19	-	-	0.04	0.04
Cu	6.18-8.58	7.23	4.82	4.82	0.71	0.71
O & G	1.66-2.12	1.94	-	-	0-0.15	0.08

For TSS, BOD5, Total P, and TKN, we applied the tasseled cap transformation (Crist and Cicone, 1984) on the six bands of the Landsat ETM+ image. This transformation emphasizes vegetation and soil, both of which are components of open land. We used the greenness (Figure 9.1), wetness (Figure 9.2), and haze (Figure 9.3) layers from the resulting six-layer image and applied an ISODATA (Iterative Self-Organizing Data Analysis Technique) (Richards, 1986). The ISODATA procedure

groups the pixels according to the similarity of their digital numbers. The result of this procedure showed that open land was separated from all other classes. However, these classes also included water. Hence, we examined the bimodal histogram of the NIR band and found that the threshold to separate water was a digital number of 32. The procedure just described constituted the first classification using only spectral data (Figure 9.4). However, because the areas where the ocean meets the beach has a mixed spectral signature from both land covers, these pixels were classified to non-open land. Hence a buffer distance of 5 pixels (142.5 meters) was used to correct the misclassification (Figure 9.5). We then incorporated neighborhood information to the second classification. The idea is that neighboring pixels have a tendency to have similar classes. If a pixel A, for example, has been classified as TSS, high loading, and at least three of its immediate neighbors in the north, east, west, and south directions have also been classified as such, then pixel A retains that category. If not, the class is replaced by the majority value in a 3 by 3 filter. Figure 9.6 demonstrates a part of the neighborhood analysis just described. The graphic model essentially makes an image (called Threshold in Figure 9.6) with pixels showing the number of neighbors that has a similar class as the pixel of interest. Figure 9.7 shows the third classification incorporating neighborhood information just described.



0 1 km

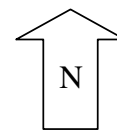


Figure 9.1: “Greenness” component of the tasseled cap transformation



0 1 km

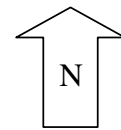


Figure 9.2: “Wetness” component of the tasseled cap transformation



0 1 km

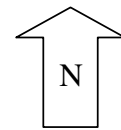


Figure 9.3: “Haze” component of the tasseled cap transformation

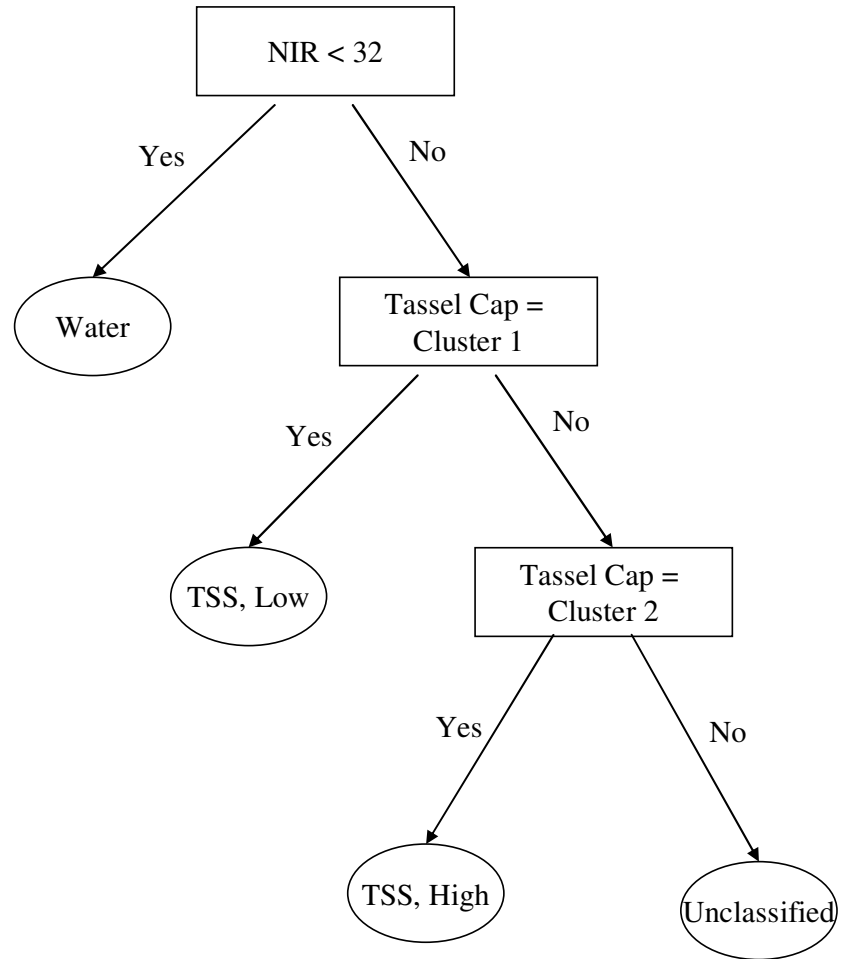


Figure 9.4: TSS loadings classification using spectral data (similar flowcharts for BOD5, Total P, and TKN)

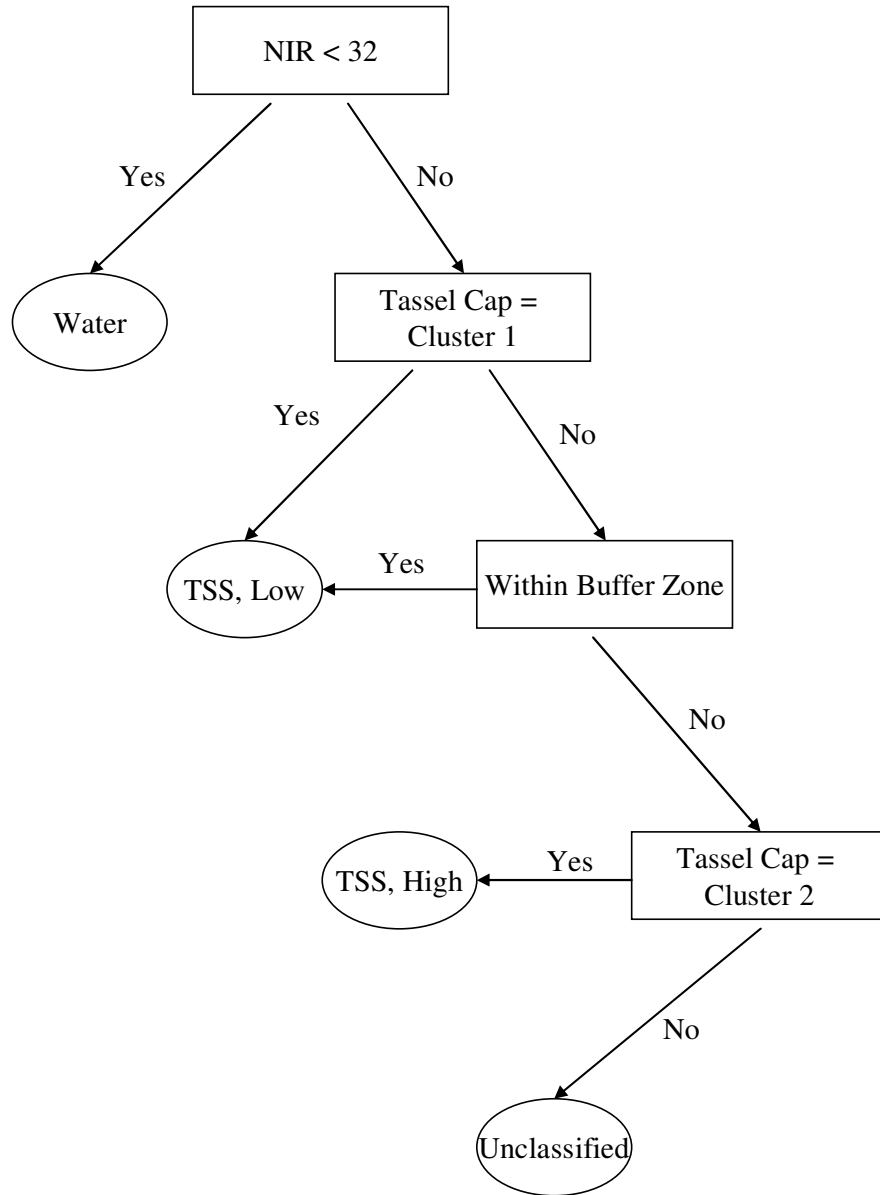


Figure 9.5: TSS loadings classification using spectral data and buffer zone (similar flowcharts for BOD5, Total P, and TKN)

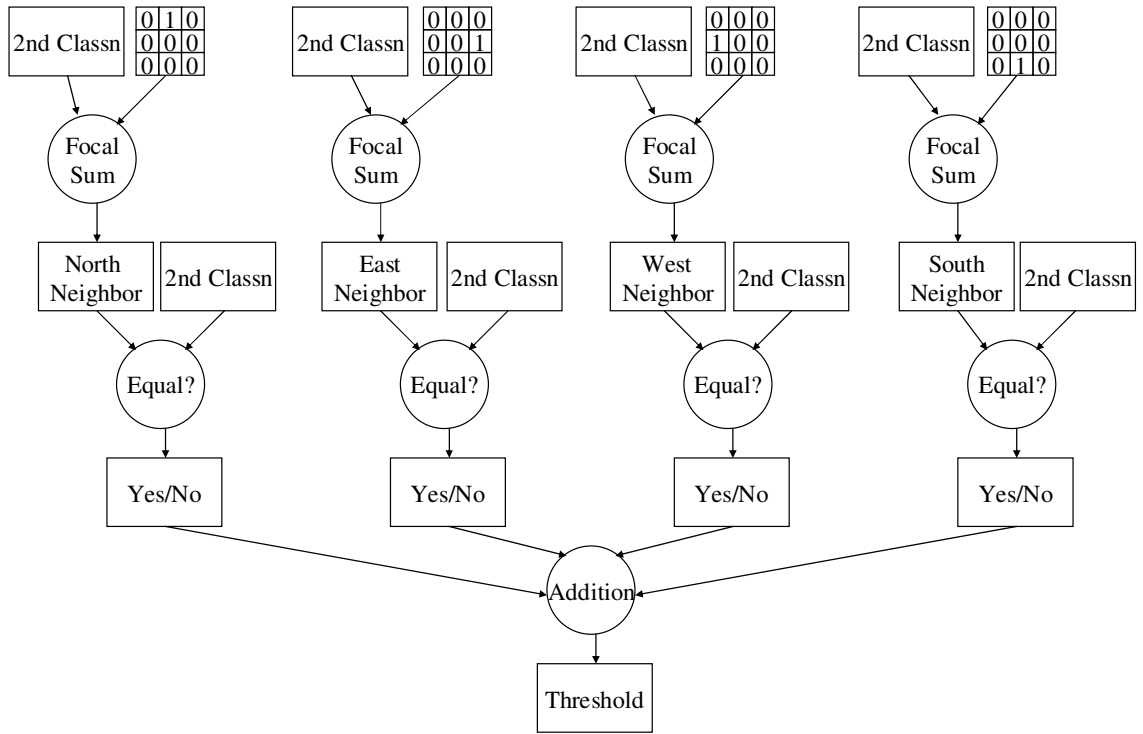


Figure 9.6: Neighborhood analysis

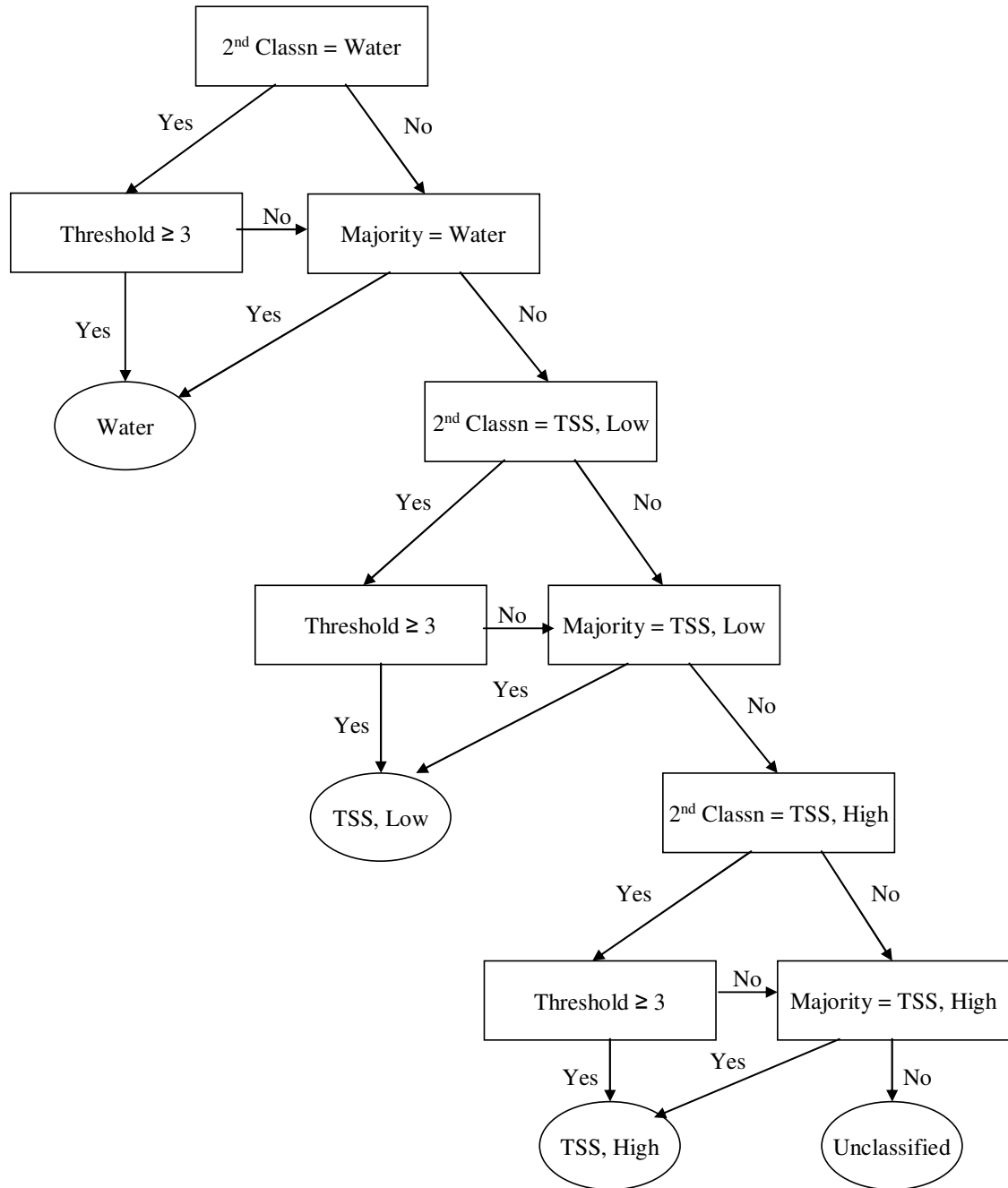


Figure 9.7: TSS loadings classification using spectral data, buffer zone, and neighborhood information (similar flowcharts for BOD5, Total P, and TKN)

For copper, similar tasks were performed except that there was a need to separate single-family from the non-open areas. The spectral signature of single-family is very distinct. We drew a training area on the raw image, generated the statistics, and used these parameters to make the rules. For oil and grease, the same steps were done. In this case, however, the single-family areas were merged to open land. Figures 9.8 to 9.13 display the flowcharts of the knowledge-based classification with spectral and ancillary data. Standard GIS operations were regularly used for spatial analysis.

9.3.3 Accuracy Assessment

We used 1,040 randomly generated test pixels (3.4% of the study area) to evaluate the quality of our classifications. The identities of several of these test pixels were derived from the SCAG land use map, but because the SCAG classification is not optimized for environmental purposes, the identities of some test pixels were incorrect for our study. In this case, the identities were manually recognized using the raw image and the aerial photographs. For example, airport, considered as other urban area, is actually composed of impervious surfaces and soil. Hence, test pixels falling on the soil were identified as open land. We observed the same for public because it is actually composed of different types of land cover. This class is particularly problematic because it has no distinct spectral signature.

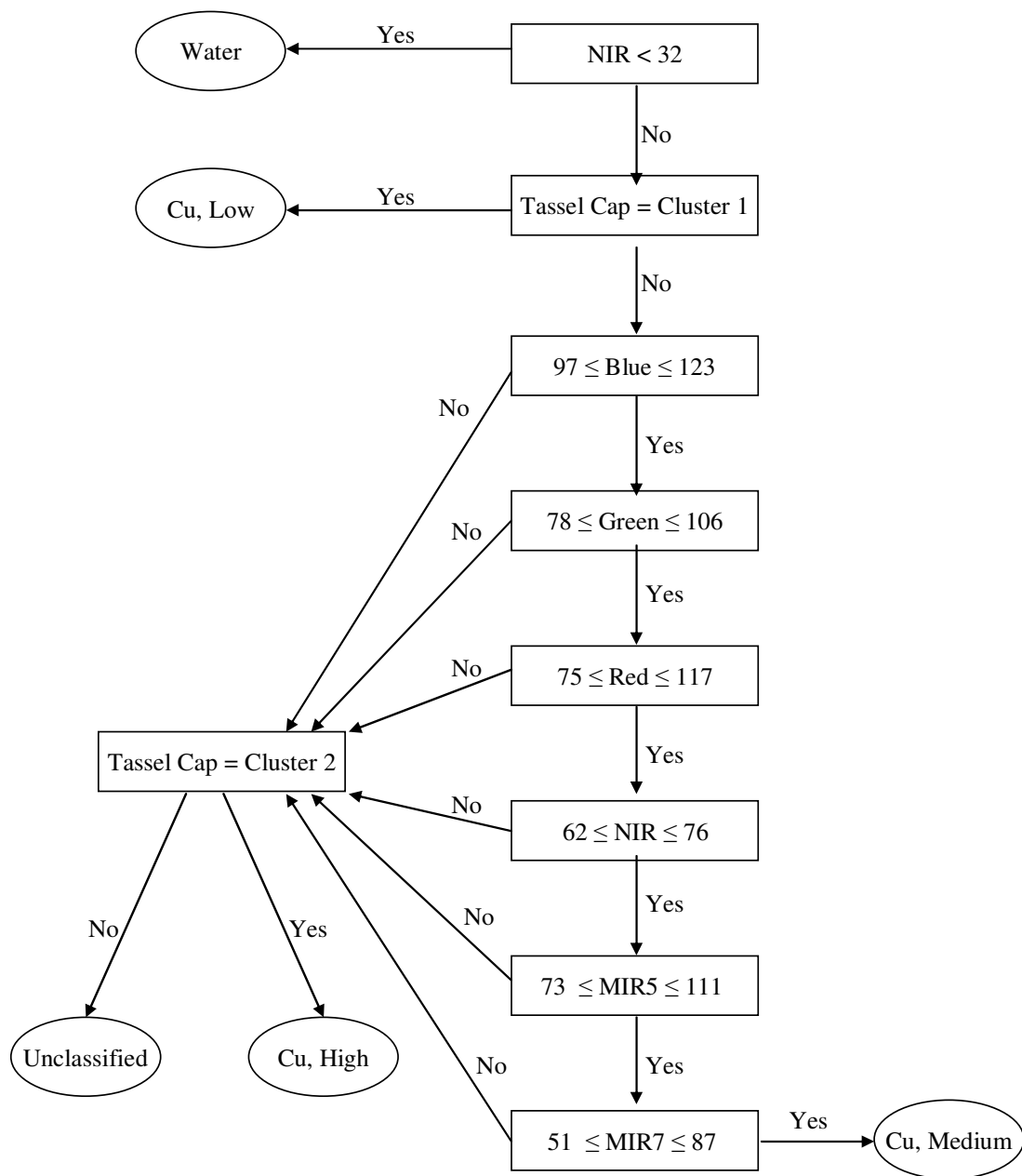


Figure 9.8: Copper loadings classification using spectral data

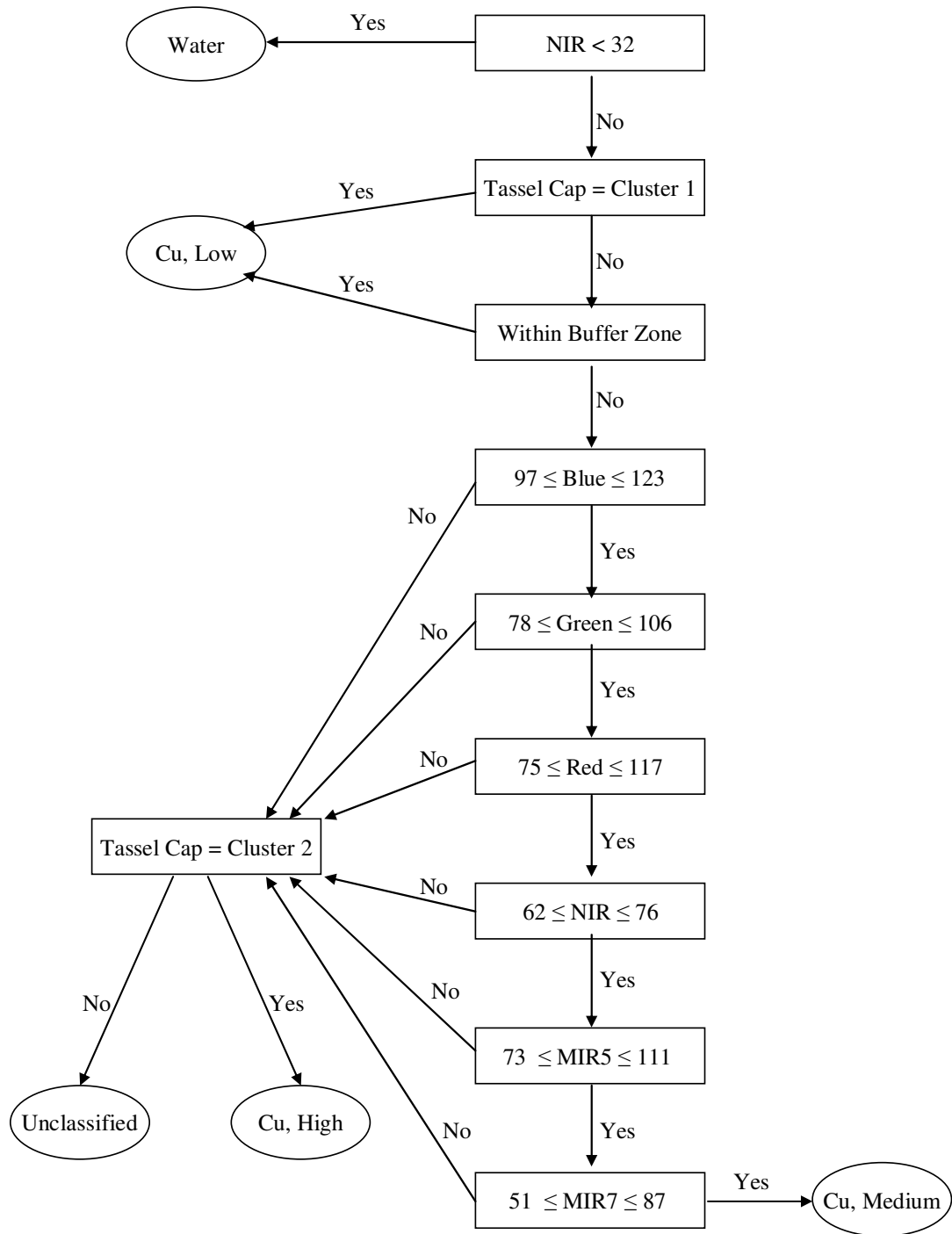


Figure 9.9: Copper loadings classification using spectral data and buffer zone

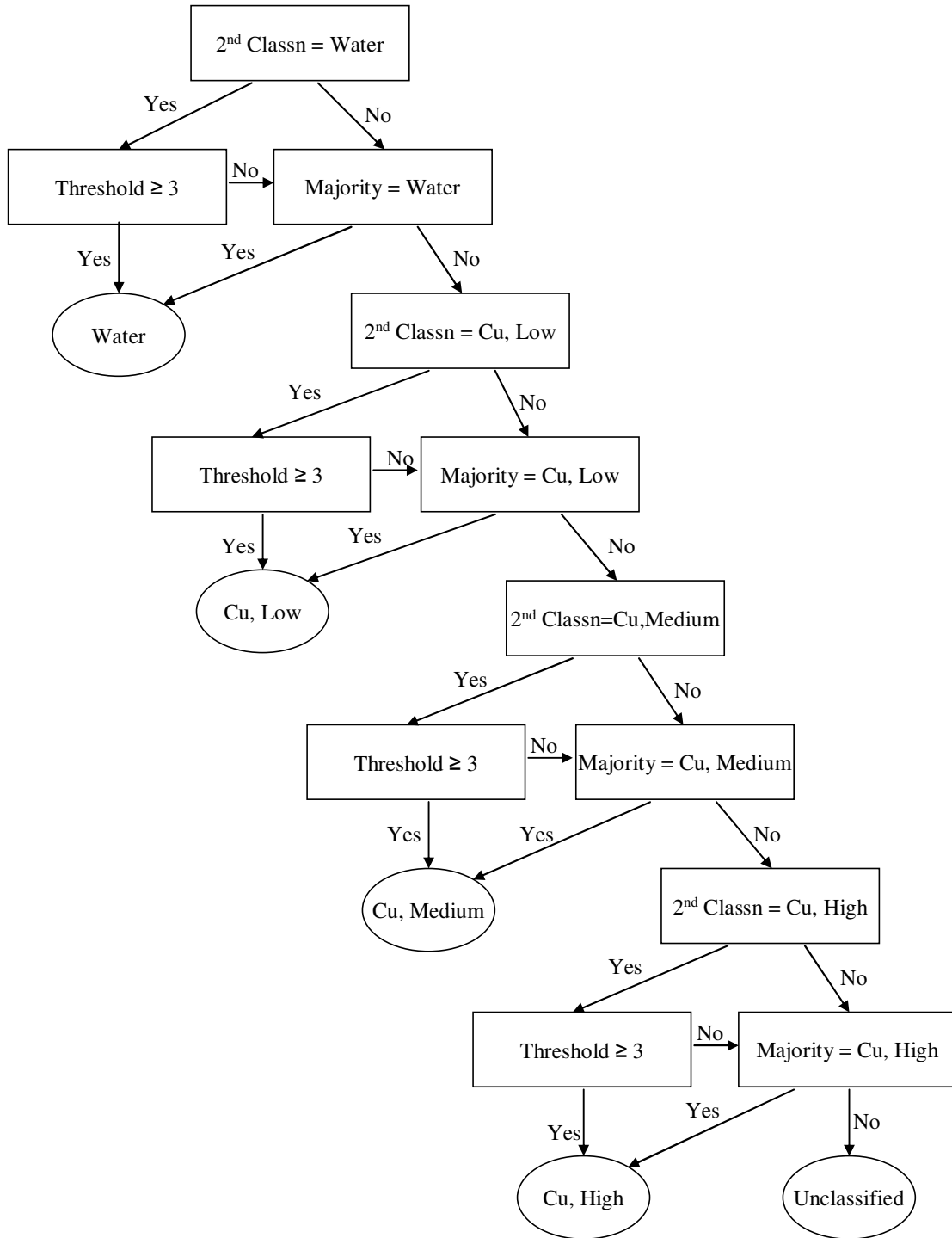


Figure 9.10: Copper loadings classification using spectral data, buffer zone, and neighborhood information

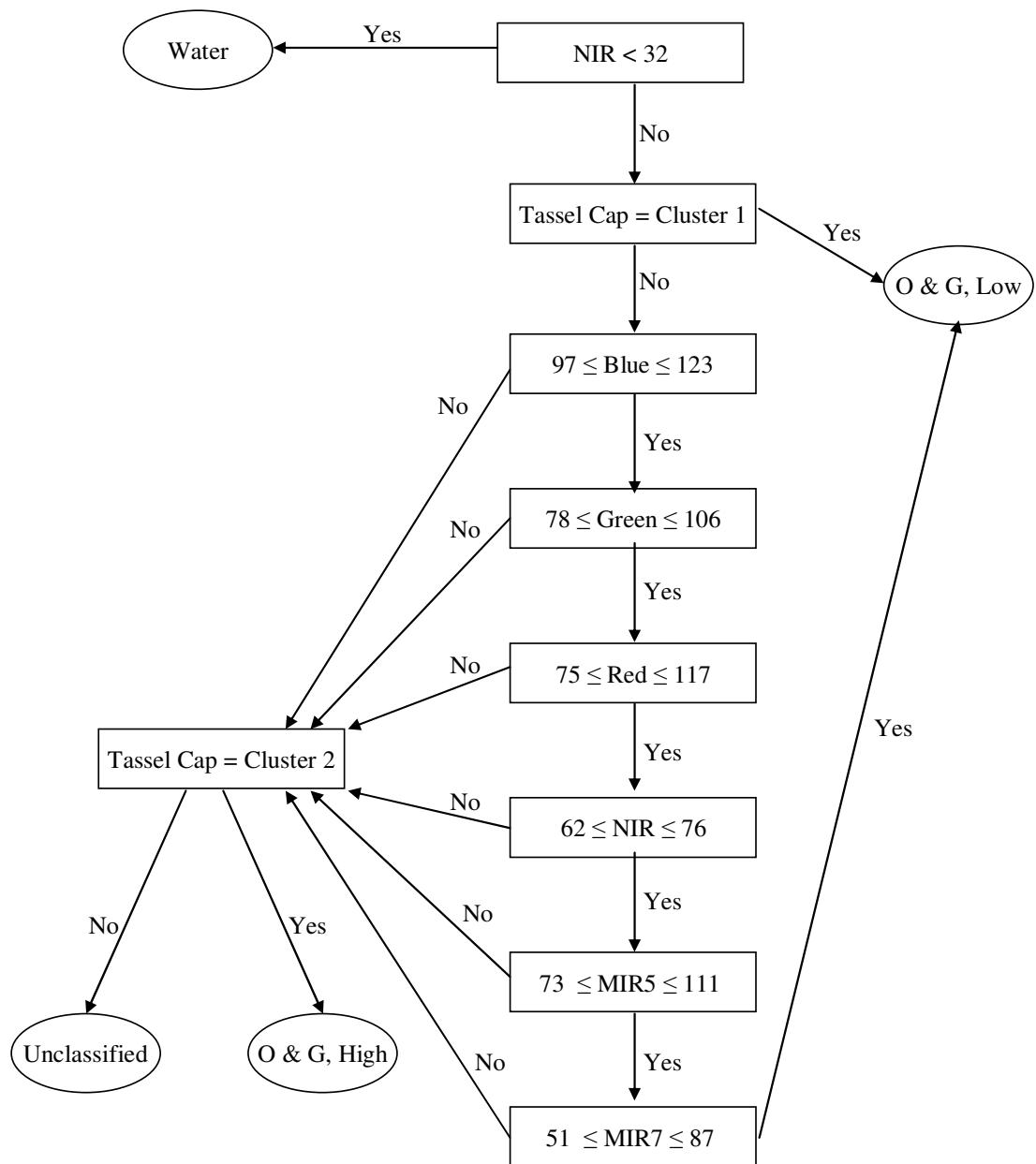


Figure 9.11: O & G loadings classification using spectral data

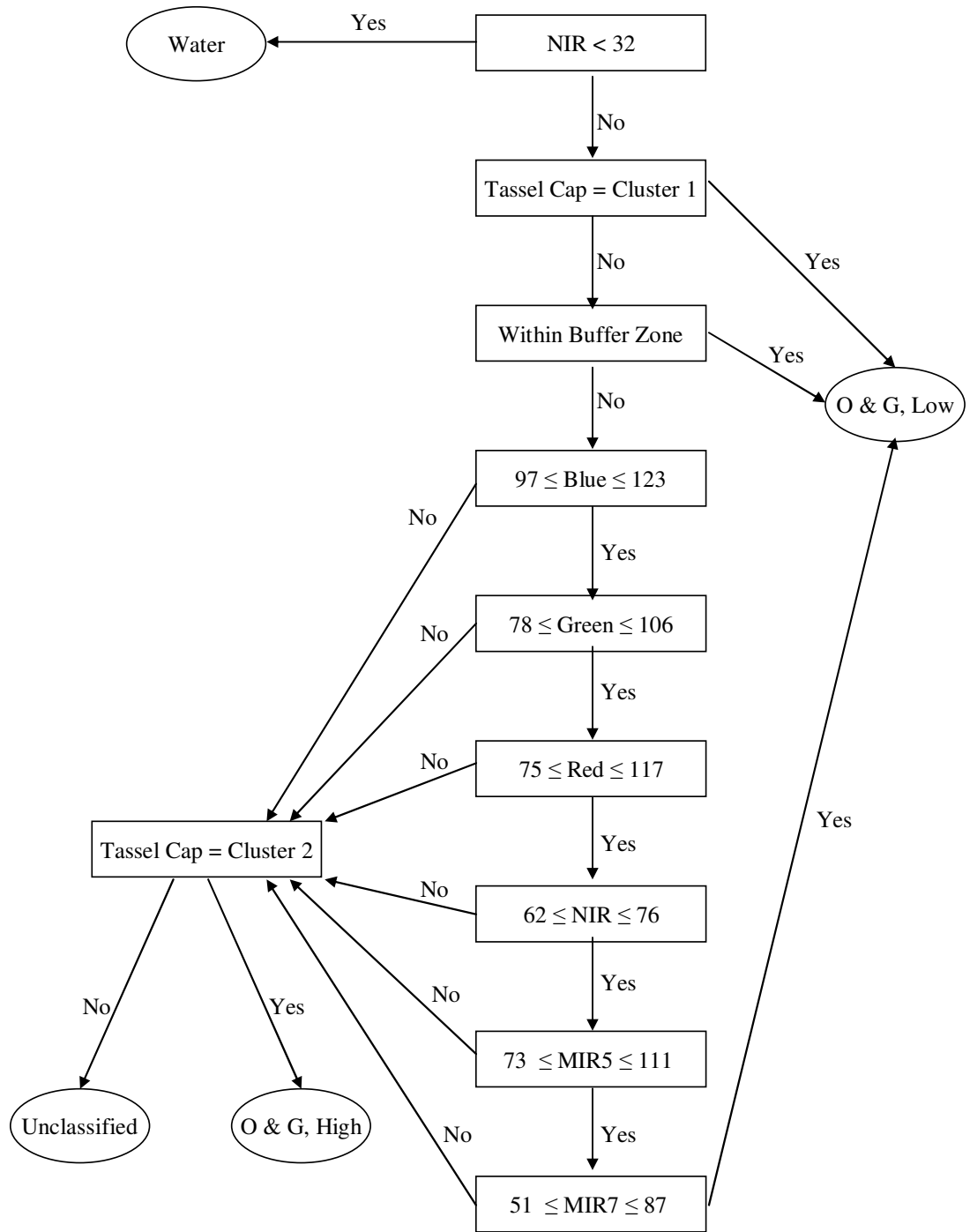


Figure 9.12: O & G loadings classification using spectral data and buffer zone

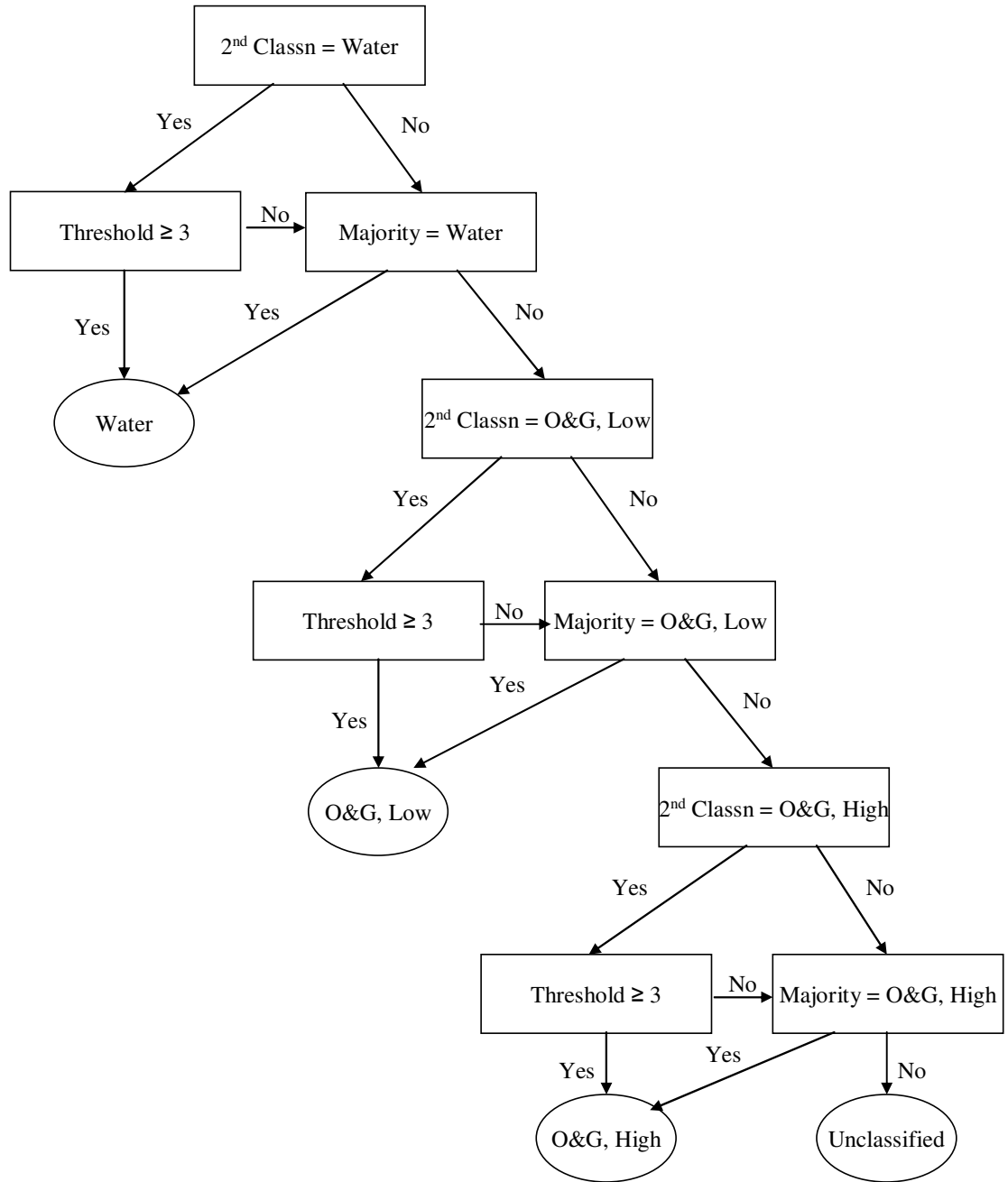


Figure 9.13: O & G loadings classification using spectral data, buffer zone, and neighborhood information

9.4 Results and Discussion

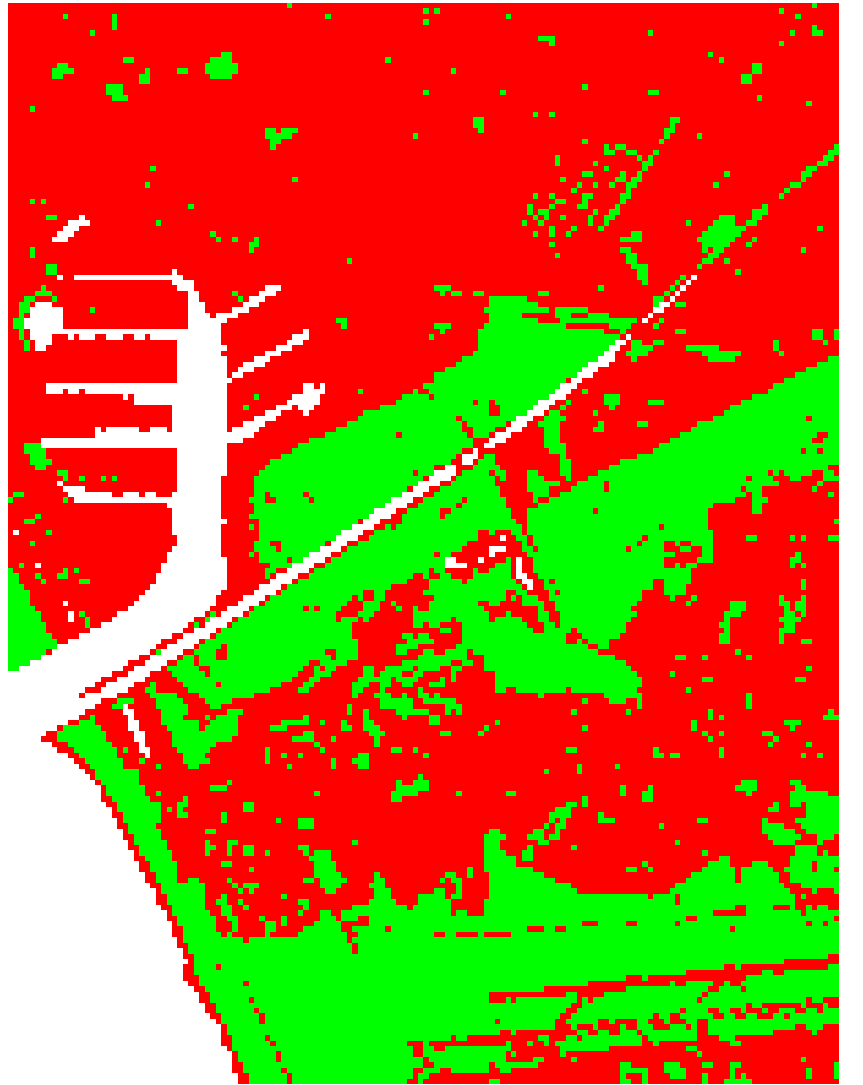
Figures 9.14 to 9.22 show the classified images. Error matrices are presented in Tables 9.4 to 9.12. Table 9.13 is a summary of the nine classifications. Overall accuracy is defined as the sum of the correctly identified pixels divided by the total number of test pixels. For individual classes, however, producer's and user's accuracies (both called locational accuracies) are more meaningful parameters. For example, for TSS, BOD5, Total P, and TKN, in the classification using spectral information only, 92.5% (producer's accuracy) of the pixels in the study area were classified correctly by the producer of the map as high loading areas. A user of the map who goes to the field and finds an area classified as high loading, has a 94.6% (user's accuracy) chance that indeed the area has a high loading of TSS, BOD5, Total P, and TKN. Also, since water is not an area of interest to us, it is omitted from the table. All locational accuracies for water are high (from 93.9% to 100%) which means it is highly separable. Unlike other studies, the water area is not masked because as another land cover having a spectral signature of its own, it can be separated by an appropriate rule, in this case, using only the NIR band. We must also remember that water contributes to the overall accuracy.

We inspect the classifications using only spectral data. For TSS, BOD5, Total P, and TKN, we simply needed to separate the open areas (low loading) from the non-open areas (high loading). We found that the tasseled cap transformation coupled with ISODATA was a satisfactory way to separate open land from non-open land (92.3% overall accuracy). Surprisingly, with this transformation, beach was also correctly classified to open land. This is difficult to do using the raw bands and even

transformations like the normalized difference vegetation index ((NIR band – red band) / (NIR band + red band)). Beach is normally confused with impervious surface, although their material components are different. Identifying the pollutant levels for copper and oil and grease involved the recognition of single-family residential. The lower accuracies observed (85.5% for copper, 87.1% for oil and grease) may be due to the confusion of impervious surfaces in the single-family residential with the impervious surfaces in all other classes. Also, there are areas designated as single-family residential in the SCAG land use map, but their spectral signature is different from the usual signature.

We expected that with the addition of ancillary data, the classifications would improve. There was evident misclassification in the area where the ocean meets the beach because of the mixing of the two land cover types. The buffer zone solved this problem. Indeed, all the classifications improved with the addition of the buffer zone. At this point, we call these as second classifications.

In the third classifications, the general effect of the neighborhood analysis was less clear. For TSS, BOD5, Total P, and TKN, the overall accuracy and the PA/LL were the same as in the second classification. PA/HL and UA/LL increased, but UA/HL actually decreased. For copper, the addition of the neighborhood information increased the overall accuracy, PA/HL, UA/ML, and UA/LL. However, UA/HL and PA/LL decreased. PA/ML remained the same. For oil and grease, most of the accuracy measures actually dropped. Visually, however, the classifications involving the neighborhood functions looked better. Because of its filtering procedure, small clumps of misclassifications were actually removed.



0 1 km

High Loading
Low Loading

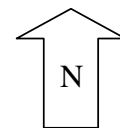
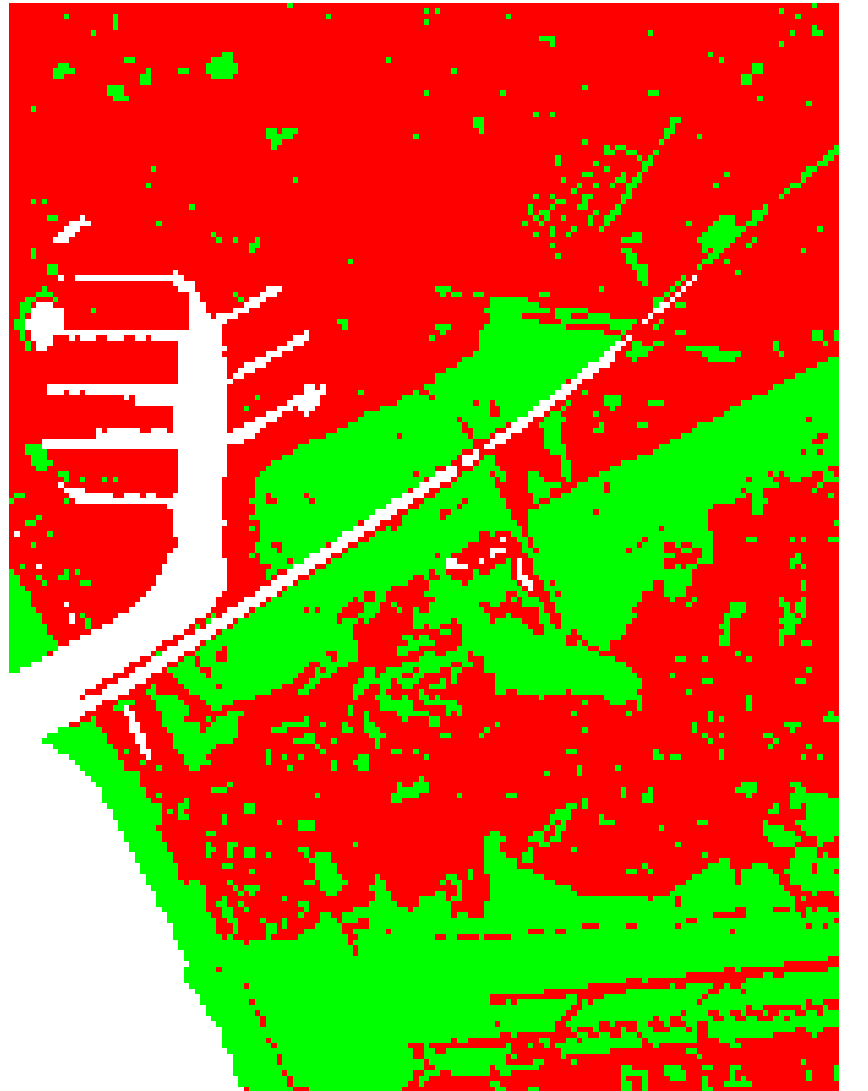


Figure 9.14: TSS, BOD5, Total P, and TKN loadings using spectral data



0 1 km

High Loading
Low Loading

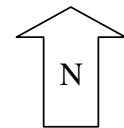
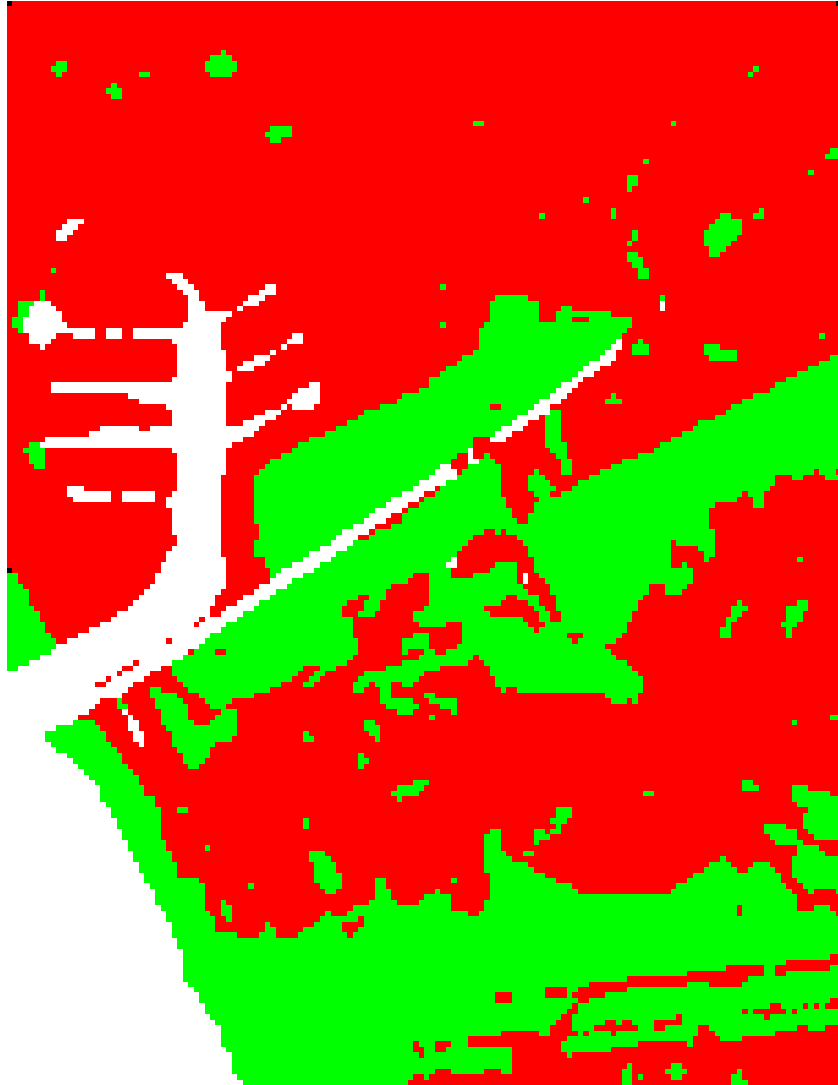


Figure 9.15: TSS, BOD5, Total P, and TKN loadings using spectral data and buffer zone



0 1 km

High Loading
Low Loading

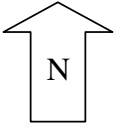
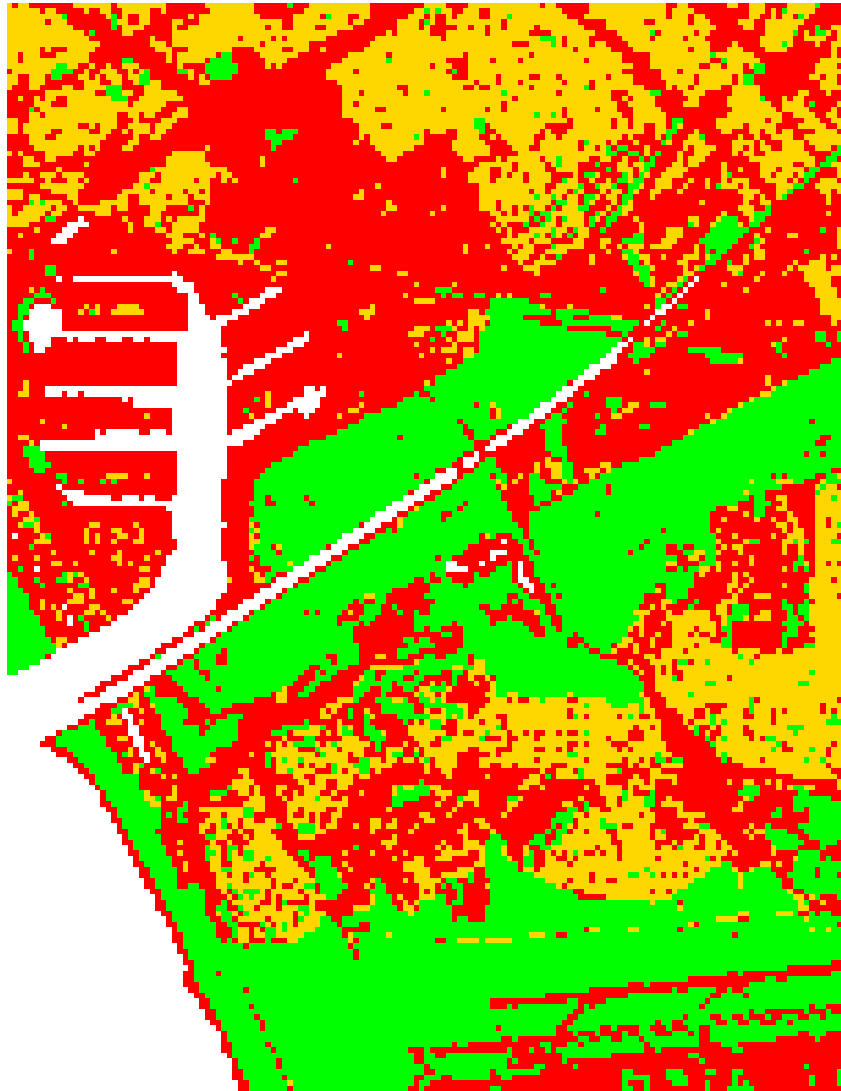


Figure 9.16: TSS, BOD5, Total P, and TKN loadings using spectral data, buffer zone, and neighborhood information



0 1 km

- High Loading
- Medium Loading
- Low Loading

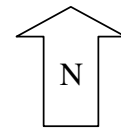
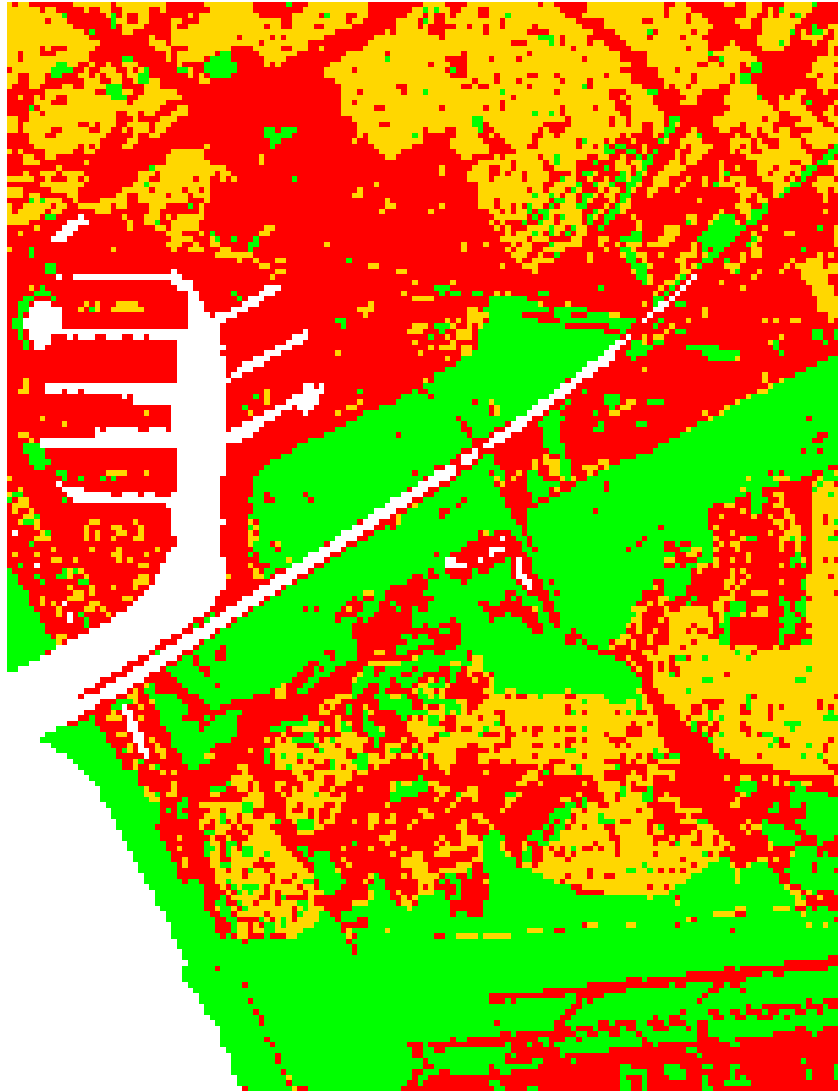


Figure 9.17: Copper loadings using spectral data



0 1 km

- High Loading
- Medium Loading
- Low Loading

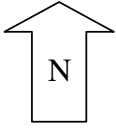
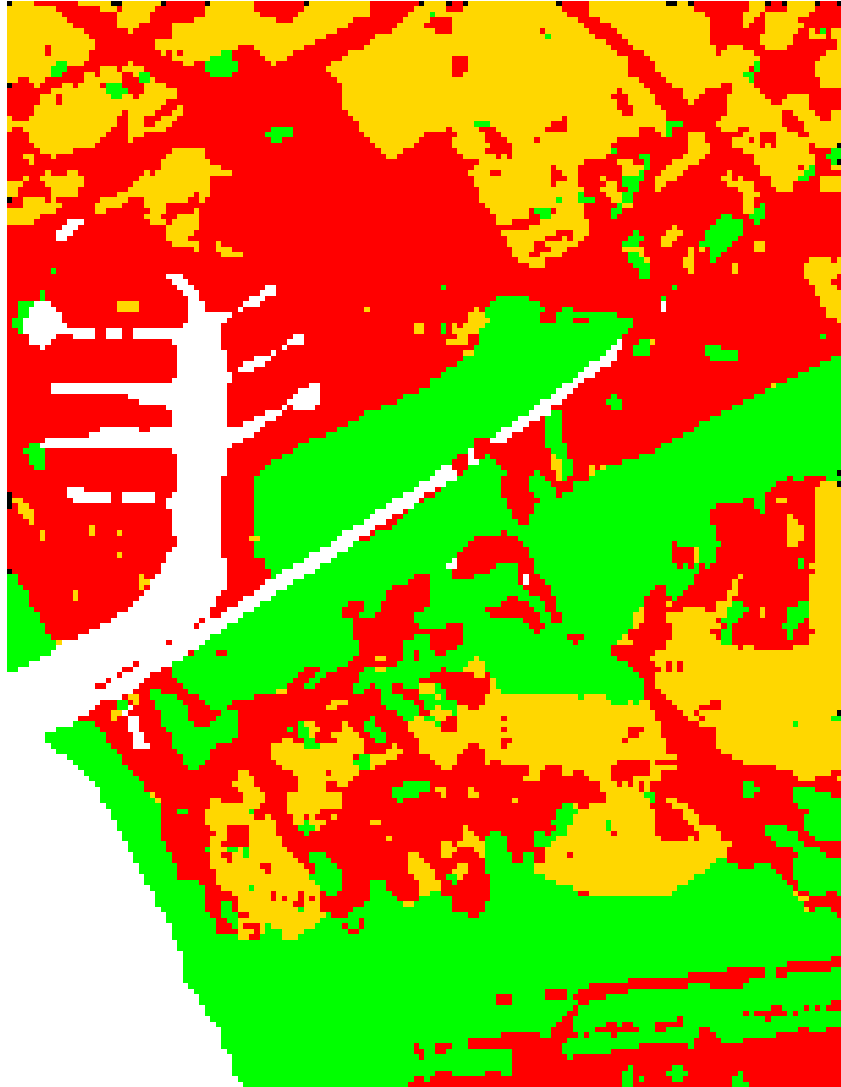


Figure 9.18: Copper loadings using spectral data and buffer zone



0 1 km

- High Loading
- Medium Loading
- Low Loading

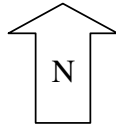
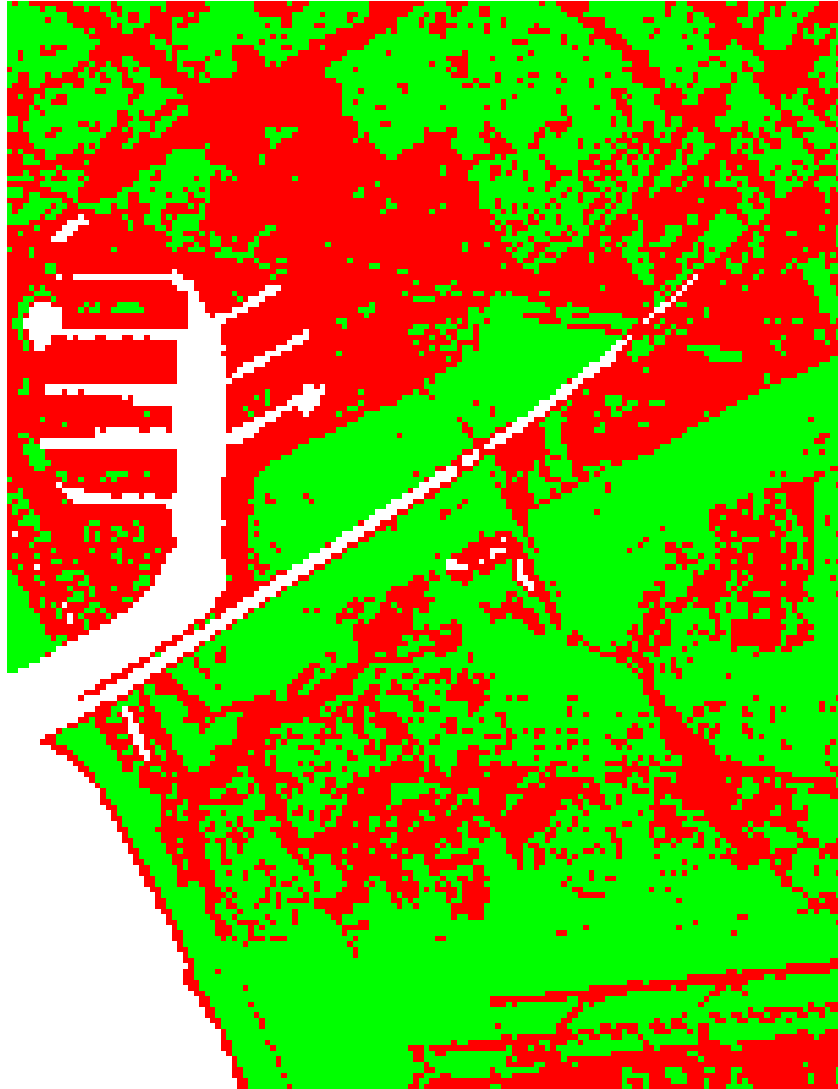


Figure 9.19: Copper loadings using spectral data, buffer zone, and neighborhood information



0 1 km

High Loading

Low Loading

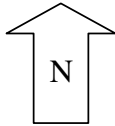


Figure 9.20: O & G loadings using spectral data



0 1 km

High Loading
Low Loading

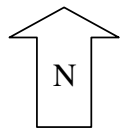
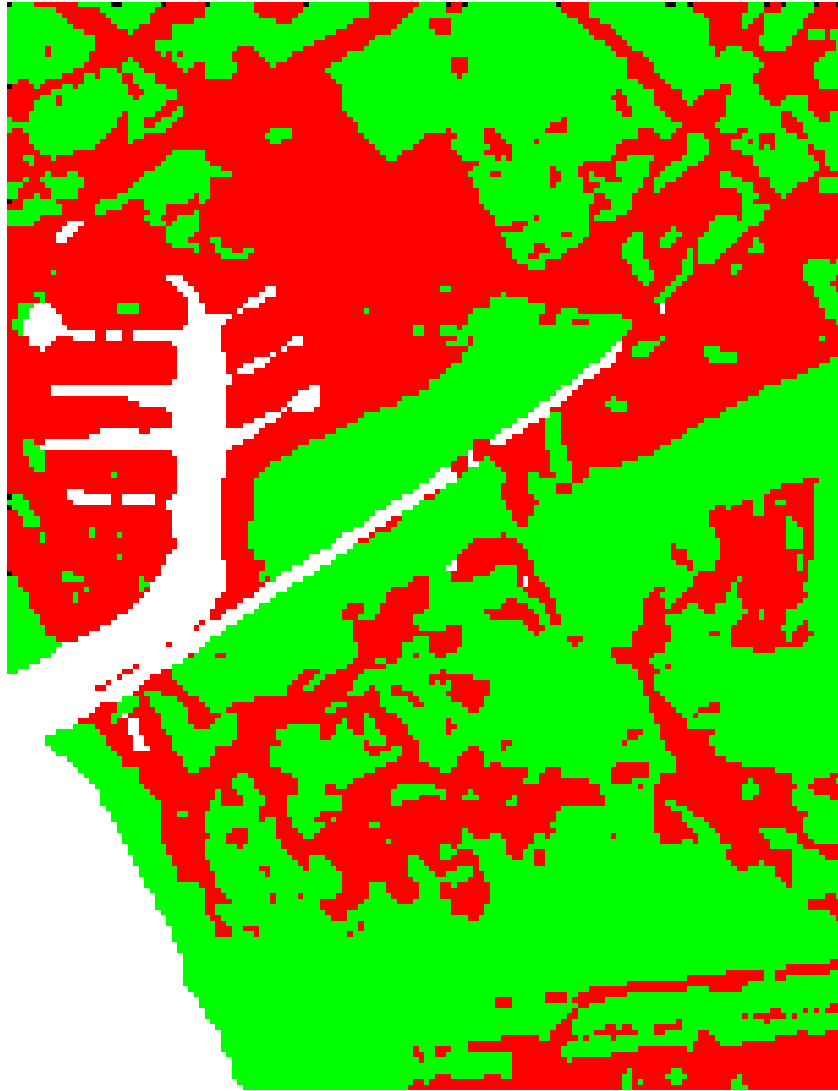


Figure 9.21: O & G loadings using spectral data and buffer zone



0 1 km

High Loading
Low Loading

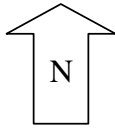


Figure 9.22: O & G loadings using spectral data, buffer zone, and neighborhood information

Table 9.4: Error matrix for TSS, BOD5, Total P, and TKN, using spectral data

		Reference			
		Water	Low	High	Row Total
Classi- fication	Water	111	0	0	111
	Low	0	272	47	319
	High	4	29	577	610
	Column Total	115	301	624	1040
Producer's Accuracy		User's Accuracy			
Water	= 96.5%	Water	= 100%		
Low	= 90.4%	Low	= 85.3%		
High	= 92.5%	High	= 94.6%		
Overall Accuracy = 92.3%					

Table 9.5: Error matrix for TSS, BOD5, Total P, and TKN, using spectral data and buffer zone

		Reference			
		Water	Low	High	Row Total
Classi- fication	Water	111	0	0	111
	Low	0	277	47	324
	High	4	24	577	605
	Column Total	115	301	624	1040
Producer's Accuracy		User's Accuracy			
Water	= 96.5%	Water	= 100%		
Low	= 92.0%	Low	= 85.5%		
High	= 92.5%	High	= 95.4%		
Overall Accuracy = 92.8%					

Table 9.6: Error matrix for TSS, BOD5, Total P, and TKN, using spectral data, buffer zone, and neighborhood information

		Reference			
		Water	Low	High	Row Total
Classi- fication	Water	108	0	2	110
	Low	0	277	42	319
	High	7	24	580	611
	Column Total	115	301	624	1040
Producer's Accuracy		User's Accuracy			
Water	= 93.9%	Water	= 98.2%		
Low	= 92.0%	Low	= 86.8%		
High	= 92.9%	High	= 94.9%		
Overall Accuracy = 92.8%					

Table 9.7: Error matrix for copper, using spectral data

		Reference				
		Water	Cu, Low	Cu, Medium	Cu, High	Row Total
Clas- sifi- cation	Water	111	0	0	0	111
	Cu, Low	0	275	14	50	339
	Cu, Medium	0	1	151	17	169
	Cu, High	4	25	40	352	421
	Column Total	115	301	205	419	1040
Producer's Accuracy		User's Accuracy				
Water	= 96.5%	Water	= 100.0%			
Cu, Low	= 91.4%	Cu, Low	= 81.1%			
Cu, Medium	= 73.6%	Cu, Medium	= 89.3%			
Cu, High	= 84.0%	Cu, High	= 83.6%			
Overall Accuracy = 85.5%						

Table 9.8: Error matrix for copper, using spectral data and buffer zone

		Reference				
		Water	Cu, Low	Cu, Medium	Cu, High	Row Total
Classi- fication	Water	111	0	0	0	111
	Cu, Low	0	280	14	50	344
	Cu, Medium	0	1	151	17	169
	Cu, High	4	20	40	352	416
	Column Total	115	301	205	419	1040
Producer's Accuracy			User's Accuracy			
Water	=	96.5%	Water	=	100.0%	
Cu, Low	=	93.0%	Cu, Low	=	81.4%	
Cu, Medium	=	73.6%	Cu, Medium	=	89.3%	
Cu, High	=	84.0%	Cu, High	=	84.6%	
Overall Accuracy = 86.0%						

Table 9.9: Error matrix for copper, using spectral data, buffer zone, and neighborhood information

		Reference				
		Water	Cu, Low	Cu, Medium	Cu, High	Row Total
Classi- fication	Water	108	0	0	2	110
	Cu, Low	0	278	11	46	335
	Cu, Medium	0	0	151	13	164
	Cu, High	7	23	43	358	431
	Column Total	115	301	205	419	1040
Producer's Accuracy			User's Accuracy			
Water	=	93.9%	Water	=	98.2%	
Cu, Low	=	92.4%	Cu, Low	=	83.0%	
Cu, Medium	=	73.6%	Cu, Medium	=	92.1%	
Cu, High	=	85.4%	Cu, High	=	83.1%	
Overall Accuracy = 86.1%						

Table 9.10: Error matrix for O & G, using spectral data

		Reference			
		Water	O & G, Low	O & G, High	Row Total
Classi- fication	Water	111	0	0	111
	O & G, Low	0	444	68	512
	O & G, High	4	62	351	417
	Column Total	115	506	419	1040
Producer's Accuracy		User's Accuracy			
Water	= 96.5%	Water	= 100.0%		
O & G, Low	= 87.7%	O & G, Low	= 86.7%		
O & G, High	= 83.8%	O & G, High	= 84.2%		
Overall Accuracy = 87.1%					

Table 9.11: Error matrix for O & G, using spectral data and buffer zone

		Reference			
		Water	O & G, Low	O & G, High	Row Total
Classi- fication	Water	111	0	0	111
	O & G, Low	0	449	68	517
	O & G, High	4	57	351	412
	Column Total	115	506	419	1040
Producer's Accuracy		User's Accuracy			
Water	= 96.5%	Water	= 100%		
O & G, Low	= 88.7%	O & G, Low	= 86.8%		
O & G, High	= 83.8%	O & G, High	= 85.2%		
Overall Accuracy = 87.6%					

Table 9.12: Error matrix for O & G, using spectral data, buffer zone, and neighborhood information

		Reference			
		Water	O & G, Low	O & G, High	Row Total
Classi- fication	Water	108	0	2	110
	O & G, Low	0	448	68	516
	O & G, High	7	58	349	414
	Column Total	115	506	419	1040
Producer's Accuracy		User's Accuracy			
Water	= 93.9%	Water	= 98.2%		
O & G, Low	= 88.5%	O & G, Low	= 86.8%		
O & G, High	= 83.3%	O & G, High	= 84.3%		
Overall Accuracy = 87.0%					

Table 9.13: Comparison of classifications

Accuracy Parameter	TSS, BOD5, Total P, TKN			Cu			O & G		
	S	S, B	S, B, N	S	S, B	S, B, N	S	S, B	S, B, N
OA	92.3	92.8	92.8	85.5	86.0	86.1	87.1	87.6	87.0
PA/HL	92.5	92.5	93.0	84.0	84.0	85.4	83.8	83.8	83.3
UA/HL	94.6	95.4	94.9	83.6	84.6	83.1	84.2	85.2	84.3
PA/ML	-	-	-	73.7	73.7	73.7	-	-	-
UA/ML	-	-	-	89.4	89.4	92.1	-	-	-
PA/LL	90.4	92.0	92.0	91.4	93.0	92.4	87.8	88.7	88.5
UA/LL	85.3	85.5	86.8	81.1	81.4	83.0	86.7	86.8	86.8

All values are in per cent.

S = Spectral data

B = Buffer zone

N = Neighborhood information

OA = Overall Accuracy

PA/HL = Producer's Accuracy (High Loading)

UA/HL = User's Accuracy (High Loading)

PA/ML = Producer's Accuracy (Medium Loading)

UA/ML = User's Accuracy (Medium Loading)

PA/LL = Producer's Accuracy (Low Loading)

UA/LL = User's Accuracy (Low Loading)

9.5 Conclusions

We can determine pollution levels from satellite images directly because pollutant loadings are associated with specific land cover whose spectral signatures are unique. As a first step, it is necessary to identify open land because it generates little amounts of pollutants. The tasseled cap transformation coupled with ISODATA is a satisfactory way to do this. Single-family, which can be separated using the raw image, is another land use that is distinct from others because it is composed of both impervious surface and lawns. Multiple-family, commercial, and industrial areas are composed mainly of impervious surfaces, like roofs and parking lots, hence they have high runoff coefficients. This may be one of the reasons why they have high pollutant loadings. Misclassifications can be solved by ancillary data, such as distance from a specific object. The effect of neighborhood information, however, is less clear. But visually, the neighborhood functions seem to improve the classification because it removes the salt and pepper appearance of the images. This performs the same task as post-classification smoothing.

9.6 References

Clarke, K.C. (1995) *Analytical and Computer Cartography, 2nd Edition*, Prentice-Hall, Inc., Upper Saddle River, New Jersey.

Crist, E.P. and Cicone, R.C. (1984) A physically-based transformation of Thematic Mapper data- The TM tasseled cap. *IEEE Transactions on Geoscience and Remote Sensing*, 22 (3): 256-263.

Jackson, P. (1999) *Introduction to Expert Systems, 3rd Edition*, Addison-Wesley, U.S.A.

Johnsson, K. and Kanonier, J. (1991) Knowledge based land-use classification. In *Proceedings of the International Geoscience and Remote Sensing Symposium IGARSS '91*, 3-6 June, Espoo, Finland, pp. 1847-1850.

Middelkoop, H. and Janssen, L.L.F. (1991) Implementation of temporal relationships in knowledge based classification of satellite images. *Photogrammetric Engineering and Remote Sensing*, 57 (7): 937-945.

Park, M.H. and Stenstrom, M.K. (2004) A new classification system for urban stormwater pollutant loading: A case study in the Santa Monica Bay area. In *Proceedings of the IWA Diffuse Pollution Conference*, 24-29 October, Kyoto, Japan, Paper 2-E-IV-4.

Richards, J.A. (1986) *Remote Sensing Digital Image Analysis: An Introduction*, Springer-Verlag, Germany.

Stenstrom, M.K., Silverman, G.S., and Bursztynsky, T.A. (1984) Oil and grease in urban stormwaters. *Journal of Environmental Engineering*, 110 (1): 58-72.

Stenstrom, M.K. and Strecker, E. (1993) *Assessment of Storm Drain Sources of Contaminants to Santa Monica Bay, Vol. I, Annual Pollutants Loadings to Santa Monica Bay from Stormwater Runoff*, UCLA-ENG-93-62, University of California, Los Angeles, California.

Wong, K.M., Strecker, E.W., and Stenstrom, M.K. (1997) GIS to estimate storm-water pollutant mass loadings. *Journal of Environmental Engineering*, 123 (8): 737-745.

Chapter 10

Assessing the Accuracy of Classifications for Pollutant Loadings Estimation

10.1 Introduction

In Chapter 9, we identified different levels of pollution for TSS, BOD5, Total P, TKN, Cu, and O & G. To evaluate the quality of the classifications, error matrices were assembled, and overall accuracy values were computed. However, this measure assumes that all misclassification errors are equally serious. We propose a method that weighs the errors, and suggest measures that reflect the accuracy of the classifications with more specificity.

10.2 Methodology

Annual pollutant loadings previously calculated are shown in Table 10.1. We designated the pollution levels as high, medium, and low. Table 10.2 displays the range of values for each pollution level. We also computed the average if applicable. With ERDAS Imagine 8.7, we segregated the imagery to areas that had high, medium, and low loading for each pollutant using knowledge-based classification techniques coupled with standard GIS operations. We applied the ISODATA procedure on a tasselled cap transformation using the greenness, wetness, and haze components computed from the

six raw bands of blue, green, red, near infrared, and the two mid-infrared bands. This resulted in the separation of open land from non-open land. Single-family residential was likewise distinguished using the six raw bands. Only the near infrared band was utilized to segregate water. Using only spectral data (first classification), the area where the beach met the ocean showed open land misclassified to non-open land. In the second classification, a buffer distance of five pixels (142.5 m) corrected this error. Neighborhood analysis was employed in the third classification. To keep its value in the second classification, a pixel should have at least three of its neighbors (in the north, east, west, and south directions) in the same category. Otherwise, it was replaced by the value in the majority image that was processed from a 3 x 3 filter.

Table 10.1: Annual pollutant loadings

Pollutant	Land Use						
	SF	MF	Co	P	LI	OU	O
TSS	14.70	15.83	17.31	15.44	17.31	18.01	6.37
BOD5	0.86	1.13	1.35	1.20	1.35	1.29	0.02
Total P	43.08	46.73	41.35	36.88	41.35	53.18	6.76
TKN	0.22	0.18	0.19	0.17	0.19	0.20	0.04
Cu	4.82	7.54	6.92	6.18	6.92	8.58	0.71
O & G	0.15	1.66	2.12	1.89	2.12	1.89	0

SF = Single-Family
 MF = Multiple-Family
 Co = Commercial
 P = Public
 LI = Light Industrial
 OU = Other Urban
 O = Open

Loadings are in kg/year except for Total P and Cu which are in g/year.

Table 10.2: Range and average loadings for the different pollution levels

Pollutant	High Loading-Range	High Loading-Average	Medium Loading-Range	Medium Loading-Average	Low Loading-Range	Low Loading-Average
TSS	14.70-18.01	16.43	-	-	6.37	6.37
BOD5	0.86-1.35	1.20	-	-	0.02	0.02
Total P	36.88-53.18	43.76	-	-	6.76	6.76
TKN	0.17-0.22	0.19	-	-	0.04	0.04
Cu	6.18-8.58	7.23	4.82	4.82	0.71	0.71
O & G	1.66-2.12	1.94	-	-	0-0.15	0.08

The next task was to quantify the quality of the classifications. This was done first by assembling error matrices. We tested 1,040 randomly generated pixels which were 3.4% of the study area. These points were mainly checked from aerial photos and field visit. The land use digital map published by the Southern California Association of Governments (SCAG) was not used fully because there was no one-to-one correspondence between its categories and the classes we have designated. For example, “other urban” areas in the SCAG data have both open land and built-up areas. This illustrates that land use data from public records are often incompatible with environmental objectives.

Overall accuracy is the most common measure of evaluating the quality of classifications, although it does not take location into account. The kappa coefficient factors in the effect of chance in the classification (Lillesand and Kiefer, 1994). For example, a kappa value of 78% indicates that the classification is 78% better than a classification that resulted from random assignment. Therefore, kappa is lower than the overall accuracy. Both measures were computed using ERDAS Imagine 8.7. We believe

that the weighted equivalents of overall accuracy and kappa will provide more specific measures of accuracy.

The arrangement shown in Table 10.3 is used to assess the weighted overall accuracy and weighted kappa coefficient (Naesset, 1996). This is similar to an error matrix except that the cell values are not absolute observations and computed values but proportions.

Table 10.3: Proportion of pixels distributed into k classes

		Reference					Total
		1	2	$k - 1$	k	
Classification	1	p_{11}	p_{12}	$p_{1\ k-1}$	p_{1k}	p_{1+}
	2	p_{21}	p_{22}	$p_{2\ k-1}$	p_{2k}	p_{2+}

	$k - 1$	$p_{k-1\ 1}$	$p_{k-1\ 2}$	$p_{k-1\ k-1}$	$p_{k-1\ k}$	p_{k-1+}
	k	p_{k1}	p_{k2}	$p_{k\ k-1}$	p_{kk}	p_{k+}
Total	p_{+1}	p_{+2}	p_{+k-1}	p_{+k}	1	

(from Naesset, 1996)

To make this table, we divide all the original values in the error matrix by the total number of test points. Let

$$p_{i+} = \sum_{j=1}^k p_{ij} \quad (10.1)$$

be the proportion of pixels classified into class i in the classified image, and

$$p_{+j} = \sum_{i=1}^k p_{ij} \quad (10.2)$$

be the proportion of pixels confirmed as class j in the reference image. Let w_{ij} be the weight associated with the i,j th cell in the error matrix. If

$$p_{\sigma} = \sum_{i=1}^k \sum_{j=1}^k w_{ij} p_{ij} \quad (10.3)$$

is the weighted agreement or weighted overall accuracy, and

$$p_c = \sum_{i=1}^k \sum_{j=1}^k w_{ij} p_{i+} p_{+j} \quad (10.4)$$

is the weighted chance agreement, Cohen (1968) defines weighted kappa as

$$K_w = \frac{p_{\sigma} - p_c}{1 - p_c} \quad (10.5)$$

To calculate for the weighted overall accuracy and weighted kappa, we need to assign a weight for each cell in the error matrix to reflect the severity of the misclassification error. Fleiss *et al.* (1969) state that weights are limited to the interval $0 \leq w_{ij} \leq 1$ for $i \neq j$, and that the weight for perfect agreement is 1 (i.e., $w_{ii} = 1$). Naeset (1996) suggested that weights may reflect the loss of utility because of misclassification. If $U_{c,j}$ is the utility when a pixel is correctly classified into class j and $U_{E,ij}$ is the utility when a pixel belonging to class j is wrongly classified into class i , then the weight is

$$w_{ij} = U_{E,ij}/U_{c,j} \quad (10.6)$$

The benefit of creating a pollutant loading map is to be able to identify areas generating high levels of pollution. Therefore, initially, we thought of quantifying the value of best management practices (BMPs). However, BMPs can vary depending on the type of pollutants. In addition, it may be difficult to determine the dollar value of the benefit arising from a BMP. Next, we looked at the average or representative values associated with high, medium, and low loadings. If we put the absolute values of pollutant loadings in the equation above, we may have a value of zero in the denominator. Amounts over- or underestimated from the misclassification errors can also produce zeroes in the denominator.

Cicchetti and Allison (1971) proposed a way of assigning weights specifically for ordinal data. Perfect agreement is assigned a weight of 1, and the worst disagreement is assigned a weight of zero. Weights of other cases of misclassifications are determined linearly. Because our classification is in ordinal scale, this procedure is applicable. However, we have modified it so that the weights were linearly related to the amount of pollutant loadings. The difference between TSS low loading and TSS medium loading, for example, is not the same as the difference between BOD5 low loading and BOD5 medium loading.

To demonstrate how weights are calculated, we take copper as an example. Similar procedures were applied to the other pollutants. Complete agreement is assigned a weight of 1, and the worst disagreement is assigned a weight of zero (Table 10.4) When we misclassify an actual water pixel to high loading, we are “putting” high amounts of loading to an area where there is none generated. Misclassifying medium to high loading

or vice-versa has a less serious effect because the over- or underestimated amount is smaller than in the worst misclassification case. In Table 10.4, we need to compute for the weights a , b , c , d , and e . Note that the severity of error associated with misclassifying low to high loading, for example, is as severe as misclassifying high to low loading, hence they have the same weight.

Table 10.4: Agreement weight matrix for copper with variable weights to be computed

	Water	Cu, Low	Cu, Medium	Cu, High
Water	1	a	b	0
Cu, Low	a	1	e	c
Cu, Medium	b	e	1	d
Cu, High	0	c	d	1

In Table 10.5, the weights are related to the pollutant loadings. In the second and third columns, when the loading is zero, the weight is one, and when the loading is 7.23, the weight is zero. For the last column, when the loading is 0, the weight is also zero. When the loading is 7.23, the weight is one. By simple ratio and proportion, we computed for the values of a , b , c , and d . Using these values, the weight e was calculated by averaging the weights of its neighbors in the north, east, west, and south directions. Table 10.6 shows the completed agreement weight matrix for copper. Similar tables were made for TSS, BOD5, Total P, TKN, and O & G (Tables 10.7-10.11). After the weight matrices were computed, weighted overall accuracy and weighted kappa coefficients were calculated using STATA 8.2.

Table 10.5: Relationship of copper loadings to weights

	Loading	Weights	Weights
Water	0	1	0
Cu, Low	0.71	<i>a</i>	<i>c</i>
Cu, Medium	4.82	<i>b</i>	<i>d</i>
Cu, High	7.23	0	1

Table 10.6: Agreement weight matrix for copper

	Water	Cu, Low	Cu, Medium	Cu, High
Water	1.00	0.90	0.33	0
Cu, Low	0.90	1.00	0.61	0.10
Cu, Medium	0.33	0.61	1.00	0.67
Cu, High	0	0.10	0.67	1.00

Table 10.7: Agreement weight matrix for TSS

	Water	TSS, Low	TSS, High
Water	1	0.61	0
TSS, Low	0.61	1	0.39
TSS, High	0	0.39	1

Table 10.8: Agreement weight matrix for BOD5

	Water	BOD5, Low	BOD5, High
Water	1	0.98	0
BOD5, Low	0.98	1	0.02
BOD5, High	0	0.02	1

Table 10.9: Agreement weight matrix for Total P

	Water	Total P, Low	Total P, High
Water	1	0.85	0
Total P, Low	0.85	1	0.15
Total P, High	0	0.15	1

Table 10.10: Agreement weight matrix for TKN

	Water	TKN, Low	TKN, High
Water	1	0.79	0
TKN, Low	0.79	1	0.21
TKN, High	0	0.21	1

Table 10.11: Agreement weight matrix for O & G

	Water	O & G, Low	O & G, High
Water	1	0.96	0
O & G, Low	0.96	1	0.04
O & G, High	0	0.04	1

10.3 Results and Discussion

Tables 10.12-10.14 summarize the results of all the calculations. The addition of the buffer zone improved the classification. However, the effect of the neighborhood analysis is hard to tell. In some cases the accuracy increased, but in other cases, the accuracy decreased, or remained the same.

Overall accuracy values and kappa coefficients were the same for TSS, BOD5, Total P, and TKN for each group of classifications. This was because there were only two states for these pollutants, low loading and high loading, which basically meant separating open land from non-open land. This qualitative assignment of pollution levels did not take into account the difference in magnitudes between pollution levels. With the weighted equivalents of the overall accuracy and kappa coefficient, we observed that these pollutants showed different values, indicating the fact, for example, that among TSS, BOD5, Total P, and TKN, TSS loading classification was the best classified. We

also observed that weighted overall accuracy was always higher than overall accuracy. But weighted kappa coefficient could be smaller or larger than kappa coefficient. Naeset (1996) states that these values depend on the dataset and the weights applied.

Table 10.12: Accuracy measures for classification with spectral data (in per cent)

Pollutant	Overall Accuracy	Weighted Overall Accuracy	Kappa	Weighted Kappa
TSS	92.3	95.2	86.0	86.9
BOD5	92.3	92.4	86.0	84.2
Total P	92.3	93.4	86.0	85.0
TKN	92.3	93.8	86.0	85.4
Cu	85.5	90.8	79.2	78.8
O & G	87.1	87.6	78.0	73.6

Table 10.13: Accuracy measures for classification with spectral data and buffer zone (in per cent)

Pollutant	Overall Accuracy	Weighted Overall Accuracy	Kappa	Weighted Kappa
TSS	92.8	95.4	86.9	87.7
BOD5	92.8	92.9	86.9	85.2
Total P	92.8	93.8	86.9	85.9
TKN	92.8	94.2	86.9	86.3
Cu	86.0	91.2	79.9	79.8
O & G	87.6	88.1	78.9	74.5

Table 10.14: Accuracy measures for classification with spectral data, buffer zone, and neighborhood information (in per cent)

Pollutant	Overall Accuracy	Weighted Overall Accuracy	Kappa	Weighted Kappa
TSS	92.8	95.3	86.8	87.2
BOD5	92.8	92.9	86.8	85.1
Total P	92.8	93.7	86.8	85.7
TKN	92.8	94.1	86.8	86.1
Cu	86.1	91.0	80.0	79.3
O & G	87.0	87.5	77.9	73.3

10.4 Conclusions

The weighted equivalents of the overall accuracy and the kappa coefficient provide a new way to look at accuracy measures for assessing the quality of maps made from automated classification of remotely sensed data. This becomes more important especially when classifying ordinal data. Since levels of pollution are only designated as high, medium, and low, these more specific accuracy measures will give better information to users and serve as a guide in designing best management practices.

10.5 References

Cicchetti, D.V. and Allison, T. (1971) A new procedure for assessing reliability of scoring EEG sleep recordings. *American Journal of EEG Technology*, 11: 101-109.

Cohen, J. (1968) Weighted kappa: Nominal scale agreement with provision for scaled disagreement or partial credit. *Psychological Bulletin*, 70: 213-220.

Fleiss, J.L., Cohen, J., and Everitt, B.S. (1969) Large sample standard errors of kappa and weighted kappa. *Psychological Bulletin*, 72: 323-327.

Lillesand, T.M. and Kiefer, R.W. (1994) *Remote Sensing and Image Interpretation*, 3rd Edition, John Wiley & Sons, Inc., U.S.A.

Naesset, E. (1996) Use of the weighted Kappa coefficient in classification error assessment of thematic maps. *International Journal of Geographical Information Systems*, 10 (5): 591-603.

Chapter 11

Conclusions and Future Work

The automated classification of satellite imagery can provide an efficient alternative to traditional methods in obtaining important information for stormwater management. Many studies in the literature proved that the results of the stormwater modeling effort in terms of pollutant loadings or hydrographs, for example, remain satisfactory even with input parameters processed from satellite data. One of these critical parameters is land use and/or land cover because it is associated with impervious areas which determine runoff rates and volumes. Land use/land cover is also related to the types and quantities of pollutants generated in a parcel of land. Emerging technologies, such as neural networks and knowledge-based systems, can improve the accuracy of automated land use/land cover classification.

We have demonstrated that the combined technologies of satellite remote sensing, knowledge-based systems, and geographic information systems (GIS) can be used to map impervious surfaces and distinguish areas with different levels of pollution. Spectral data from the raw image and transformations can provide rules for the knowledge base. Many transformations have been attempted, but the normalized difference vegetation index (NDVI) and the tasseled cap transformation proved to be the most appropriate for this particular study. The use of ancillary data, such as the distance from a specific object,

refined the classification. However, the addition of more ancillary data, such as neighborhood information, did not necessarily enhance the classification. Validation using aerial photographs, SCAG data, and field visit verified that the classifications were satisfactory. The addition of ancillary data is often necessary in automated classification because spectral signatures sometimes overlap, especially in urban areas which exhibit much structural complexity and heterogeneity. Incorporation of ancillary data is best done through a knowledge-based system coupled with GIS. We have substantiated that this method is superior to statistical methods alone using only spectral data. We also proposed more specific methods to report the accuracy of classifications. These measures are the weighted overall accuracy and the weighted kappa coefficient. We suggested ways to compute weights associated with the severity of misclassification errors. This led to more specificity in evaluating the quality of classifications of different pollutant levels.

There are various ways that the techniques utilized here can be applied to other endeavors. The most useful is probably to apply the same exact knowledge base to another study area. We will see if the knowledge base is applicable in an area with a different climate and culture. When vegetation, soil, or level of activity, for example, are different, how robust is our knowledge base? Are modifications required? For impervious surface detection, it is probably better to use a higher resolution image because most impervious surface, for example, roads and highways, are narrower than the pixel resolution. We may also encounter other types of land cover, other than the ones considered in this investigation. An example is a desert area.

We can estimate different levels of pollution in other areas as well. In a smaller city, or a rural area, where activity is less, pollutants may have lower concentrations, and impervious surface area may be less. These factors should be considered in the classifications. We can also add other contaminants like chemical oxygen demand, nitrite and nitrate, soluble phosphorus, lead, and zinc. Needless to say, the choice of pollutants is dependent on the availability of their concentrations for validation purposes. Some contaminants may be more important than others, too. Oil and grease, for example, is probably significant in urban areas, but not in rural areas where parking lots are fewer.

We can also maximize the amount of spectral information available. For example, in this study, we used the six reflective bands of the Landsat ETM+ which has a 30 m resolution. The panchromatic (15 m resolution) and the thermal (60 m resolution) bands were not utilized. Hence, they can be included in the knowledge base. However, issues in resampling should be considered because of the differences in resolution. The reflective bands also have their equivalents in other images like SPOT or IKONOS. These other types of images can be tried as well.

The raw images are always useful, but most of them are actually highly correlated. This means there is a repetition of information between some bands. Transformations have been developed to accentuate features of interest to the analyst. We have worked on the NDVI image, the most popular vegetation index image, but we can also look at other vegetation index images. The mere development of the other vegetation index images warrants their study. We may also try other transformations, such as indices, in which particular soil components are emphasized (e.g., iron oxide). Indices are

especially valuable in areas with high variations in topography because it can remove effects due to shadows. The principal components transformation should also be tried. However, we must be careful in using this procedure because it is a statistical transformation, unlike others which are related to the physical properties of the earth surface features.

The addition of other ancillary data is highly recommended. Adding elevation and their associated parameters like slope and aspect were not useful for this site, because it is relatively flat. We proved that elevation was not an important ancillary data from our observations during the field visit. Multi-family residential areas, for example, can be found both in the valleys and in the hills. For another study area where differences in elevation are significant, then elevation can be added in the knowledge base. This parameter can be easily processed from a digital elevation model (DEM). These are available in various resolutions, too. An analyst must choose the resolution most compatible to the satellite image he is working on. Other ancillary data that may be helpful are zoning information and housing density. Neighborhood information is another type of ancillary data. We have concluded that it may not necessarily increase the accuracy of the classification. In the future, we can vary the kernel size and observe the effect on the classification. Moreover, we can assign a different threshold in the rules and/or conditions. We can also consider other neighbors, such as the northeast, northwest, southeast, and southwest neighbors.

After selecting the images, we evaluate the utility of their spectral content by using separability measures. We used Jeffries-Matusita distances here, but there are

others such as divergence and transformed divergence. However, we must be aware of their properties, and we should not blindly use these measures without examining them first. If we do this, we can interpret these separability measures in a more meaningful way. Also, in delineating training areas, we should take into account the variability of a particular class. More homogeneous classes like vegetation, for example, need a few or even one large training area, while urban areas, which has greater variability, should have more training areas.

After the classification procedure, we must report the quality of the classifications. The overall accuracy and the kappa coefficient are the standard measures but their weighted equivalent should be tried. Perhaps, the difficulty in this procedure lies in the calculation of weights. In the literature, there are no fast rules in making the weights, but it generally depends on the application, and the data that are available.

An extension of this study that can be more involved is to actually include the parameters acquired from satellite imagery to stormwater models. We can compare results of these models with those whose input parameters were obtained manually. This process will take time as stormwater modeling requires a great deal of input parameters. The model results can be in terms of hydrographs or runoff volumes. Validation procedures may also be an issue because data may not always be available, especially for smaller watersheds.

We have demonstrated the utility of satellite data for stormwater management applications. The availability of more image types and the development of more advanced computing technologies make the use of satellite data an attractive alternative

to traditional, manual methods which are slow, difficult, and expensive. It is hoped that more planners and engineers consider the use of satellite data in acquiring information relevant for stormwater management.

Appendix: Abbreviations and Acronyms

A	drainage area
AGNPS	Agricultural Non-Point Sources
ANN	artificial neural network
ANSWERS	Areal Non-point Source Watershed Environment Response Simulation
B	Buffer zone
BMP	best management practice
BOD	biochemical oxygen demand
BOD ₅ , BOD ₅	biochemical oxygen demand
C	event mean concentration
cm	centimeter
Co	Commercial
COD	chemical oxygen demand
Cu	copper
DEM	digital elevation model
DN	digital number
EMC	event mean concentration
ETM	Enhanced Thematic Mapper
GCP	ground control point
GIS	Geographic Information System
GPS	Global Positioning System

GWLF	Generalized Watershed Loading Functions
HEC	Hydrologic Engineering Center
I	fraction of impervious surface of a land parcel
IAR	Impervious Surface at Residential
IFOV	instantaneous field of view
ISODATA	Iterative Self-Organizing Data Analysis Technique
J-M	Jeffries-Matusita
KBS	knowledge-based system
km	kilometer
L ₁	Loadings (kg/yr)
L ₂	Loadings (g/yr)
LACDPW	Los Angeles County Department of Public Works
lbs	pounds
LI	Light Industrial
m	meter
MF	Multiple-Family
MICE	Map Image Congruency Evaluation
MIR	mid-infrared
MIR5	mid-infrared band 5
MIR7	mid-infrared band 7
MSIAS	multispectral image analysis system
MSS	Multi-spectral Scanner

MXL	maximum likelihood
N	neighborhood information
NDVI	Normalized Difference Vegetation Index
NIR	near-infrared
NO _{2&3}	nitrite and nitrate
NSTORM	total number of storms per year
O	Open
OA	Overall Accuracy
OU	Other Urban
O & G	oil and grease
P	Public
PA/HL	Producer's Accuracy (High Loading)
PA/LL	Producer's Accuracy (Low Loading)
PA/ML	Producer's Accuracy (Medium Loading)
PL	pollutant loadings per year
RBV	Return Beam Vidicon
RBF-NN	radial-basis-function neural network
RC	runoff coefficient
RF	rainfall
RV	runoff volume per storm event
RVA	total volume of runoff per year
S	spectral data

SALT	Sloping Agricultural Land Technology
SCAG	Southern California Association of Governments
SCS	Soil Conservation Service
SD	standard deviation
SF	Single-Family
SLAMM	Source Loading and Management Model
SP	soluble phosphorus
sq cm	square centimeter
sq km	square kilometer
sq m	square meter
SSE	sum of squared error
STORM	Storage Treatment Overflow Runoff Model
SWAT	Soil and Water Assessment Tool
SWMM	Storm Water Management Model
TIR	thermal infrared
TKN	total Kjeldahl nitrogen
TM	Thematic Mapper
TN	total nitrogen
TP	total phosphorus
TSS	total suspended solids
TVR	total volume of water produced from rainfall per storm event
UA/HL	User's Accuracy (High Loading)

UA/LL	User's Accuracy (Low Loading)
UA/ML	User's Accuracy (Medium Loading)
UCLA	University of California, Los Angeles
USGS	United States Geological Survey
UTM	Universal Transverse Mercator
WGS	World Geodetic System
WMS	Watershed Modeling System